THE STUDY OF NUCLEAR EQUATION OF STATE USING STOPPING AND ANISOTROPIC FLOW

A THESIS

submitted to the

THAPAR UNIVERSITY, PATIALA

for the degree of

DOCTOR OF PHILOSOPHY

IN THE FACULTY OF SCIENCE

By

Mandeep Kaur

Regn. No. 901112019

SCHOOL OF PHYSICS AND MATERIALS SCIENCE

THAPAR UNIVERSITY

PATIALA-147004, PUNJAB (INDIA)

Dedicated to

My Beloved Parents and Husband

THAPAR UNIVERSITY, PATIALA

CANDIDATE'S DECLARATION

I hereby certify that the work which is being presented in this thesis entitled "**THE STUDY OF NUCLEAR EQUATION OF STATE USING STOPPING AND ANISOTROPIC FLOW**" is partial fulfillment of the requirements for the award of degree of Doctor of Philosophy and submitted in the School of Physics and Materials Science, Thapar University, Patiala, is an authentic record of my own work carried out during a period from July 2011 to May 2016 under the supervision of **Dr. Suneel Kumar**, Associate Professor, Thapar University, Patiala. The matter presented in this thesis has not been submitted by me in part or full for the award of any other degree in any other university or institute.

Mandeep Kaur

(Mandeep Kaur)

This is to certify that the above statement made by the candidate is correct to the best of our knowledge.

S Kumar

Supervisor

(Dr. Suneel Kumar)

M Sharma

Head of Department

(Dr. Manoj K. Sharma)

O P Pandey

Dean R & SP

(Dr. O. P. Pandey)

S Dhiman

External examiner

(Dr. S. K. Dhiman)

Date: 25|5|2016

Acknowledgements

The ironic truth of life is that it has many ups and downs. But I am fortunate enough that God has always blessed me with optimistic and motivated surroundings. I am forever grateful to God for all he has done for me. I would like to acknowledge all those who made my dream come true. However, these few words cannot fully express my gratitude for all of them.

Firstly, from the core of my heart, I would like to thank my esteemed supervisor Dr. Suneel Kumar, Associate Professor, School of Physics and Materials Sciences (SPMS), Thapar University, Patiala, for not only shaping my academic career, but also for showing me what a researcher should strive to be; patient, punctual, thorough, passionate and personable. I am truly grateful to him for his support and invaluable guidance.

I would like to express my sincere gratitude to Prof. Prakash Gopalan, Director, Thapar University and Shri Gurbinder Singh, Registrar, Thapar University, Patiala.

I am also thankful to Dr. O. P. Pandey, Dean of Research and Sponsored Projects for his constant moral support to accomplish this task and providing the possible research facilities in various disciplines.

I will always be deeply indebted to Dr. Manoj K. Sharma, Professor and Head, School of Physics and Materials Science, Thapar University, Patiala, for providing all the necessary facilities in the department. I extend my sincere thanks to Prof. Kulbir Singh. I would also like to acknowledge the valuable suggestions of the members of the doctoral committee, Dr. Alka Upadhyay and Dr. A. K. Lal. My sincere thanks also goes to all the faculty and staff of the SPMS for their kind support and motivation. Many thanks to the head of Centre of Information and Technology Management (CITM) for providing the supercomputing facility. Special thanks to Mr. Harcharanjit Singh for helping me to tackle the problems related to Scientific Linux.

I would like to thank my seniors Dr. Sanjeev Kumar, Dr. Varinderjit Kaur, Dr. Karan Singh Vinayak, Dr. Anupriya and Dr. Rajni for their guidance and help whenever I bothered them. I highly appreciate my lab mates Navjot, Rubina, Aman, Sangeeta, Amandeep and Deepshikha and many other research scholars here at Thapar University, for their pleasant company and for making this experience an enjoyable and memorable one.

I acknowledge with thanks the co-operation and encouragement extended by Dr. R. K. Puri, Professor, Panjab University, and his students Dr. Sakshi Gautam, Sukhjeet, Rajni and Mandeep for their fruitful discussions and novel views.

On a more personal note, I would like to express gratitude to my dearest friends Ms. Kamaldeep Kaur, Mrs. Gurvinder Kaur and Mrs. Kirandeep Sandhu. They have been the essential supporters throughout this journey. I deeply appreciate my close and ever cheerful friend Mrs. Kanchan for being with me and encouraging me to achieve my goal.

I don't really have words to express my gratitude towards my parents (Sdn. Joginder Kaur and S. Wajinder Singh). I might not be the person I am today without your unconditional love, support and inspiration. I am indebted to my parents for their time, efforts and belief in me. I also thank my brother S. Iqbal Singh and bhabhi Sdn. Kawaljeet Kaur for their co-operation and help to achieve this goal. Feeling gratitude towards my in-laws Sdn. Manjit Kaur and S. Gurmeet Singh, for their continuous support to make this end possible. I highly appreciate the joyful company of Gudiya, Priya, Money, Harpreet, Hardeep and Amandeep. You people always made me feel special and motivated me to accomplish this task. I really enjoyed and cherished the moments spent with my nephew Agamroop Singh. His smiling and cute face and enthusiasm for playing and dancing refreshed my mind during the frustrating hours of my doctorate degree.

Finally, I owe so much to my husband S. Rajbir Singh, whose love, patience, and understanding made the final finishing of the thesis a lot more easier and paved the way to achieve this academic goal. I am grateful to him for his everlasting support and motivation towards this end. I thank you to make me realize that how meaningful and beautiful my life is.

The financial assistance from Department of Science and Technology (DST) and then from University Grants Commission (UGC), New Delhi, under the "Maulana Azad National Fellowship For Minority Students Scheme" is gratefully acknowledged.

Mandeep Kaur

Patiala

May, 2016.

(Mandeep Kaur)

List of Publications :

A. Journals :

1. Dependence of the energy of vanishing flow on different components of the nuclear potential.
   Mandeep Kaur, Varinderjit Kaur and Suneel Kumar,
   Phys. Rev. C **88**, 054620 (2013).

2. Study of various potentials in heavy-ion collisions at intermediate energies.
   Varinderjit Kaur, Mandeep Kaur and Suneel Kumar,
   Nucl. Data Sheets **118**, 333 (2014).

3. On the momentum distribution of particles participating in nuclear stopping.
   Mandeep Kaur and Suneel Kumar,
   Pramana J. Phys. **84**, 101 (2015).

4. Contribution of different components of interaction potential towards the global nuclear stopping.
   Mandeep Kaur and Suneel Kumar,
   Indian J. Phys. **89** (9), 967-972 (2015).

5. Rapidity dependence of fragment production: Role of various components of NN potential.
   Mandeep Kaur, Manpreet Kaur, Varinderjit Kaur and Suneel Kumar,
   (To be submitted).

6. Effect of isospin dependent spatial and momentum constraints on transverse flow.
   Mandeep Kaur, Kamaldeep Kaur and Suneel Kumar,
   (To be submitted).

B. Symposia/Workshops/Conferences:

7. Role of momentum dependent interactions in nuclear stopping.
   Mandeep Kaur, Sanjeev Kumar and Suneel Kumar,
   Proceedings of the DAE Symp. on Nucl. Phys. **55**, 498 (2010).

8. N/Z dependence of nuclear stopping for Ca isotopes.
   Mandeep Kaur and Suneel Kumar,
   Proceedings of the DAE Symp. on Nucl. Phys. **56**, 800 (2011).

9. Effect of different potentials on anisotropic flow.
   Mandeep Kaur, Varinderjit Kaur and Suneel Kumar,
   Proceedings of the DAE Symp. on Nucl. Phys. **57**, 710 (2012).

10. Momentum distribution of particles participating in nuclear stopping.
    Mandeep Kaur and Suneel Kumar,
    Proceedings of the DAE Symp. on Nucl. Phys. **58**, 312 (2013).

11. Effect of isospin dependent spatial correlation on clusterization.
    Mandeep Kaur and Suneel Kumar,
    Proceedings of 75 years of Nuclear Fission, BARC, Mumbai p.50 (2014).

12. Effect of isospin-dependent spatial and momentum constraints on flow.
    Kamaldeep Kaur, Mandeep Kaur and Suneel Kumar,
    Zakopane Conference on Nuclear Physics, p.193 Sep. (2014).

13. Phase space analysis of nuclear stopping due to fragments.
    Mandeep Kaur, Kamaldeep Kaur and Suneel Kumar,
    Proceedings of the DAE Symp. on Nucl. Phys. **59**, 444 (2014).

Contents

List of Figures

List of Tables

ABSTRACT

The present study sheds light on the theoretical aspects of equation of state of nuclear matter by studying the influence of various components of interaction potential as well as nucleon-nucleon cross section on the critical observables of heavy-ion collisions such as collective flow, nuclear stopping and multifragmentation. The dynamic microscopic theory- *Isospin-dependent Quantum Molecular Dynamics* (IQMD) model is used to carry out the present study.

Chapter 1 describes the general introduction of the nuclear physics. The importance of heavy-ion collisions at intermediate energy regime to understand the reaction dynamics under extreme conditions is discussed. The dynamics of mass symmetric and mass asymmetric heavy-ion collisions is described. It also outlines the various observables to study the equation of state in the aforesaid energy regime such as collective flow, nuclear stopping and multifragmentation followed by the theoretical and experimental review of these observables.

Chapter 2 presents a brief survey of various primary models used in the literature to study the reaction dynamics. The Isospin-dependent Quantum Molecular Dynamics model (IQMD) model used to carry out the present study is explained in detail. The secondary models (used to analyze the phase space generated by the primary model) such as Minimum Spanning Tree (MST), its updated versions MSTP, isoMST and GEMINI model are also discussed.

In **Chapter 3** the importance of various components of nucleon-nucleon interaction potential towards the transverse directed flow $\langle P_x^{dir} \rangle$ and $\langle P_x/A \rangle$ as well as their balance energies is discussed for the reactions ${}^{58}_{26}$Fe+${}^{58}_{26}$Fe, ${}^{58}_{28}$Ni+${}^{58}_{28}$Ni, ${}^{86}_{36}$Kr+${}^{93}_{41}$Nb and ${}^{197}_{79}$Au+${}^{197}_{79}$Au. The results of our calculations are also compared with the experimental measurements. Our calculations for the considered energy range clearly demonstrate the dominance of the Coulomb potential and momentum-dependent interactions over the other components of nuclear potential for the lighter colliding systems. The symmetry potential also contribute significantly in the collision of heavier nuclei. In addition, the directed transverse flow (v_1) of light fragments is studied for the semi-central collisions of the reaction ${}^{197}_{79}$Au+${}^{197}_{79}$Au at incident energy ranging between 40 and 250 MeV/nucleon. The cluster recognition

method is optimized by applying different isospin-dependent spatial and momentum constraints.

In **Chapter 4** the effect of isospin content as well as the contributions of various components of nucleon-nucleon interaction potential on stopping ratio of protons and neutrons for the reaction $^{120}_{50}$Sn+$^{120}_{50}$Sn is presented. It is observed that the momentum dependent interactions affect the nuclear stopping to a larger extent compared to the other components of the nucleon-nucleon interaction potential. The isospin-dependent nucleon-nucleon cross section is also found to affect the stopping in central heavy-ion collisions. The momentum distribution of particles participating in nuclear stopping to get a better insight into the stopping of various charged fragments is also investigated. The comparison of measured and calculated values of stopping for protons reveals the significance of these constraints. Maximum stopping is obtained for the particles lying in the lowest range of the momentum distribution at all incident energies.

In **Chapter 5** the importance of various components of nucleon-nucleon interaction potential in the fragment production within different rapidity domains for the central collisions of the reactions $^{120}_{50}$Sn+$^{120}_{50}$Sn , $^{82}_{36}$Kr+$^{158}_{64}$Gd, $^{56}_{26}$Fe+$^{184}_{74}$W, $^{35}_{17}$Cl+$^{205}_{81}$Tl at incident energy ranging between 50 and 110 MeV/nucleon is investigated. Moreover, the role of different components of nucleon-nucleon interaction potential with increase in mass asymmetry is also explored by keeping the total mass of the system fixed. The charge distribution of fragments under the influence of various sets of components of interaction potential is also investigated and the results are compared with the experimental data for symmetric reactions.

Chapter 6 describes the conclusions and significance of the work done in this thesis along with the prospect for the extension of present work.

Chapter 1

Introduction

" The important thing is not to stop questioning. Curiosity has its own reason for existing"..............Albert Einstein

1.1 Introduction

Nuclear physics was originated as a scientific discipline with the unintentional discovery of radioactivity by H. Becquerel in 1896 [1]. Soon after this a series of brilliant experiments were performed nearly spontaneously leading to the discovery of fundamental particles and interactions between them [2–4]. For instance, nucleus as a heavy centre of the atom was discovered by E. Rutherford in 1911 [2]. The field of nuclear physics comprises of various phenomena covering a broad span; from the interactions of elementary particles, the foundation of nuclear reactions, to the structure of universe. The impact of nuclear physics extends well beyond the understanding of structure and properties of nucleus. It has benefited the society through many innovative applications in nuclear medicine, national security, nuclear power generation, climate research and agriculture, etc. Fig. 1.1 illustrates different ways through which nuclear physics enters our world. The rare natural happenings in the universe such as supernovae explosion, neutron stars, big-bang, and the evolution of life on earth is still a question of open debate. Unfortunately, these phenomena are inaccessible in the space and time to be used for the investigation of reaction dynamics under the extreme conditions of nuclear density, temperature and pressure. Various theoretical models have also been developed for the understanding of properties of atomic nuclei, its structure, nuclear interactions as well as the laws governing the nuclear interactions [5–9]. Bethe-Weizsäcker mass formula based on Liquid drop model

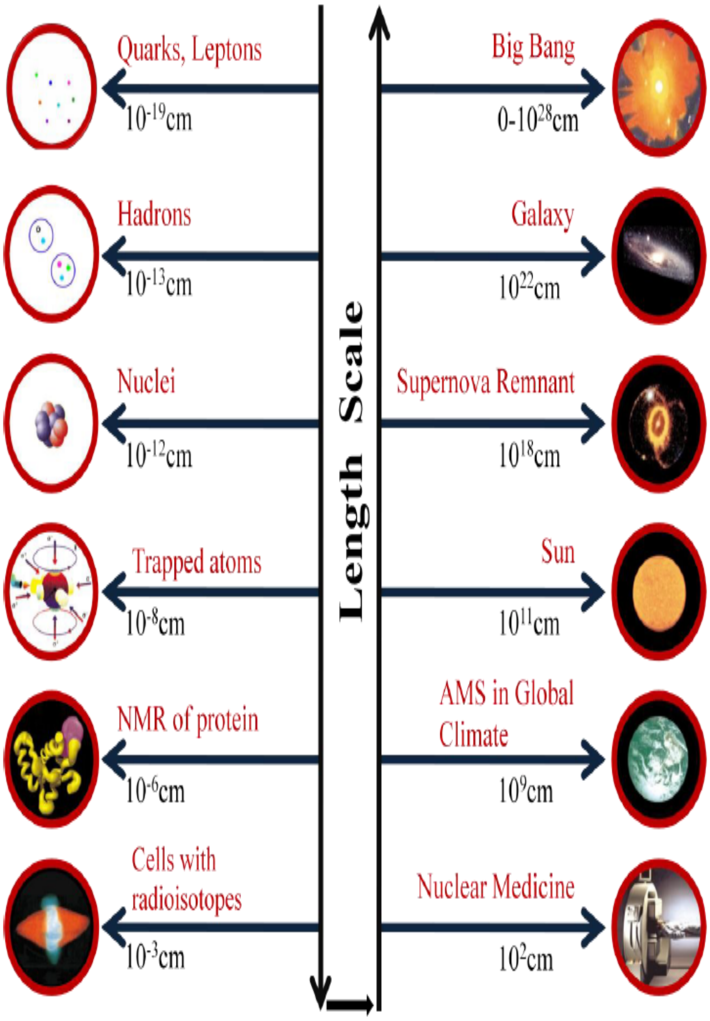

Figure 1.1: An illustration of various channels in which nuclear physics enters into our world. Figure is taken from Ref. [10].

[5] was the pioneer to provide the simplest but powerful theoretical description of the average properties of nuclei. Bethe-Weizsäcker mass formula for calculating the binding energies of nuclei involve the contributions from volume term, surface term, Coulomb term, asymmetry term as well as the pairing term. Mathematically, the binding energy is given by the formula:

$$B(A,Z) = a_v A - a_s A^{2/3} - a_c Z(Z-1)A^{-1/3} - a_a \frac{(A-2Z)^2}{A} + \delta a_p A^{-3/4} \tag{1.1}$$

Here, A and Z are the mass and charge of a nucleus. The binding energy for symmetric nuclear matter (N = Z) in the absence of surface and Coulomb interactions is found to be about -16 MeV corresponding to normal nuclear matter density (ρ_0)=0.17 fm^{-3}. The constants in Eq. 1.1 are experimentally determined fitting parameters and the values of a_s, a_c and a_a are 17.804 MeV, 0.7103 MeV and 23.69 MeV, respectively [11]. The predicted binding energies along with the observed ones are shown in Fig. 1.2. The figure reveals the importance of various terms involved in the Weizsäcker mass formula. The contribution of various terms lead to lower the binding energy for large value of mass (A). Later on, Malik

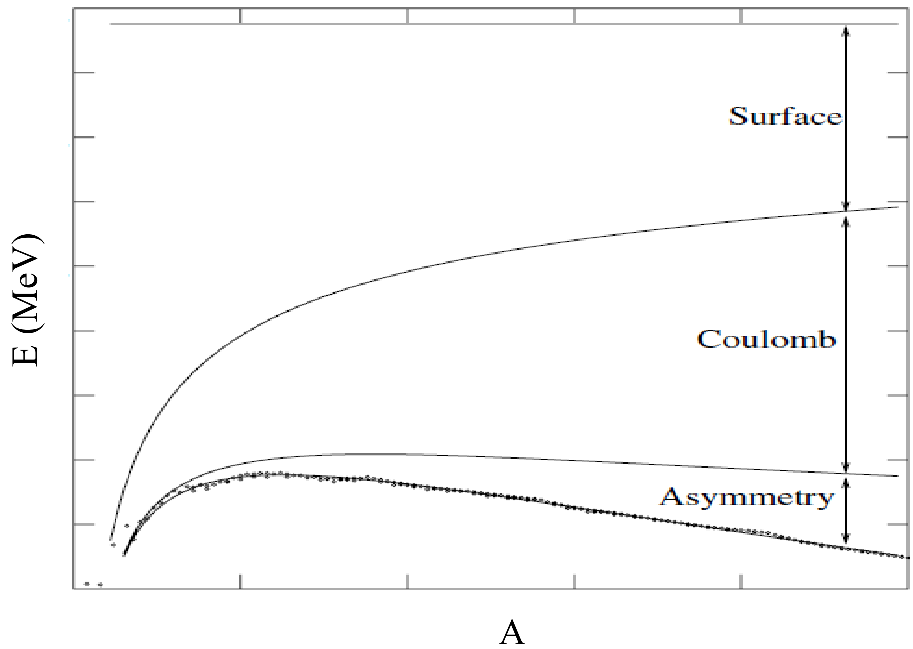

Figure 1.2: The predictions of mass formula and observed binding energies as a function of A. Only even-odd combinations of A and Z are considered where the pairing term of mass formula vanishes. Figure is taken from Ref. [11].

et al. [7], proposed a model for the mechanism of cluster formation and tunneling of nuclear interaction barrier for a radioactive nuclei. Rath *et al.* [8], investigated the complete fusion excitation function at near barrier energies. Similarly, the structure of nucleon self-energy in nuclear matter is investigated by using various realistic models [9]. These models are very useful to describe the low density (E $\leq$ 10 MeV/nucleon) phenomena such as fission, fusion, cluster-radioactivity, and formation of super-heavy nuclei, etc. On the other hand, the main interest to study the high energy (E $>$ 2 GeV/nucleon) heavy-ion collisions is to leap into the unexplored space of quark-gluon plasma [12]. However, at intermediate energies (10 MeV/nucleon $<$E $\leq$ 2 GeV/nucleon), various interesting observable phenomena emerged such as collective flow, nuclear stopping, subthreshold particle production and multifragmentation [13–19]. Heavy-ion (A $\geq$ 4) collisions in this energy regime offer a virtual ground for the investigation of hot and dense nuclear matter under the extreme conditions of thermodynamic variables such as temperature, pressure and density. The relationship between these thermodynamic variables is well known as nuclear matter equation of state (EOS). The knowledge of EOS of nuclear matter is of considerable interest to study different phases of nuclear matter as well as their possible phase transitions occurring at densities other than the normal nuclear matter density (ρ_0). Fig. 1.3 displays the nuclear matter phase diagram in terms of temperature and density. Low temperature and density corresponds to the liquid phase of nuclear matter. However, the nuclear matter in the form of quark-gluon plasma is supposed to exist under extreme conditions of temperature and density. At low density and high temperature, hadron gas is formed and towards the low temperature and high density, condensed phase of nuclear matter is observed. Interestingly, the liquid-gas phase transition of phase diagram extends

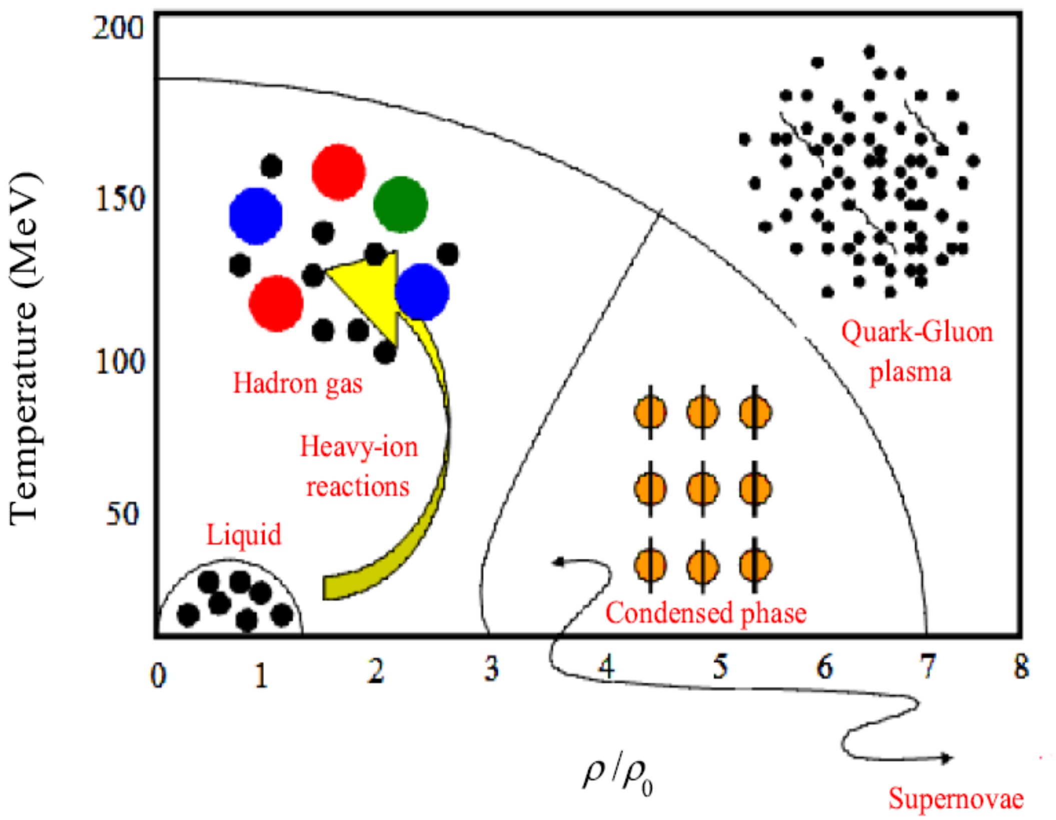

Figure 1.3: Schematic phase diagram in terms of temperature and scaled density (ρ/ρ_0). Figure is taken from Ref. [13].

over a wide range of temperature and density and hides a variety of phenomena in itself. The major phenomena are multifragmentation, nuclear stopping and anisotropic flow. It becomes very difficult to generate this kind of high temperature and pressure situation in real world, but can be studied by simulated heavy-ion collisions theoretically. The study of these phenomena using heavy-ion collisions of mass symmetric reactions is common and studied in literature extensively. However, to understand the mechanism of these phenomena for asymmetric nuclear matter is a challenge till date. Our main focus in this thesis will be to study the nuclear equation of state of nuclear matter using heavy-ion collisions of mass symmetric and mass asymmetric reaction systems.

1.2 Equation of state of symmetric nuclear matter

The equation of state of infinite nuclear matter describes its global properties by studying the relationship between three thermodynamical variables, the density, temperature and pressure. In nuclear physics, one generally uses energy/nucleon (E/A) to pin down the behaviour of matter as a function of density. Incompressibility or compression modulus (K), the key parameter (or the characteristic property of nuclear matter) to extract information about the EOS is given by the relation:

$$K = 9\left[\frac{d}{d\rho}\left(\rho^2\frac{\partial(E/A)}{\partial\rho}\right)\right]_{\rho=\rho_0}, \tag{1.2}$$

Here, E/A is the energy per particle at normal nuclear matter density ρ_0 . Fig. 1.4 indicates two possible EOS (soft with K= 200 MeV and hard with K=380 MeV) corresponding to two different incompressibilities. Normally, the nuclear matter is assumed to be symmetric (N=Z). However, for asymmetric nuclear matter (N$\neq$Z), due to unequal isospin content, the symmetry energy term contribute significantly. Therefore, the isospin dependent nuclear EOS of asymmetric nuclear matter is of utmost importance as it help us to understand the heavy-ion collisions by treating the isospin degree of freedom explicitly. The study of isospin dependent nuclear EOS is crucial to understand a large variety of astrophysical phenomena, involving widely different scales of space and time. The pursuit of investigations like internal structure, maximum mass, maximum radii and moments of inertia of neutron stars has made this field very fascinating [20]. Just like asymmetric nuclear matter, mass asymmetric reactions also play an important role to understand various aspects of heavy-ion collisions. A brief review of mass symmetric and asymmetric reactions has been provided in the following section.

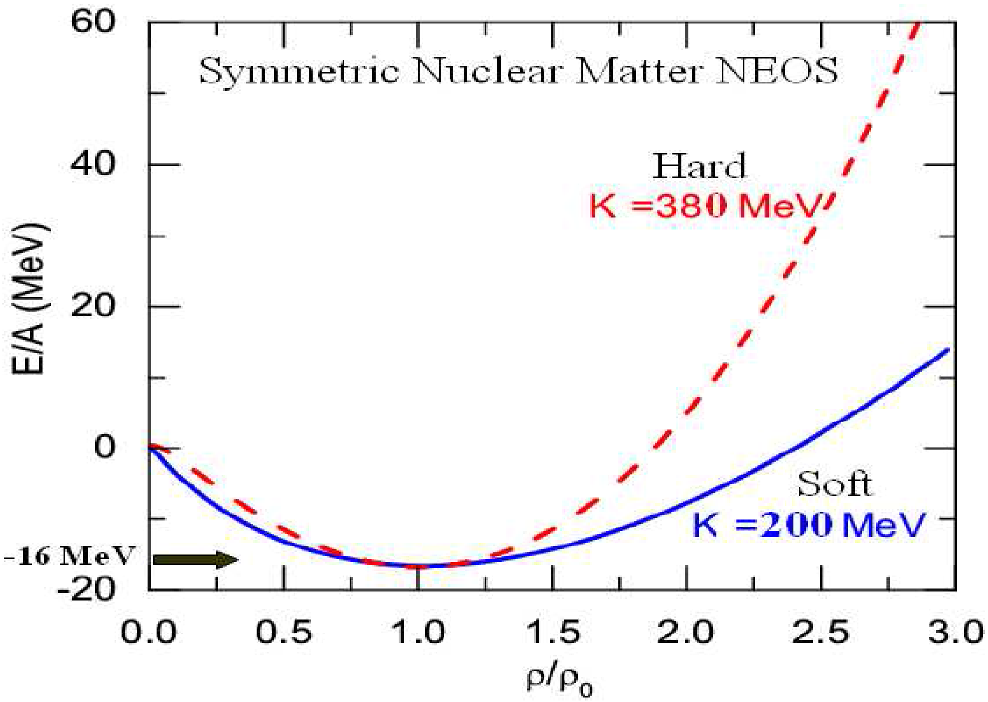

Figure 1.4: Hard and Soft EOS in terms of density dependence of energy per nucleon. Figure is taken from Ref. [13].

1.3 Dynamics of mass symmetric and mass asymmetric heavy-ion collisions

The theoretical and experimental attempts carried out for the investigation of heavy-ion collisions has divided it into two categories, namely, the mass symmetric and mass asymmetric heavy-ion collisions. Fig. 1.5 shows the snapshot of phase space in Z-X plane for the central collision of mass symmetric and mass asymmetric heavy-ion collision. In symmetric heavy-ion collisions, the number of nucleons in both target and projectile are same (or nearly same), however, in case of asymmetric heavy-ion collisions, the number of nucleons in projectile and target are quite different. Various physical quantities such as excitation energy, colliding geometry, equation of state and nucleon-nucleon (NN) cross section affect the outcome of a reaction. It is worth mentioning that both types of reactions respond in a quite different manner under the similar conditions of these physical ingredients. It is well known that the reaction dynamics at intermediate energy regime depends strongly on the mass asymmetry of the reaction, which is defined by the parameter $\eta = |\frac{A_T - A_P}{A_T + A_P}|$ [21]; where, A_T and A_P are the masses of target and projectile,

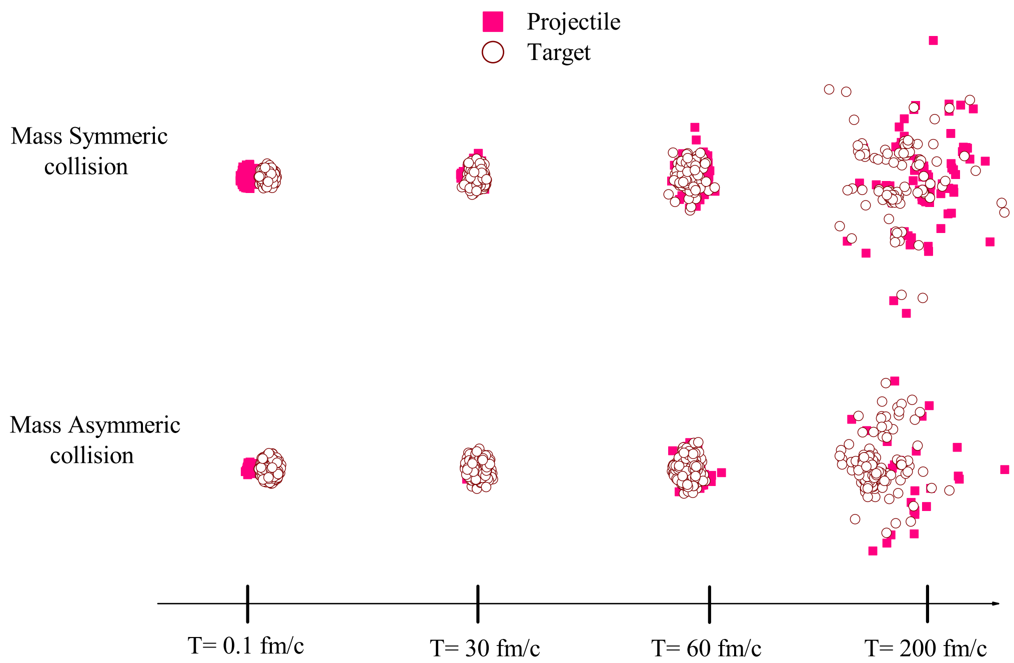

Figure 1.5: Snapshot of mass symmetric and mass asymmetric heavy-ion collision at different time steps.

respectively. In asymmetric collisions, the system is compressed to a quite small extent, as a result the energy dumped into the system is stored in the form of thermal energy. However, this is not the case for the symmetric collisions. In symmetric collisions, due to violent nucleon-nucleon collisions in relatively large participant zone, the average density of the system in the compression zone increases considerably. Thus the energy is stored in the system as compressional energy, which can be found in the fast radial expansion of the system at the later stage of the reaction. Figure 1.6 shows the density evolution for the central collision of a mass symmetric and mass asymmetric heavy-ion collision at three different incident energies. One can clearly see that in case of mass symmetric collisions, highly compressed matter is formed which expands faster at the later stage of the reaction as compared to the mass asymmetric collisions.

Lot of studies are available in the literature to study the influence of these physical conditions on various interesting observables such as collective flow, nuclear stopping and multifragmentation at intermediate energy regime by taking into account the symmetric collisions [22–25]. In contrast, very few are available which focus on asymmetric collisions [26–30]. The energy at which multifragmentation begins is found to increase with increase

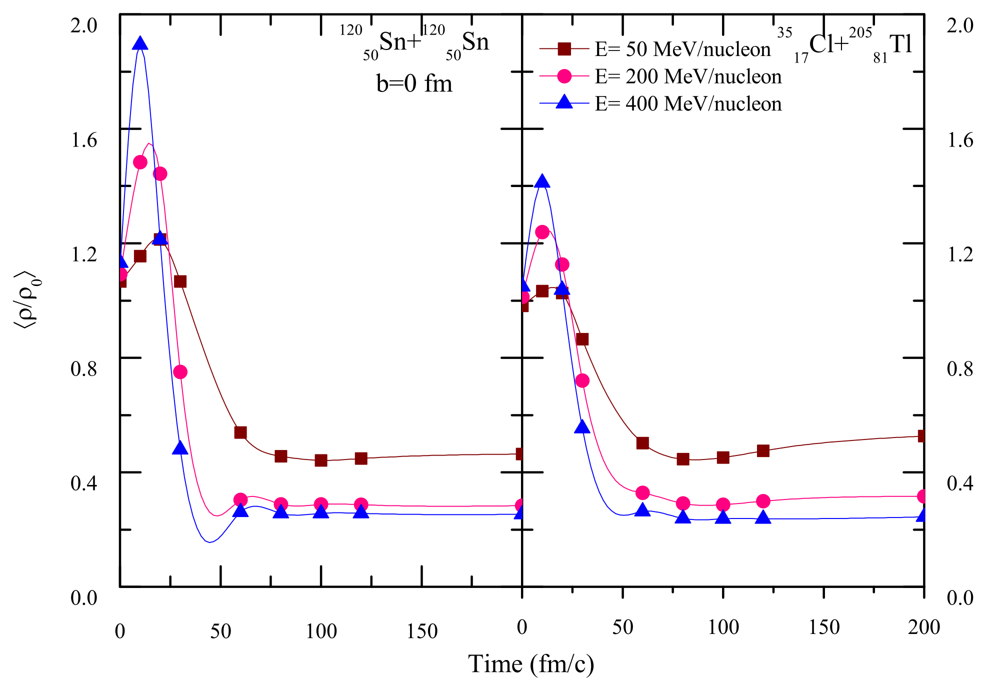

Figure 1.6: Density profile for central collision of mass symmetric (left) and mass asymmetric (right) reaction at different incident energies.

in mass asymmetry of the reaction [31]. Moreover, the results obtained for the central collision of asymmetric reaction are found to be comparable to that of symmetric reaction at peripheral colliding geometry. In order to get better insight into the influence of various physical ingredients on the reaction dynamics of heavy-ion collisions the observables like collective flow, nuclear stopping and multifragmentation have a significant role to play. It is worth noting that these observables also help us to extract the nuclear EOS under the extreme conditions of temperature, pressure and density. The aforementioned equation of state is attained by means of compression and thermalization achieved in heavy-ion reaction which consequently result into fragment production, collective flow and nuclear stopping respectively.

1.4 Phenomena occurring at intermediate energy regime

1.4.1 Collective flow

The azimuthal momentum distribution of particles emitted in a heavy-ion collision namely, the collective flow, is useful to understand properties of hot and dense nuclear matter. The compressed nuclear matter expands radially and anisotropically at the later stage of the reaction due to the pressure gradient generated depending on the colliding geometry. Radial expansion refers to the thermal motion of outgoing particles. On the other hand, the anisotropic expansion refers to the spatial orientation of particle momenta. The combined effect of both radial and anisotropic expansion is known as collective flow. The phrase "Collective" is meant by the common property of many ejectiles e.g. same velocity or same direction. For the central heavy-ion collisions, the pressure gradient is radially symmetric and boost the particles isotropically outward. This give rise to radial flow. However, the non-central collisions would result in anisotropic flow. Anisotropic flow is of various types, namely, directed flow, transverse flow, elliptic flow, triangular flow and higher order flows. These names refers to the shape of azimuthal distribution at midrapidity.

The **directed flow** takes place within the reaction plane (the plane that contains the beam axis and the line joining the centeriods of incoming nuclei) and hence also named as "in-plane" flow or "sidewards" flow. The emission of different fragments and particles are inclined preferably towards 0^o in the forward hemisphere and 180^o in the backward hemisphere in the reaction plane. Directed flow has been reported to be sensitive towards the various entrance channels such as mass of the system, colliding geometry as well as the incident energy of the projectile [14, 15, 22, 32–35]. Directed flow is maximum for the semi-central colliding geometries. On the other hand due to symmetry in central collisions and scarce pressure gradient in peripheral collisions the directed flow vanishes. Similarly, incident energy also affect the directed flow significantly. At low value of incident energy, the attractive part of nuclear mean field dominate the reaction dynamics and thereby deflect the fragments and nucleons towards the negative scattering angles. With increase in incident energy, the repulsive behaviour of nucleon-nucleon scattering becomes important. As a result, the nucleons are deflected towards the positive scattering angles. While going from lower to higher incident energy, the directed flow disappears at an incident energy, namely, the balance energy (E_{bal}), or energy of vanishing flow (EVF). Fig. 1.7 illustrates the schematics of directed flow at three different incident energies.

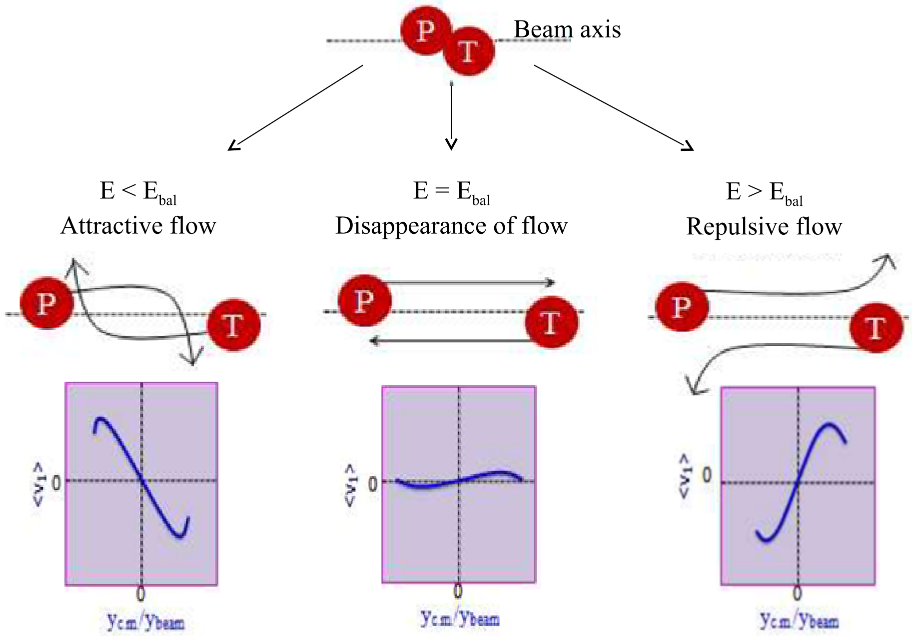

Figure 1.7: A pictorial representation of directed flow at three different incident energies.

There are several methods mentioned in literature to measure directed flow such as transverse momentum method [36], sphericity method [37], and particle pair correlation method [38]. The statistical fluctuation and finite size effects involved in the later two make these methods less preferred(hinder the use of these methods). However, the transverse momentum method is the widely used method to measure the directed flow over a wide range of incident energies. In this method, each particle is treated individually and reaction plane is determined by vector Q and Z (beam axis) direction. Here, Q is defined as $\vec{Q_i} = \sum_{j \neq i} \omega_j p_{j\perp}$ and the weight ω_j is supposed to be +1 and -1 for forward and backward centre-of-mass rapidity respectively. The spectators and participants are also separated on the basis of rapidity distribution. The statistical fluctuations and flow effects are distinguished by averaging over all events. In this method, the directed flow is measured by plotting the average transverse momentum per nucleon in the reaction plane

($\langle p_x/A\rangle = p\hat{Q}/A$) as a function of rapidity Y(i) [13].

$$Y(i) = \frac{1}{2}\ln\frac{E(i) + P_z(i)c}{E(i) - P_z(i)c} \tag{1.3}$$

where $E(i)$ and P_z are respectively, total energy and longitudinal momentum of i^{th} particle. The slope of the curve signifies the strength of directed flow.

One can also use a more integrated quantity known as directed transverse flow $\langle P_x^{dir}\rangle$), which is defined as

$$\langle P_x^{dir}\rangle = \frac{1}{A}\sum_i^A sign\{Y(i)\}P_x(i) \tag{1.4}$$

where $P_x(i)$ is transverse momentum of i^{th} particle along x direction and $Y(i)$ is the rapidity distribution. $\langle P_x^{dir}\rangle$ is defined over the entire rapidity region. In this definition, all the rapidity bins are taken into account in the measurement of $\langle P_x^{dir}\rangle$.

The distribution of emitted particles can also be characterized by the Fourier expansion of azimuthal distribution of particles with respect to the reaction plane [39].

$$\frac{dN}{d\phi} \propto [1 + 2\sum_{n=1}^{\infty} v_n\cos(n\phi)] \tag{1.5}$$

where ϕ is azimuthal angle between the transverse momentum of the particles and the reaction plane. In the coordinate system, we assume the beam axis along the Z-axis and the X-axis is labeled as impact parameter axis. The coefficients of Fourier expansion represent the order of flow. The first harmonic coefficient v_1 represents the transverse flow. Mathematically v_1 can be described as:

$$v_1 \ = \ \langle\cos\phi\rangle \ = \ \langle\frac{p_x}{p_t}\rangle \tag{1.6}$$

where p_x and p_y are the projection of particle transverse momentum parallel and perpendicular to the reaction plane respectively and $p_t = \sqrt{p_x^2 + p_y^2}$ is defined as transverse momentum. In the present thesis, we have concentrated on directed flow and transverse flow.

1.4.2 Nuclear Stopping

Collisions suffered by the nucleons of one nucleus with that of other nucleus are not independent of each other, rather, these collisions make this process a lot more complex phenomena. As a result of these collisions, the nucleons get slow down and transfer the initial longitudinal energy associated with them into transverse degree of freedom. During this process, a large part of energy is released in the overlapping region. This phenomena is well known as nuclear stopping. In other words, the amount of stopping determines the energy lost by the nucleon in a heavy-ion collision process. Different prospectives of nuclear stopping are shown in Fig. 1.8.

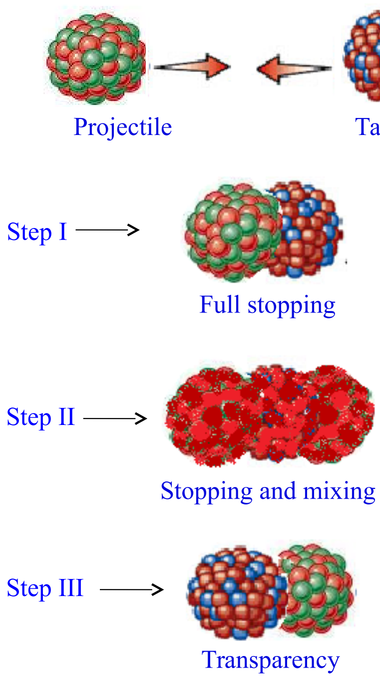

Figure 1.8: A schematic view of the movement of projectile and target.

The first one shows the case of full stopping, where the nucleons of target and projectile are repelled by each other just as two hard spheres. However, the second one "stopping and mixing" shows the complete memory loss due to breakage of correlations among the nucleons. In this case, the matter is highly compressed and the system is thermalized to a large extent. This case prevails at intermediate energy heavy-ion collisions. The third one shows "transparency" of nuclear matter, which is observed at very high values of incident energy. At such high energies, the cross section becomes very small and the nucleons of target and projectile just passes through each other without interacting with each other. This is in analogy with the large crowd of bees. Nuclear stopping depends on various entrance channels such as incident energy [40], colliding geometry [25], combined mass and asymmetry of colliding nuclei [26,41] as well as their orientation [42]. Nuclear stopping is also found to be sensitive towards different equation of states and nucleon-nucleon cross sections [43].

1.4.3 Multifragmentation

Nuclear multifragmentation is characterized by increasing excitation energy and expanding system volume. The collision of heavy-ions at intermediate energies produces hot and dense nuclear matter that disintegrate into large number of small, heavy and medium size pieces. Analysis of fragment production in heavy-ion collisions is very useful for better understanding of nuclear matter equation of state as well as the properties of hot and dense nuclear matter. The phenomena of nuclear multifragmentation takes place in three simple steps. The first step involves the formation of excited nuclear matter. In the second step, the excited nuclear matter undergoes expansion and thereby produces large number of free nucleons and fragments. These fragments are highly excited and immediately undergo de-excitation into cold and stable fragments at the final stage of this process. Fig. 1.9 shows a typical sketch of multifragmentation.

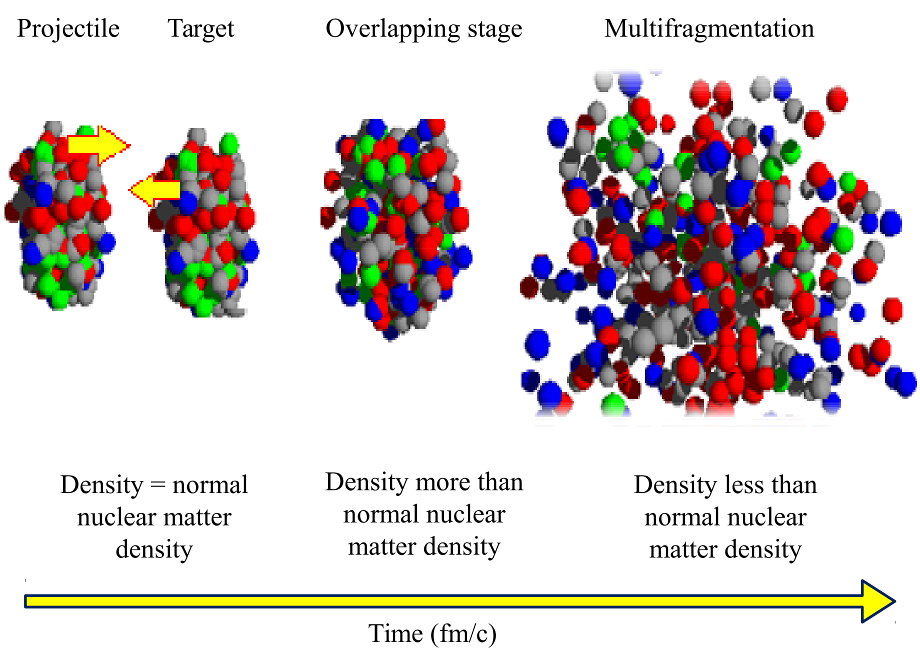

Figure 1.9: A schematic representation of nuclear multifragmentation process.

There have been considerable progress in the field of heavy-ion collisions to study nuclear multifragmentation, both theoretically as well as experimentally. Studies revealed that just like collective flow and nuclear stopping, multifragmentation also depends on various entrance channels like incident energy [19, 44], impact parameter [45, 46], mass of colliding systems [47] and mass asymmetry of the reaction [27–30]. For multifragmentation to occur, the impact parameter should be small and the incident energy is required to be large enough to ensure sufficient deposition of energy onto the target nucleus.

1.5 Review of theoretical studies in heavy-ion collisions at intermediate energies

Heavy-ion collisions at intermediate energy regime provide us the possibility to look for nuclear dynamics and nuclear properties via anisotropic flows, nuclear stopping and multifragmentation. It offers better understanding of the well known equation of state of nuclear matter. The total interaction potential of a heavy-ion collision is a combination of Skyrme potential, Yukawa potential, Coulomb potential, momentum dependent potential and symmetry potential. Nucleon-nucleon interaction potential can be reduced to density dependence. Therefore, nuclear EOS, which depends upon density, can be better understood through the variation of these interaction potentials. The variation of these potentials affect the nuclear EOS. However, the order of including these potentials does not affect the final result. Since last twenty years or so, nuclear physicists have made considerable progress to understand the role of various components of nucleon-nucleon interaction potential through anisotropic flow, nuclear stopping and multifragmentation. A brief review of these attempts is given below.

1.5.1 Theoretical attempts to study anisotropic flow

As mentioned earlier, the investigation of anisotropic flow on various observables has revealed much interesting physics. Detailed theoretical studies have shown that the strength of transverse flow and the balance energy can provide better insight into the nuclear equation of state as well as nucleon-nucleon cross section. Li *et al.* [48] have studied the isospin dependence of collective flow for the reactions $^{48}_{20}$Ca+ $^{58}_{26}$Fe and $^{48}_{24}$Cr+ $^{58}_{28}$Ni within the framework of isospin-dependent Boltzmann-Uehling-Uhlenbeck (IBUU) model [49]. The isospin effects have been explained in terms of competition between various mechanisms, such as Coulomb energy, symmetry energy, nucleon-nucleon cross section, the surface properties of colliding nuclei and so on. The neutron-rich system is found to show significantly stronger negative deflection and has higher balance energy. Similar conclusions are obtained by Chen *et al.* [50] by studying the flow of different fragments for the reactions $^{58}_{26}$Fe+$^{58}_{26}$Fe and $^{58}_{28}$Ni+$^{58}_{28}$Ni at 55 MeV/nucleon. The importance of momentum dependent interactions (MDI) towards the anisotropic flow has been studied widely [51–59]. The flow value is found to be higher in case of soft momentum dependent (SMD) EOS compared to hard EOS for the reactions $^{93}_{41}$Nb+$^{93}_{41}$Nb and $^{40}_{20}$Ca+$^{40}_{20}$Ca at 400 MeV/nucleon [51,52]. However, Peilert *et al.* [53] have shown an entirely contradictory conclusion for the reaction $^{197}_{79}$Au+ $^{197}_{79}$Au at 400 and 800 MeV/nucleon. Sood *et al.* [54] have studied the role of momentum dependent interactions in transverse flow as well as its disappearance for central heavy-ion collisions over a wide range of masses from 24 to 394 and found that the inclusion of momentum dependent interactions explains the EVF for $^{12}_{6}$C+$^{12}_{6}$C, which otherwise was not possible with static hard EOS. Jain *et al.* [55] reported the significance of momentum dependent interactions and nucleon-nucleon cross section on neutron-proton directed flow for the reactions $^{40}_{20}$Ca+$^{40}_{20}$Ca, $^{58}_{28}$Ni+$^{58}_{28}$Ni, $^{101}_{44}$Ru+$^{101}_{44}$Ru, $^{124}_{50}$Sn+ $^{124}_{50}$Sn, $^{124}_{47}$Ag+$^{124}_{47}$Ag and $^{197}_{79}$Au+ $^{197}_{79}$Au. Di Toro *et al.* [56] investigated the neutron-proton transverse flow and elliptic flow for the reaction $^{124}_{50}$Sn+ $^{124}_{50}$Sn at an incident energy 1.5 GeV/nucleon. Both are found to be sensitive towards the symmetry energy. In addition to transverse and elliptic flow, the neutron-proton and t/^{3}He relative and differential flows are found to be sensitive towards the symmetry potential [57–59]. However, the radial flows are found to be independent of symmetry potential. Gautam *et al.* [60] have studied the effect of symmetry energy and its density dependence on flow and balance energy. The directed and elliptical flow of light fragments (n, p, $^{2}_{1}$H, $^{3}_{1}$H, $^{3}_{2}$He, $^{4}_{2}$He etc.) in $^{197}_{79}$Au+ $^{197}_{79}$Au is studied by introducing Skyrme potential energy density functional within the framework of UrQMD model at 150, 250 and 400 MeV/nucleon [61]. Recently, Bansal *et al.* [62] have studied the role of momentum dependent equation of state on directed flow and its disappearance. The dominant behaviour of Coulomb interaction in superheavy mass region has also been studied [63]. These studies indicate that a lot of work has been done to explain the anisotropic flows by studying the interplay between various potentials in heavy-ion collisions, but the relative importance among these is not yet clear. So, in the present work, we aim to look in detail the role of various components of nucleon-nucleon potential.

1.5.2 Theoretical attempts to study nuclear stopping

Numerous attempts do exist in the literature, indicating the role of various model ingredients in nuclear stopping. Here, some of the efforts are described briefly. Liu *et al.* [64] have studied the nuclear stopping for the reactions ^{20}Ne+ ^{20}Ne, ^{40}Ar+^{40}Ar, ^{80}Zn+^{80}Zn, ^{112}Sn+^{112}Sn, and ^{124}Sn+^{124}Sn at different beam energies ranging from 15 to 150 MeV/nucleon. The isospin effects are investigated by varying the neutron-proton ratio of colliding systems. The study revealed that nuclear stopping is sensitive towards the NN cross section but is insensitive to symmetry potential. Similar predictions were also made in Ref. [65, 66]. Later on, the isospin effects in terms of Coulomb and symmetry potential are investigated for the reactions ^{94}Kr+^{94}Kr, ^{94}Zr+^{94}Zr, ^{94}Mo+^{94}Mo and ^{94}Ru+^{94}Ru, ^{64}Fe+^{64}Fe, ^{89}Kr+^{89}Kr and ^{124}Sn+^{124}Sn at an incident energy of 50 MeV/nucleon. The Coulomb interaction is found to reduce the nuclear stopping and again, no sensitivity has been reported towards the symmetry potential [67, 68]. The sensitivity of momentum dependent interactions on nuclear stopping has been studied by Kumar *et al.* [69] for the reaction $^{40}_{20}$Ca + $^{40}_{20}$Ca, $^{58}_{28}$Ni + $^{58}_{28}$Ni, $^{93}_{41}$Nb + $^{93}_{41}$Nb, $^{131}_{54}$Xe + $^{131}_{54}$Xe and $^{197}_{79}$Au +$^{197}_{79}$Au over a wide range of incident energies at central and semi-central colliding geometries. The momentum dependent interactions are found to weaken the finite size effects in nuclear stopping. The sensitivity of nuclear stopping towards the different equation of state as well as nucleon-nucleon cross sections in different energy regimes has also been studied [70, 71]. Recently, Bansal *et al.* [72] have studied the nuclear stopping by varying the mass asymmetry of the reaction. The correlation between nuclear stopping and transverse flow has also been established.

1.5.3 Theoretical attempts to study multifragmentation

Numerous theoretical attempts have been made in the literature to study the nuclear multifragmentation. Few of them are briefly reviewed here. Zhang *et al.* [73] studied the isospin effects in fragmentation for the reactions ^{112,124} Sn+ ^{112,124} Sn at an incident energy 40 MeV/nucleon using IQMD model [74]. This model involves explicitly the Coulomb interaction, isospin-dependent symmetry potential and NN cross section to account for the isospin degree of freedom. The study revealed different scalings of intermediate mass fragments with the number of neutrons and charged particles between the two reacting systems. The neutron-rich system is found to emit more pre-equilibrium neutrons and less charged particles. Similarly, Liu *et al.* [67, 75, 76] studied the isospin effects for the reactions ^{76} Zn+ ^{40} Ar, ^{76} Kr+ ^{40} Ca and ^{120} Xe+ ^{40} Ca, ^{120} Cd+ ^{40} Ar at 100 MeV/nucleon and found that neutron-poor system leads to large number of IMF's compared to the neutron-rich systems. The study was further advanced to investigate the effect of Coulomb interaction and symmetry potential separately for various reactions. They found that the Coulomb interaction induces a reduction in isospin fractionation ratio (the isospin ratio of gas to liquid phase). On the other hand, the symmetry potential enhances the same. The interplay between Coulomb and symmetry potential results in reduced isospin fractionation ratio [67]. This ratio increases with increase in N/Z ratio of the system and decreases with increase in mass of the system irrespective of Coulomb interaction. Li *et al.* [77] have investigated the influence of nuclear finite-size effect on the formation and stability of fragments for the reactions ^{40} Ca+ ^{40} Ca, ^{197} Au+ ^{197} Au and ^{120} Xe+ ^{129} Sn by using improved QMD model [13] and found that the surface energy term strongly affect the stability of nuclear system as well as the yield of fragments at incident energies of a few MeV/nucleon to several tens of MeV/nucleon. Recently, Wu *et al.* [78] have discussed the competition between Coulomb and symmetry potential for the asymmetric reaction ^{40} Ar+^{197} Au at incident energies 35, 50 and 100 MeV/nucleon. Their study revealed that the competition between Coulomb and symmetry potential affect the free nucleons and light charged particles emission in the target and projectile region. In addition to this, the influence of symmetry energy at both subsaturation and supersaturation densities has been investigated by means of various observables such as isospin-diffusion, neutron to proton double ratio, light charged particles flow and giant dipole resonances etc. The momentum dependent interactions are also found to play an important role in multifragmentation [79–82]. The momentum dependent interactions strongly influence the fragment production at peripheral colliding geometries and the momentum fluctuations are useful in determining the symmetry energy in neutron/proton rich systems. With the inclusion of MDI's, the particle production is found to be reduced drastically. However, the kaon production is reduced by a factor of four by taking into account the MDI's

[13]. Recently, Imal *et al.* [83] have studied the production cross section and isotopic yield distributions of projectilelike residues in the reactions $^{112}_{50}$Sn+$^{112}_{50}$Sn and $^{124}_{50}$Sn+$^{124}_{50}$Sn by using statistical multifragmentation model (SMM). Zheng *et al.* [84] have studied the deexcitation of an excited nucleus by using Gemini model. They found that the momentum fluctuation temperature shifts down due to sequential decay. Similar results are also found in Ref. [85].

1.6 Review of experimental facilities

Many experimental efforts have been made to acquire the data for better understanding of nature and natural phenomena. Earlier, the natural accelerators available to the mankind was cosmic rays. Cosmic rays consist of 85% protons, 14% He like atoms and less than 1% are the heavier elements such as C or O [86]. It was realized later that different mass component of cosmic rays lead to different energy. But exclusive experiments needs only fixed energy as well as a fixed mass. The only possibility to achieve this was the accelerators. With the passage of time, it became possible to accelerate the heavier nuclei with the energy upto several hundred of GeV, which, at the earlier, was possible for the lighter nuclei only.

BEVALAC was the first accelerator made at the land of Berkley laboratory. The main motive behind the experiment was to get the theoretician and experimentalist aware of the problems and hazards of the way from medium energy heavy-ion collisions (HIC) to EOS. Later on several accelerators were built. Some of them are at : Michigan State University (USA), GANIL(France), Relativistic Heavy Ion collider (RHIC) (USA), Superconducting Supercollider (SSC) at BNL (USA), Superconducting Cyclotron (SC) at Texas (USA), superconducting cyclotron and CHIMARA detector at INFN, Catania (Italy), SIS accelerator at GSI (Germany) and Vivitron accelerator in Strasbourg (France), Superconducting Cyclotron (SC) facility and its updated version i.e. Radioactive Ion Beam (RIB) facility at Variable Energy Cyclotron Centre (VECC), Kolkata (India).

1.6.1 Experimental attempts to study anisotropic flow

The National Superconducting Cyclotron Laboratory (NSCL) at Michigan State University (MSU), USA is the pioneer to predict the isospin effects in collective transverse flow for the reactions of $^{58}_{26}$Fe+$^{58}_{26}$Fe and $^{58}_{28}$Ni+$^{58}_{28}$Ni at incident energy of 55 MeV/nucleon and found that neutron-rich system has exhibited larger flow (greater negative deflection) [87]. The energy of vanishing flow is also measured and neutron-rich system is found to have higher energy of vanishing flow at all measured impact parameters. The FOPI collaboration at GSI (Germany) measured the directed flow for the reactions $^{197}_{79}$Au+$^{197}_{79}$Au at incident energies ranging between 90 and 400 MeV/nucleon [88]. Similar study is also carried out by INDRA collaboration at GSI (Germany) for the reactions of $^{197}_{79}$Au+$^{197}_{79}$Au at 40 and 150 MeV/nucleon and measured the directed and elliptic flows [32]. FOPI collaboration have measured the neutron and proton transverse flows and found it to be sensitive towards symmetry energy [89]. Recently, FOPI collaboration also studied the central heavy-ion collisions for the reactions $^{40}_{20}$Ca+$^{40}_{20}$Ca, $^{58}_{28}$Ni+$^{58}_{28}$Ni, $^{96}_{44}$Ru+$^{96}_{44}$Ru, $^{96}_{40}$Zr+$^{96}_{40}$Zr, $^{129}_{54}$Xe+CsI and $^{197}_{79}$Au+$^{197}_{79}$Au at different incident energies ranging between 120 MeV/nucleon and 1.5 GeV/nucleon [90]. The transverse rapidity distribution and radial flow has been measured for all the reactions. Russotto *et al.* [91] defined the ratio of directed and elliptic flow of neutrons with respect to hydrogen isotopes for the reactions of $^{197}_{79}$Au+$^{197}_{79}$Au at 400 MeV/nucleon as a probe for symmetry energy. The results are compared with theoretical predictions of Ultra relativistic Quantum Molecular Dynamics (UrQMD) model. The NIMROD-ISiS (Neutron Ion Multiplicity for Reaction Oriented Dynamics with Indiana Silicon investigation Sphere) collaboration at Texas A & M University (TAMU) in USA is also working actively in this field. The transverse flow of fragments for the reactions of ^{70}Zn+^{70}Zn, $^{64}_{28}$Ni+$^{64}_{28}$Ni and ^{64}Zn+^{64}Zn at 35 MeV/nucleon is measured by Kohley *et al.* [92]. The measurements have shown that flow decreases with increase in the neutron content of a fragment. Moreover, the effects of mass, charge and isospin-dependent components are also studied. The increased production of the neutron-rich light charged particles (LCPs) in midrapidity region has also been reported. Recently, the experimental results are also compared with various models like Antisymmetrised Molecular Dynamics (AMD), Constrained Molecular Dynamics (CoMD) and Stochastic Mean Field (SMF) [93]. However, results vary with models, the good thing is that with every calculation, better agreement with the data with stiff form of the symmetry energy has been observed.

1.6.2 Experimental attempts to study nuclear stopping

Nuclear stopping can be viewed as the efficiency of converting the incoming longitudinal energy of colliding matter into other degrees of freedom in the course of reaction. Experimentally, nuclear stopping has been measured by FOPI collaboration for the systems $^{40}_{20}$Ca+$^{40}_{20}$Ca, $^{58}_{28}$Ni+$^{58}_{28}$Ni, $^{96}_{44}$Ru+$^{96}_{44}$Ru, $^{129}_{54}$Xe+CsI and $^{197}_{79}$Au+$^{197}_{79}$Au at incident energies ranging between 90 MeV/nucleon and 1930 MeV/nucleon [90]. The study revealed that for the heaviest system, a broad plateau extended from 200 to 800 MeV/nucleon corresponding to maximum stopping is observed [88, 90]. However, the situation is quite different in case of low energy domain (10 to 100 MeV/nucleon). Lehaut *et al.* [94] analyzed the same for the central collisions of symmetric and asymmetric reactions such as $^{197}_{79}$Au+$^{197}_{79}$Au, $^{129}_{54}$Xe+ $^{118}_{50}$Sn, $^{58}_{28}$Ni+$^{58}_{28}$Ni by using 4π multi-detector INDRA. Nuclear stopping was reported to be highly sensitive towards the isospin dependence of the in-medium nucleon-nucleon cross section. The study concluded that a minimal value of stopping occurs around 35 MeV/nucleon irrespective of the system size. Moreover, a rapid decrease in stopping as a function of incident energy was observed upto 40 MeV/nucleon. Recently, stopping ratio of protons has been measured by 4π array INDRA for central collisions of various reactions in the Fermi energy domain [95]. The relationship between stopping ratio and mean free path (λ_{NN}) of nucleons is established. Mean free path is found to have a maximum (λ_{NN} = 9.5 $\pm$ 2 fm) around 35 MeV/nucleon and decreases towards an asymptotic value (λ_{NN} = 4.5 $\pm$ 1 fm) at 100 MeV/nucleon. In addition to this, the in medium effects are also found to affect the nucleon-nucleon cross section significantly.

1.6.3 Experimental attempts to study multifragmentation

In 1930's the first experiment was performed by using cosmic rays as the projectiles and ionisation chambers and Geiger counters as detectors. As a result, slow nuclear fragments with their mass greater than the mass of α-particles, and lighter than those of fission fragments were emitted. These fragments were named as intermediate mass fragments (IMF's) ($3 \leq Z \leq 20$). Later on, the same was observed experimentally by Perfilov and Lozkin [96]. In 1982, Jakobsson *et al.* observed a multiple emission of IMF's in the emulsion irradiated by the carbon beam of 250 MeV/nucleon at Berkeley Bevalac [97]. This result developed new interest in nuclear physicists toward multifragmentation. Warwick *et al.* [98] found that for beam energies higher than 35 MeV/nucleon the reaction channel is dominated by nuclear multifragmentation. Studies carried out by Purdue University group [99] and Dubna group [100] revealed the importance of nuclear multifragmentation to get new insights into the problem of heavy-ion collisions such as phase transition and equation of state of nuclear matter. A number of sophisticated but complicated detectors including forward and 4π designs were created to study each and every aspect in detail. BEVALAC accelerator situated at Lawrence Berkeley Laboratory in California was the first to study the multifragmentation. After this attempt, various accelerators (mentioned earlier) have made good progress in the field of heavy-ion collisions to understand multifragmentation. The availability of new experimental facilities at Dubna, Brookhaven and CERN have made it possible to have a beam of ultra-relativistic energies. The Emulsion experiment [97, 101] provided the opportunity to study fission, multifragmentation, liquid-gas phase transition as well as vaporization at intermediate energies. The Berkeley group investigated the role of entrance-channel mass asymmetry for incident energy ranging between 50 and 110 MeV/nucleon [102–104]. The main focus was on different parameters like excitation energy, angular distribution, velocity distribution as well as cross section. The EOS collaboration at BEVALAC intent to study the phase transition in nuclear matter through the process of multifragmentation. Various critical exponents like surface energy, volume energy, symmetry energy and entropy etc. are extracted by taking into account the mass asymmetric sets of reactions [105]. Similar investigation for symmetric reaction of ${}^{197}_{79}$Au+${}^{197}_{79}$Au are also available in the literature [106]. The main focus of the National Superconducting Cyclotron Laboratory (NSCL) of Michigan State University (MSU) has been to study the asymmetric reactions like ${}^{129}_{54}$ Xe + ${}^{12}_{6}$C, ${}^{27}_{13}$Al, ${}^{51}_{23}$V , ${}^{64}_{29}$Cu, ${}^{89}_{39}$Y (50 MeV/nucleon), ${}^{36}_{18}$Ar + ${}^{197}_{79}$Au, ${}^{129}_{54}$Xe + ${}^{197}_{79}$Au (50-110 MeV/nucleon), ${}^{40}_{18}$Ar + ${}^{64}_{29}$Cu, ${}^{108}_{47}$ Ag, ${}^{197}_{79}$Au (at 17-115 MeV/nucleon) [107–109]. The major emphasis of the Superconducting Cyclotron of the Laboratori Nationali del Sud of INFN (Italy) is to explore some interesting facts about symmetric reactions of ${}^{93}_{41}$Nb + ${}^{93}_{41}$Nb (at 17, 23, 30 and 38 MeV/nucleon) and ${}^{116}_{50}$Sn + ${}^{116}_{50}$Sn (at 29.6, 38 MeV/nucleon) [110]. Recently, Isospin collaboration at INFN (Italy) studied the isospin effects for non-central collisions of neutron-rich $^{124}_{50}$Sn + $^{64}_{28}$Ni and neutron-deficient $^{112}_{50}$Sn + $^{68}_{28}$Ni systems at 35 MeV/nucleon [111]. The FOPI and ALADIN group at GSI performed a systematic study on multifragmentation over a wide range of masses with incident energies ranging from 100 to 1000 MeV/nucleon [45, 46, 112–117]. Experimental observations shed light on the particle evaporation to multi fragment emission and at last total disassembly and shattering of the nuclear matter after the reaction. ALADIN collaboration also described the most interesting phenomenon of multifragmentation i.e. the rise and fall in multiplicity for the reaction of $^{197}_{79}$Au+$^{197}_{79}$Au. The fragment multiplicities and correlations are found to obey universal behavior. The secondary beams have extended the domain of the study to isospin plane [118, 119]. The NIMROD collaboration at TAMU focuses on the reaction dynamics in Fermi energy domain of the HICs [120–123]. The multiplicity and charge distribution, energy and velocity spectra has been observed for the reactions of $^{64}_{30}$Zn + $^{58}_{28}$Ni (26 MeV/nucleon), $^{197}_{79}$Au (at 47 MeV/nucleon), $^{92}_{42}$Mo (at 35 and 47 MeV/nucleon), $^{40}_{18}$Ar + $^{112}_{50}$Sn (40 MeV/nucleon) and $^{27}_{13}$Al + $^{124}_{50}$Sn (at 55 MeV/nucleon) [121]. The EOS for isospin asymmetric nuclear matter has also been investigated by this collaboration [124]. An extensive analysis for the observables such as symmetry energy, isotropic and isobaric yield ratio, average N/Z ratio for the reactions of $^{124}_{50}$Sn + $^{124}_{50}$Sn, $^{124}_{54}$Xe + $^{124}_{50}$Sn, $^{112}_{50}$Sn + $^{112}_{50}$Sn at 28 MeV/nucleon has been performed [122, 124]. These properties are also studied by using different beams with projectiles $^{40}_{18}$Ar, $^{40}_{20}$Ca, $^{58}_{26}$Fe and $^{58}_{28}$Ni on $^{58}_{26}$Fe and $^{58}_{28}$Ni targets at 25, 30, 33, 40, 45, 47 and 53 MeV/nucleon [124, 125]. These findings revealed that the isotopic distribution of the hot primary fragments are found to vary over a wide range and are extended towards the neutron drip line. With the passage of time, the mass dependence of the nuclear caloric curve has also been reported [123]. The, INDRA group at GANIL (France) has also made remarkable achievements in the field of nuclear multifragmentation. This group mainly concentrate on the system size effects, the role of system size in entrance channel as well as Coulomb instabilities, kinetic energy spectra and fragment velocity correlation in case of nearly asymmetric reactions of $^{36}_{18}$Ar + $^{58}_{28}$Ni, $^{155}_{64}$ Gd + $^{238}_{92}$U and $^{129}_{54}$Xe + ^{nat}Sn (at 30-95 MeV/nucleon), $^{58}_{28}$Ni +$^{58}_{28}$Ni (32-90 MeV/nucleon), $^{208}_{82}$Pb + $^{197}_{79}$Au (at 29 MeV/nucleon) and $^{36}_{18}$Ar + KCl [29, 47, 126]. The entrance channel effects on the asymmetric reactions has been explored in the mass range 58 to 181 and beam energy between 24 to 90 MeV/nucleon [28]. In addition to this, the symmetric reaction of $^{197}_{79}$Au + $^{197}_{79}$Au for the excitation energy between 40 and 150 MeV/nucleon has also been studied by this group [44]. It is concluded that the shattering of the projectile into pieces results in the formation of fragments and the phenomenon is termed as multifragmentation [127]. The bimodal behavior of heaviest fragment distribution in the projectile fragmentation has also been investigated by ALADIN-INDRA collaboration [128]. It has also been observed that the isospin effect has a significant role at semi-peripheral collisions for the reaction $^{58}_{28}$Ni + $^{197}_{79}$Au at intermediate energies [129].

1.7 Organisation of thesis

Despite many efforts, the relative contribution of various components of nuclear potential such as Skyrme potential, Yukawa potential, Coulomb potential, momentum dependent interaction and symmetry potential towards the various promising observables of heavy-ion collisions at intermediate energy is not yet clear. Therefore, the main motive of the present work is to study the role of different components of nuclear potential on various observables such as multifragmentation, collective flow and nuclear stopping at intermediate energy regime. In addition to this, the study on the effect of various momentum constraints on flow of fragments and nuclear stopping is also included in the present work.

The thesis is organized as follow:

In **Chapter 2**, a brief survey of various primary and secondary models used in the literature to study the reaction dynamics has been presented. The Isospin-dependent Quantum Molecular Dynamics (IQMD) model used to carry out the present study is discussed in detail. The chapter is followed by explanation of various clusterization techniques.

In **Chapter 3**, the importance of various components of nucleon-nucleon interaction potential towards the transverse directed flow for the reactions $^{58}_{26}$Fe+$^{58}_{26}$Fe, $^{58}_{28}$Ni+$^{58}_{28}$Ni, $^{86}_{36}$Kr+$^{93}_{41}$Nb and $^{197}_{79}$Au+$^{197}_{79}$Au is discussed. Our results of extracted balance energies has been compared with the experimental data. In addition to this, the cluster recognition method has been optimized to study the directed flow of fragments for the reaction $^{197}_{79}$Au+$^{197}_{79}$Au.

In **Chapter 4**, a systematic study of nuclear stopping is presented by studying the role of various components of nucleon-nucleon interaction potential and nucleon-nucleon cross section for the reaction $^{120}_{50}$Sn+$^{120}_{50}$Sn for a wide range of incident energy and impact parameters. In addition to this, the momentum distribution of particles participating in nuclear stopping has been investigated to get a better insight into the stopping of various charge fragments. The results obtained are compared with the experimental findings of FOPI collaborations.

In **Chapter 5**, the importance of various components of nucleon-nucleon interaction potential towards multifragmentation is studied within different rapidity domains for the central collisions of the reactions $^{120}_{50}$Sn+$^{120}_{50}$Sn , $^{82}_{36}$Kr+$^{158}_{64}$Gd, $^{56}_{26}$Fe+$^{184}_{74}$W, $^{35}_{17}$Cl+$^{205}_{81}$Tl at incident energy ranging between 50 and 110 MeV/nucleon. Moreover, the role of different components of nucleon-nucleon interaction potential towards mass asymmetry is also explored by keeping the total mass of the system fixed. The results are compared with the experimental data for the symmetric collisions.

In **Chapter 6**, the results are concluded followed by an outlook of the work.

Bibliography

[1] H. Becquerel, Comptes Rendus **122**, 420421 (1896).

[2] E. Rutherford, Philosophical Magazine **21**, pp. 669-688 (1911); E. Rutherford, Philosophical Magazine, **24**, 669 (1912).

[3] J. Chadwick, Letter to editor, Nature **192**, 312 (1932); Proc. Roy. Soc. (London) **A136**, 692 (1932).

[4] O. Hahn, F. Strassmann, Naturewissenchaften **27**, 203 (1939); L.Meitner, O.R. Frisch, Nature **143**, 204 (1939).

[5] N. Bohr and J. Archibald Wheeler, Phys. Rev. **56**, 426 (1939).

[6] G.H. Bhat, J.A. Sheikh, Y. Sun, and U. Garg, Phys. Rev. C **86**, 047307 (2012).

[7] S.S. Malik and Raj K. Gupta, Phys. Rev. C **39** 1992 (1989).

[8] P.K. Rath, Phys. Rev. C **79**, 051601(R) (2007).

[9] T. Frick, Kh. Gad, and H. Müther, P. Czerski, Phys. Rev. C, **65**, 034321 (2002).

[10] G. Kaur, Ph.D. Thesis, Thapar University, Patiala (INDIA) (2015) (http://hdl.handle.net/10266/3779).

[11] J.L. Basdevant, J. Rich and M. Spiro, Fundamentals in nuclear physics,Springer, (2005).

[12] A. Bonasera, Phys. Rev. C **60**, 065212 (1999); S. Terranova and A.Bonasera, Phys. Rev. C **70** 024906 (2004).

[13] J. Aichelin, Phys. Rep. **202**, 233 (1991).

[14] G.D. Westfal *et al.*, Phys. Rev. Lett. **71**, 1986 (1993); D. Klakow, G. Welke, and W. Bauer, Phys. Rev. C **48**, 1982 (1993); M.J. Huang *et al.*, Phys. Rev. Lett. **77**, 3739 (1996).

[15] C.A. Ogilvie *et al.*, Phys. Rev. C **40**, 2592 (1989); B. Blattel *et al.*, *ibid.* **43**, 2728 (1991).

[16] J.C. Angelique *et al.*, Nucl. Phys. A **614**, 261 (1997); A. Andronic *et al.*, *ibid.* A **679**, 765 (2001).

[17] A.B. Larionov, W. Cassing, C. Greiner, and U. Mosel, Phys. Rev. C **62**, 064611 (2000).

[18] S. Kumar, S. Kumar, and R.K. Puri, Phys. Rev. C **81**, 014611 (2010).

[19] L. Phair *et al.*, Phys. Lett. B **285**, 10 (1992); M.B. Tsang *et al.*, Phys. Rev. Lett. **71**, 1502 (1993).

[20] J.M. Lattimer, M. Prakash, Science, **304**, 536 (2004); J.M. Lattimer, M. Prakash, Phys. Rep. **442**, 109-165 (2007).

[21] J. Maruhn and W. Greiner, Phys. Rev. Lett. **32**, 548 (1974).

[22] Q. Pan and P. Danielewicz, Phys. Rev. Lett. **70**, 2062 (1993); G.F. Bertsch, W. G. Lynch and M.B. Tsang, Phys. Lett. B **189**, 384 (1987).

[23] Y. Zhang, Z. Li, and P. Danielewicz, Phys. Rev. C **75**, 034615 (2007); L.W. Chen and C.M. Ko, Phys. Lett. B **634**, 205 (2006).

[24] W.J. Llope *et al.*, Phys. Rev. C **51**, 1325 (1995).

[25] G.E. Cooper, Nucl. Phys. A **661**, 362 (1999).

[26] V. Kaur, S. Kumar and R.K. Puri, Nucl. Phys. A **861**, 37 (2011).

[27] R. Sun *et al.*, Phys. Rev. C **61**, 061601 (2000).

[28] J. Colin *et al.*, Phys. Rev. **67**, 064603 (2003).

[29] J.D. Frankland *et al.*, Phys. Rev. C **71**, 034607 (2005); J.D. Frankland *et al.*, Nucl. Phys. A **689**, 940 (2001).

[30] S. Goyal, Phys. Rev. C **84**, 044614 (2011).

[31] J. Singh, Ph.D. Thesis, Panjab University, Chandigarh (2001).

[32] J. Lukasik *et al.*, Phys. Lett. B **608**, 223 (2005).

[33] A. Insolia, U. Lombardo, N.G. Sandulescu and A. Bonasera, Phys. Lett. B **334**, 12 (1994).

[34] A. Andronic *et al.*, Phys. Rev. C **67**, 034907 (2003).

[35] W.M. Zhang *et al.*, Phys. Rev. C **42**, R491 (1990); D. Beavis *et al.*, *ibid.* C **45**, 299 (1992); B. Hong *et al.*, *ibid.* C **66**, 034901 (2000).

[36] P. Danielwicz and G. Odyniec, Phys. Lett. B 157, 146 (1985); J. W. Harris *et al.*, Nucl. Phys. A **471**, 241c (1987).

[37] H.A. Gustafsson, *et al.*, Phys. Rev. Lett. **52**, 1590 (1984).

[38] W.G. Meyer, H. H. Gutbrod, Ch. Lunker and A. Sandoval, Phys. Rev. C **22**, 179 (1980).

[39] S. Voloshin, Y. Zhang, Z. Phys. C **70**, 665 (1996).

[40] S. Kumar, S. Kumar, and R.K. Puri, Phys. Rev. C **81**, 014601 (2010).

[41] Z. Li *et al.*, Nucl. Phys. A **559**, 603 (1993); A. Jain, S. Kumar, and R.K. Puri, Phys. Rev. C **84**, 057602 (2011).

[42] X.G. Cao *et al.*, Phys. Rev. C **81**, 061603(R) (2010).

[43] B. Hong *et al.*, Phys. Rev. C **71**, 034902 (2005); T. Gaitanos, C. Fuchs and H.H. Wolter, Phys. Lett. B **609**, 241 (2005).

[44] J. Lukasik *et al.*, Phys. Rev. C **66**, 064606 (2002).

[45] C.A. Ogilvie *et al.*, Phys. Rev. Lett. **67**, 1214 (1991)

[46] J. Hubele *et al.*, Phys. Rev. C **46**, R1577 (1992).

[47] N. Marie *et al.*, Phys. Rev. C **58**, 256 (1998); W. Loveland *et al.*, *ibid.* C **59**, 1472 (1999).

[48] B.A. Li, Z.Z. Ren, C.M. Ko, and S.J. Yennello, Phys. Rev. Lett. **76**, 4492 (1996).

[49] B.A. Li and S.J. Yennello, Phys. Rev. C **52**, R1746 (1995).

[50] L.W. Chen, F.S. Zhang, and G.M. Jin, Phys. Rev. C **58**, 2283 (1998).

[51] J. Zhang, S. Das Gupta, C. Gale, Phys. Rev. C **50**, 1617 (1994).

[52] D.T. Khoa, N. Ohtsuka, M.A. Matin, A. Faessler, S.W. Huang, E. Lehmann, and R.K. Puri, Nucl. Phys. A **547**, 671 (1992).

[53] G. Peilert, H. Stöcker, W. Greiner, A. Rosenhauer, A. Bohnet, and J. Aichelin, Phys. Rev. C **39**, 1402 (1989).

[54] A.D. Sood and R.K. Puri, Eur. Phys. J. A **30**, 571-577 (2006).

[55] A. Jain, K.S. Vinayak, S. Kumar, Ann. of Phys. **334**, 334 (2013).

[56] M.D. Toro *et al.*, Nucl. Phys. A **782**, 267c (2007).

[57] B.A. Li, Phys. Rev. Lett. **85**, 4221 (2000).

[58] B.A. Li, Phys. Rev. Lett. **88**, 192701 (2002); *ibid.* Nucl. Phys. A **708**, 365 (2002).

[59] G.C. Yong, B.A. Li, and L.W. Chen, Phys. Rev. C **74**, 064617 (2006); G.C. Yong, B.A. Li, L.W. Chen, and W. Zuo, *ibid.* C **73**, 034603 (2006).

[60] S. Gautam, A.D. Sood, R.K. Puri, and J. Aichelin, Phys. Rev. C **83**, 034606 (2011); S. Gautam, R. Kumari, and R. K. Puri, Phys. Rev. C **86**, 034607 (2012).

[61] Y. Wang *et al.*, Phys. Rev. C **89**, 34606 (2014).

[62] R. Bansal and S. Gautam, Phys. Rev. C **91**, 024615 (2015).

[63] R. Bansal, S. Gautam, R.K. Puri and J. Aichelin, Eur. Phys. J. A **51** 2, (2015).

[64] J.Y. Liu, W.J. Guo, S.J. Wang, W. Zuo, Q. Zhao, and Y.F. Yang, Phys. Rev. Lett. **86** 975 (2001).

[65] Y.F. Yang, J.Y. Liu, W. Zuo, W.J. Guo, and Q. Zhao, Chin. Phys. Lett. **18** 1040 (2001).

[66] J.Y. Liu, W.J. Guo, Y.Z. Xing, W. Zou and X.G. Lee, Phys. Rev. C **67** 024608 (2003).

[67] J.Y. Liu, W.J. Guo, Y.Z. Xing, X.G. Li, and Y.Y. Gao, Phys. Rev. C **70** 034610 (2004).

[68] J.Y. Liu, W.J. Guo, Y.Z. Xing, and X.G. Li, Chin. Phys. Lett. **21** 1914 (2004).

[69] S. Kumar and S. Kumar, Chin. Phys. Lett. **27** 062504 (2010).

[70] G.Q. Zhang, Y.G. Ma, X.G. Cao, C.L. Zhou, X.Z. Cai, D.Q. Fang, W.D. Tian, and H. W. Wang, Phys. Rev. C **84** 034612 (2011)

[71] M.H. Zhao *et al.*, Phys. Rev. C 89, 037001 (2014).

[72] R. Bansal, A. Jain and S. Kumar, Indian J. Phys. **89** 10, 1077 (2015).

[73] F.S. Zhang, L.W. Chen, Z.Y. Ming and Z.Y. Zhu, Phys. Rev. C **60**, 064604 (1999).

[74] C. Hartnack, R.K. Puri, J. Aichelin, J. Konopka, S.A. Bass, H. Stöcker and W. Greiner, Eur. Phys. J. A bf 1, 151 (1998); C. Hartnack, J. Aichelin, H. Stöcker, and W. Greiner, Mod. Phys. Lett. A **9**, 1151 (1994); C. Hartnack, J. Aichelin, H. Stocker, and W. Greiner, Phys. Lett. B **336**, 131 (1994).

[75] J.Y. Liu *et al.*, Phys. Rev. C **63**, 054612 (2001).

[76] J.Y. Liu, Y.Z. Xing and W.J. Guo, Chin. Phys. Lett. **20**, 832 (2006).

[77] C. Li, J. Tian, L. Ou, and N. Wang, Phys. Rev. C **87**, 064615 (2013).

[78] Q. Wu *et al.*, phys. Rev. C **91**, 014617(2015).

[79] S. Kumar and R.K. Puri, Phys. Rev. C **60**, 054607 (1999); Y.K. Vermani and R.K. Puri, DAE symposium on Nuclear Physics, IIT Roorkee (India), 22-26 December (2008).

[80] J. Singh, S. Kumar, and R.K. Puri, Phys. Rev. C **63**, 054603 (2001).

[81] M. Colonna, J. Rizzo, P. Comaz, and M.D. Toro, nucl-th/0707.3902; V. Baran, M. Colonna, M.D. Toro, and V. Greco, Phys. Rev. Lett. **86**, 4492 (2001); J. Rizzo, M. Colonna, and A. Ono, Phys. Rev. C **76**, 024611 (2007).

[82] A. Ono, P. Danielewicz, W.A. Friedman, W.G. Lynch, and M.B. Tsang, Phys. Rev. C **70**, 041604(R) (2004).

[83] H. Imal *et al.*,Phys. Rev. C **91** 034605 (2015).

[84] H. Zheng, G. Bonasera, J. Mabiala, P. Marini, and A. Bonasera, Eur. Phys. J. A **50**, 167 (2014).

[85] F. Zhang, C. Li, L. Zhu, H. Liu and F.S. Zhang, Phys. Rev. C **91**, 034617 (2015).

[86] E. Schopper, Naturwissenschaftler **5**, 557 (1937); I. I. Gurevich *et al.*, Dokl. Akad. Nauk SSSR **18**, 169 (1938)

[87] R. Pak *et al.*, Phys. Rev. Lett. **78**, 1022 (1997); *ibid.* **78**, 1026 (1997).

[88] A. Andronic *et al.*, Phys. Rev. C **64**, 041604(R) (2001).

[89] W. Trautmann *et al.*, Prog. Part. Nucl. Phys. **62**, 425 (2009).

[90] W. Reisdorf *et al.*, Nucl. Phys. A **848**, 366 (2010).

[91] P. Russotto *et al.*, Phys. Lett. B **697**, 471 (2011).

[92] Z. Kohley *et al.*, Phys. Rev. C **83**, 044601 (2011).

[93] Z. Kohley *et al.*, Phys. Rev. C **85**, 064605 (2012).

[94] G. Lehaut *et al.* (INDRA collaboration), Phys. Rev. Lett. **104**, 232701 (2010).

[95] O. Lopez *et al.* (INDRA collaboration), Phys. Rev. C **90**, 064602 (2014).

[96] O.V. Lozkin and N.A. Perfilov, J. Exp. Theo. Phys. **31**, 913 (1956).

[97] B. Jakobsson *et al.*, Z. Phys. A **307**, 293 (1982).

[98] A.I. Warwick *et al.*, Phys. Rev. C **27**, 1083 (1983).

[99] J.E. Finn *et al.,* Phys. Rev. Lett. **49**, 1321 (1982); A.S. Hirsh *et al.*, Phys. Rev. C. **29**, 508 (1984).

[100] V. Avdeichikov *et al.*, Yad. Fiz. **48**, 1736 (1988).

[101] S.R. Souza *et al.*, Phys. Rev. C **50**, 257 (1994).

[102] L. Phair *et al.*, Phys. Rev. Lett. **75**, 213 (1995); L. Phair *et al.*, Phys. Rev. Lett. **77**, 822 (1996).

[103] T.C. Sangster *et al.*, Phys. Rev. C **46**, 1404 (1992).

[104] D.R. Bowman *et al.*, Nucl. Phys. A **523**, 386 (1991).

[105] N.T. Porlie, Nucl. Phys. A **681**, 253 (2001); B.K. Srivastva *et al.*, Phys. Rev. C **65**, 054617 (2002); J.B. Elliott *et al.*, Phys. Rev. C **71**, 024607 (2005); L.G. Moretto, C.O. Dorso, J.B. Elliott, and L. Phair, Phys. Rev. C **77**, 037603 (2008).

[106] A. Insolia *et al.*, Phys. Rev. C **61**, 044902 (2000).

[107] R.T. de Souza *et al.*, Phys. Lett. B **268**, 6 (1991); T. Li *et al.*, Phys. Rev. Lett. **70**, 1924 (1992); L. Phair *et al.*, Phys. Lett. B **285**, 10 (1992); D.R. Bowman *et al.*, Phys. Rev. C **46**, 1834 (1992); T. Li *et al.*, Phys. Rev. C **49**, 1630 (1994).

[108] C. Williams *et al.*, Phys. Rev. C **55**, R2132 (1997).

[109] M.B. Tsang *et al.*, Phys. Rev. Lett. **71**, 1502 (1993).

[110] S. Piantelli *et al.*, Phys. Rev. C **74**, 034609 (2006); S. Piantelli *et al.*, Phys. Rev. C **78**, 064605 (2008).

[111] R. Planeta *et al.*, Phys. Rev. C **77**, 014610 (2008).

[112] M. Begemann-Blaich *et al.*, Phys. Rev. C **48**, 610 (1993).

[113] G.F. Peaslee *et al.*, Phys. Rev. C **49**, R2271 (1994); N.T.B. Stone *et al.*, Phys. Rev. Lett. **78**, 2084 (1997); A.S. Botvina *et al.*, Phys. Rev. C **74**, 044609 (2006).

[114] B. de Schauenburg *et al.*, GSI Rep. 98-1, p. 56 (1997); W. Reisdorf, Nucl. Phys. A **630**, 15c (1998); W. Reisdorf, *et al.*, *ibid.* 2000-1, p. 45 (1999); W. Reisdorf, Hirschegg, p. 82 (1999); B. Hong *et al.*, Phys. Rev. C **66**, 034901 (2002).

[115] G. Poggi *et al.*, Nucl. Phys. A **586**, 755 (1995); J. Konopka, *et al.*, GSI Rep. 96-1, p. 65 (1995); J.P. Alard, *et al.*, *ibid.* 97-1, p. 54 (1996); N. Bastid, *et al.*, *ibid.* 98-1, p. 54 (1997); A. Andronic, *et al.*, *ibid.* 98-1, p. 55 (1997).

[116] A. Schüttauf *et al.*, Nucl. Phys. A **607**, 457 (1996).

[117] A.S. Botvina *et al.*, Nucl. Phys. A **584**, 737 (1995).

[118] W. Trautmann *et al.*, Int. J. Mod. Phys. E **17**, 1838 (2008); W. Trautmann *et al.*, Nucl. Phys. A **787**, 575 (2007).

[119] C. Sfienti *et al.*, Phys. Rev. Lett. **102**, 152701 (2009).

[120] Y.G. Ma *et al.*, Phys. Rev. C **69**, 031604 (2004).

[121] R. Wada *et al.*, Phys. Rev. C **69**, 044610 (2004); J. Wang *et al.*, Phys. Rev. C **72**, 024603 (2005); R. Wada *et al.*, Phys. Rev. C **71**, 054608 (2005).

[122] D.V. Shetty *et al.*, J. Phys. G: Nucl Part. Phys. **36** , 075103 (2009).

[123] D.V. Shetty, G.A. Souliotis, S. Galanopoulos, and S.J. Yennello, Phys. Rev. C **79**, 034603 (2009).

[124] D.V. Shetty *et al.*, Phys. Rev. C **68**, 054605 (2003).

[125] D.V. Shetty, S.J. Yenello, G.A. Souliotis, Phys. Rev. C **76**, 024606 (2007); D.V. Shetty, S.J. Yennello and G.A. Souliotis, Phys. Rev. C **75**, 034602 (2007); D.V. Shetty *et al.*, Nucl. Instr. and Meth. in Phys. Res. B **261**, 990 (2007).

[126] S. Hudan *et al.*, Phys. Rev. C **67**, 064613 (2003).

[127] L. Manduci *et al.*, Nucl. Phys. A **811**, 93 (2008).

[128] E. Bohnet *et al.*, Phys. Rev. Lett. **103**, 072701 (2009).

[129] E. Galichet, M. Colonna, B. Borderie and M.F. Rivet, Phys. Rev. C **79**, 064615 (2009); E. Galichet *et al.*, Phys. Rev. C **79**, 064614 (2009).

Chapter 2

Methodology

2.1 Introduction

Heavy-ion collisions at intermediate energies involve highly complicated non-equilibrium physics because of the complexity of nuclear forces. Moreover, the dynamics of heavy-ion collisions at intermediate energies is mainly governed by the three components namely, mean field, two body collisions and Pauli blocking. Therefore, the knowledge of these three components is essential to extract information about the nuclear equation of state of neutron-rich matter. These components play a significant role at different incident energies. At low incident energies, the mean field dominates due to lack of available free phase space. This results in nearly 4% of nucleon-nucleon binary collisions to occur. However, 96% of attempted collisions are blocked due to Pauli blocking. On the contrary, the large availability of free phase space at higher energies results in significant number of binary nucleon-nucleon collisions. In such cases, Pauli blocking is trivial (nearly 4%) and the dynamics of heavy-ion collisions is governed by the repulsive nucleon-nucleon scattering alone. On the other hand, both come to light at intermediate energy regime and the interplay between the two governs the reaction dynamics. In order to extract information about the nuclear equation of state as well as the reaction dynamics at intermediate energies, one always require a reliable theoretical tool such as transport theories and nuclear models. In a series of microscopic models, Cascade model [1, 2] was the first to study the dynamics of heavy-ion collisions from the initial stage to the final phase space of nucleon. In this model, each nucleus is considered as sphere with a collection of point like nucleons distributed over it. The nuclei are initialised towards each other at a specific impact parameter and incident velocity. However, no Fermi momenta was assigned to the nucleons. The initial position of a nucleon is allocated by using Monte Carlo sampling method. The particles are supposed to scatter elastically or inelastically after the collision depending upon the incident energy. Although the Cascade model is very successful in explaining the effective temperature as well as the entropy of the reaction, however, its use is limited to the central collisions only. Moreover, it does not involve the mean field and quantum interference effects such as Fermi momentum. The need of mean field effects led to the development of Time Dependent Hartree Fock (TDHF) theory [3]. The TDHF calculations were quite successful in describing the fusion cross section, scattering angles, deep inelastic scattering, momentum transfer at energy $\leq$ 5 MeV/nucleon. At higher incident energies, due to lack of two body collisions this approximation fails. Wong [4] originated the idea for semi-classical illustration of TDHF theory but was unable to incorporate the collision term. Later on, attempts have been made in the literature to extend the original TDHF equation i.e. extended TDHF (ETDHF) [5] in order to include the two body binary collisions by taking into account the residual nucleon-nucleon interactions. Unfortunately, ETDHF involve highly complex numerical implementation to be used for the large scale calculations of heavy-ion collisions. However, rational investigation of heavy-ion collisions at intermediate energies demand sophisticated treatment of both the nucleon-nucleon collisions and mean field effects. Furthering in this direction, a new approach named as Boltzmann-Uehling-Uhlenback (BUU) [6, 7] was developed by incorporating the nucleon-nucleon collisions within the semi classical version of ETDHF model (or Vlasov equation). This realization is also named as Landau-Vlasov (LV) [8] or Vlasov-Uehling-Uhenbeck (VUU) equation [9] or Boltzmann-Nordheim equation. These manifestations differ in their technical realization (computer programming) only. These one-body transport models do not preserve the correlations and fluctuations among the nucleons. Thus, the use of such transport models is limited to the investigation of stopping, collective flow as well as particle spectra, however, the fragment formation and description of two-particle correlation is beyond the scope of this model. The requirement to keep track of the correlations among the nucleons led to the development of Classical Molecular Dynamics (CMD) model. This N-body approach was able to treat the non-equilibrium situation at the early stage of a reaction. However, it was unable to accommodate some typical quantum effects like Pauli blocking and strong potential gradients. This issue was resolved by Aichelin and Stöcker by including the quantum features like Pauli blocking, stochastic scattering and particle production giving rise to a new approach named as Quantum Molecular Dynamics model. Till date, Quantum Molecular Dynamics (QMD) model [10] as well as many of its imroved/upgraded versions like Isospin dependent Quantum Molecular Dynamics(IQMD) [11], G-matrix QMD (GQMD) [12], Fermionic Molecular Dynamics (FMD) [13], Antisymmetric Molecular Dynamics (AMD) [14] are used quite successfully to understand the reaction dynamics of heavy-ion collisions under different circumstances. The entire study of this thesis is carried out by using IQMD model. In the following sections, we first discuss in detail the IQMD model which generate the phase space of nucleons after the collision. Various cluterization techniques are discussed in the later part of this chapter.

2.2 Isospin-dependent Quantum Molecular Dynamics model

The IQMD model developed by Hartnack *et al.* [11] is a widely used semiclassical transport model that treat the interactions of nucleons on a microscopic N-body level. This model is an extension of original QMD model, however the technical programming is based on VUU model. IQMD treats different charge states of nucleons, deltas and pions, explicitly. An important feature of this model i.e. isospin degree of freedom (component) that enter into the calculations via nucleon-nucleon scattering cross section, Coulomb potential and symmetry potential. The general structure of this model comprises of three important steps namely, initialization, propagation and binary nucleon-nucleon collisions. In addition to this, Pauli blocking of nucleon-nucleon collisions also plays an important role. In the following subsections, all these three steps along with the Pauli blocking are elaborated in detail.

2.2.1 Initialization

The target and projectile nucleons are initialized in their rest frame and their position in the phase space is determined randomly within the radius of $r \leq 1.12A^{1/3}$ and momentum $p \leq p_F$ (here, A is the atomic mass of the nucleus considered and p_F is Fermi momentum) corresponding to normal nuclear matter density ($\rho_0 = 0.17 fm^{-3}$). In IQMD model, each nucleon is represented by a Gaussian wave packet with a fixed width L and these nucleons interact via mutual two and three body forces. The wave function for describing the i^{th} nucleon having mean position r_i and mean momentum p_i is represented by

$$\psi_i(\mathbf{r},\ \mathbf{p}_i(t),\ \mathbf{r}_i(t)) \;=\; \frac{1}{(2\pi L)^{3/4}} exp\left[\frac{i}{\hbar}\ \mathbf{p}_i(t)\cdot\mathbf{r} \;-\; \frac{(\mathbf{r}\ -\ \mathbf{r}_i(t))^2}{4L}\right]. \tag{2.1}$$

In IQMD model, L depends on the size of the system. The system mass dependence of L is introduced to obtain maximum stability of density profile and lies between 4.33 fm^2 and 8.66 fm^2 for the lighter and heavier systems, respectively. The total n-body wave function is assumed to be direct product of coherent states.

$$\Phi \;=\; \prod_i \psi_i(\mathbf{r},\ \mathbf{r}_i, \mathbf{p}_i, t). \tag{2.2}$$

In a heavy-ion reaction, one always seek to understand the time evolution of the reaction. Wigner densities enable us to formulate quantum mechanics in a much simpler language and hence provide quite intuitive understanding of the reaction dynamics. Wigner density would yield the observables that depends on the phase space coordinates (r, p, t) which otherwise was not possible to achieve by solving the n-body Schrodinger equation. The Wigner transforms of the coherent states are Gaussians in phase space and are more convenient to be used in numerical calculations.

$$\begin{aligned} f_i(\mathbf{r},\ \mathbf{p}, \mathbf{r}_i(t),\ \mathbf{p}_i(t)) \;&=\; \frac{1}{(2\pi\hbar)^3}\int e^{-\frac{i}{\hbar}\mathbf{p}\cdot\mathbf{r}_{12}}\psi_i(\mathbf{r}+\frac{\mathbf{r}_{12}}{2},\ t)\ \psi_i^*(\mathbf{r}-\frac{\mathbf{r}_{12}}{2},\ t)d^3r_{12}, \\ &=\; \frac{1}{(\pi\hbar)^3}e^{-(\mathbf{r}\ -\mathbf{r}_i(t))^2/2L}\ e^{-(\mathbf{p}\ -\mathbf{p}_i(t))^2 2L/\hbar^2}, \end{aligned} \tag{2.3}$$

where $\mathbf{r}_i(t)$ and $\mathbf{p}_i(t)$ define the classical orbit or the center of the Gaussian wave packet in phase-space, whereas the squared width L is assumed to be independent of the time. The density of i^{th} particle in coordinate space and momentum space is

$$\begin{aligned} \rho_i(\mathbf{r}, \mathbf{r_i}(\mathbf{t})) \;&=\; \int f_i(\mathbf{r}, \mathbf{p}, \mathbf{r}_i(t), \mathbf{p}_i(t))\ d^3p, \\ &=\; \frac{1}{(2\pi L)^{3/2}}\ e^{-[\mathbf{r}\ -\ \mathbf{r}_i(t)]^2/2L}. \end{aligned} \tag{2.4}$$

$$\begin{aligned} g_i(\mathbf{p}, \mathbf{p_i}(\mathbf{t})) \;&=\; \int f_i(\mathbf{r}, \mathbf{p}, \mathbf{r}_i(t), \mathbf{p}_i(t))\ d^3r, \\ &=\; \left(\frac{2L}{\pi\hbar}\right)^{3/2}\ e^{-[\mathbf{p}\ -\ \mathbf{p}_i(t)]^2 2L/\hbar^2}. \end{aligned} \tag{2.5}$$

To initialize a nucleus, we have to assign the coordinates and momenta to all nucleons. In three dimensional space (inside a sphere of radius R) the center of Gaussian wave packet is uniformly distributed in polar coordinate by:

$$\begin{aligned} r &= R\, x_1^{1/3}, \\ cos\theta &= 1 \;-\; 2x_2, \\ \phi &= 2\pi\; x_3, \end{aligned}$$

where $x_1,\ x_2,\ x_3$ are the random numbers. The coordinates of nucleons are rejected if the distance between them is less than 1.5 fm. The local Fermi momentum is determined by the relation

$$P_F(\mathbf{r}_i) \;=\; \sqrt{-2mU(\mathbf{r}_i)}, \tag{2.6}$$

where $U(\mathbf{r}_i)$ is the local potential. The center of each Gaussian wave packet in momentum space is uniformly distributed in polar coordinate by:

$$\begin{aligned} p_i &= P_F(\mathbf{r}_i) x_4^{1/3}, \\ cos\theta &= 1 \;-\; 2x_5, \\ \phi &= 2\pi x_6. \end{aligned}$$

Only those distributions are taken into account which fulfil the criteria of d_{min} i.e.

$$(\mathbf{r}_i \;-\; \mathbf{r}_j)^2\; (\mathbf{p}_i \;-\; \mathbf{p}_j)^2 \geq d_{min}. \tag{2.7}$$

Typically 1 out of 50,000 initializations is accepted under present criteria. Moreover, the IQMD model also involve Lorentz contraction of nucleus coordinate distribution which plays a significant role at higher incident energies. In order to prevent the initialization of unstable nuclei, a sample of nuclei with the required stability are chosen. Besides this, two Euler angles are also chosen randomly as well. The position of all the nucleons of one nucleus is then rotated around its centre of mass. This procedure is repeated for different sets of Euler angles. Each set of Euler angles produce an absolutely different reaction without changing the stability.

2.2.2 Propagation

The successfully initialized stable nuclei are then boosted towards each other along the original Z-axis with proper center-of-mass velocity using relativistic kinematics. The center of each distribution moves along the Coulomb trajectories. This distribution is kept fixed until the distance between surfaces of the nuclei is 2 fm. The equation of motion of many-body system is, then, calculated by means of a generalized variational principle: we start from the action

$$S = \int_{t_1}^{t_2} \mathcal{L}[\Phi, \Phi^*] d\tau, \tag{2.8}$$

with the Lagrange functional

$$\mathcal{L} = \langle \Phi | i\hbar \frac{d}{dt} - H | \Phi \rangle. \tag{2.9}$$

The time evolution is obtained by the requirement that the action is stationary under the allowed variation of the wave function

$$\delta S = \delta \int_{t_1}^{t_2} \mathcal{L}[\Phi, \Phi^*] dt = 0. \tag{2.10}$$

The Hamiltonian H contains a kinetic term and mutual interactions V_{ij}, which can be interpreted as the real part of the Brückner G-matrix supplemented by the Coulomb interactions. The time evolution of the parameters is obtained by the requirement that the action is stationary under allowed variation of the wave function. This yields an Euler-Lagrange equation for each parameter. We obtain for each parameter λ, an Euler-Lagrange equation:

$$\frac{d}{dt}\frac{\partial \mathcal{L}}{\partial \dot{\lambda}} - \frac{\partial \mathcal{L}}{\partial \lambda} = 0. \tag{2.11}$$

If the true solution of the Schrödinger equation is contained in the restricted set of wave function $\psi_i(\mathbf{r},\ \mathbf{p}_i(t),\ \mathbf{r}_i(t))$, this variation of the action gives the exact solution of the Schrödinger equation. If the parameter space is too restricted, we could find the wave function in the restricted parameter space which comes closest to the solution of the Schrödinger equation. It should be noted that the set of wave functions which can be covered with spatial parameterizations is not necessarily a subspace of Hilbert-space, thus the superposition principle does not hold. For the coherent states and a Hamiltonian of the form H = $\sum_i T_i + \frac{1}{2}\sum_{ij} V_{ij}$ ($T_i =$ kinetic energy, $V_{ij} =$ potential energy), the Lagrangian and the variation can easily be calculated and we obtain:

$$\mathcal{L} = \sum_i \dot{\mathbf{r}}_i \mathbf{p}_i - \sum_{j \neq i} < V_{ij} > - \frac{3}{2Lm}, \tag{2.12}$$

$$\dot{\mathbf{r}}_i = \frac{\mathbf{p}_i}{m} + \nabla_{\mathbf{p}_i} \sum_j < V_{ij} > \ = \ \nabla_{\mathbf{p}_i} < H >, \tag{2.13}$$

$$\dot{\mathbf{p}}_i = -\nabla_{\mathbf{r}_i} \sum_{j\neq i} < V_{ij} >= -\nabla_{\mathbf{r}_i} < H >, \tag{2.14}$$

with $\mathbf{r}_i = \mathbf{r}_i + \frac{\mathbf{p}_i}{m}t$ and $\langle V_{ij}\rangle = \int d^3\mathbf{r}_1 d^3\mathbf{p}_2 \langle\psi_i^*\psi_j^*|V(\mathbf{r}_1,\mathbf{r}_2)|\psi_i\psi_j\rangle$. These equations represent the time evolution and can be solved numerically. Thus, the variational principle reduces the time evolution of the n-body Schrödinger equation to the time evolution equations $6\cdot(A_P + A_T)$. The equations of motion now show a similar structure like classical Hamilton equations.

$$\dot{\mathbf{p}}_i = -\frac{\partial\langle H\rangle}{\partial\mathbf{r}_i} \; ; \; \dot{\mathbf{r}}_i = \frac{\partial\langle H\rangle}{\partial\mathbf{p}_i}. \tag{2.15}$$

The numerical solution can be achieved in the spirit of the classical molecular dynamics [15–17]. The wave functions (other than the Gaussian in Eq. 2.1) yield more complex equation of motion for other parameters and hence the analogy to classical molecular dynamics is lost.

The total energy H_i of i^{th} particle is the sum of kinetic and potential energies:

$$H_i = T_i + V_i = T_i + \frac{1}{2}\sum_{j;i\neq j} V_{ij}^{(2)} + \frac{1}{3!}\sum_{j,k;i\neq j\neq k} V_{ijk}^{(3)}, \tag{2.16}$$

where T_i refers to the kinetic energy of i^{th} particle and $V_{ij}^{(2)}$ and $V_{ijk}^{(3)}$ are the two- and three-body interactions. The two-body interactions $V_{ij}^{(2)}$ is obtained by folding the two-body interactions with the densities of both particles.

$$\begin{aligned}
\sum_{j;i\neq j} V_{ij}^{(2)} &= \sum_{j;i\neq j} \int f_i(\mathbf{r}_i,\mathbf{p}_i,t)\; f_j(\mathbf{r}_j,\mathbf{p}_j,t)\; V(\mathbf{r}_i,\mathbf{r}_j) \qquad (2.17)\\
&\quad \times d^3r_i\; d^3r_j\; d^3p_i\; d^3p_j,\\
&= \sum_{j;i\neq j} \int f_i(\mathbf{r}_i,\mathbf{p}_i,t)\; f_j(\mathbf{r}_j,\mathbf{p}_j,t)\; t_1\\
&\quad \times\delta(\mathbf{r}_i-\mathbf{r}_j) d^3r_i\; d^3r_j\; d^3p_i\; d^3p_j,\\
&= \sum_{j;i\neq j} t_1 \int f_i(\mathbf{r}_i,\mathbf{p}_i,t)\; f_j(\mathbf{r}_j,\mathbf{p}_j,t)\\
&\quad \times d^3r_i\; d^3p_i\; d^3p_j,\\
&= \sum_{j;i\neq j} t_1 \int \frac{1}{(\pi\hbar)^3} e^{-(\mathbf{r}-\mathbf{r}_i(t))^2/2L} e^{-(\mathbf{p}-\mathbf{p}_i(t))^2 2L/\hbar^2}\\
&\quad \times\frac{1}{(\pi\hbar)^3} e^{-(\mathbf{r}-\mathbf{r}_j(t))^2/2L}\; e^{-(\mathbf{p}-\mathbf{p}_j(t))^2 2L/\hbar^2}\; d^3r_i\; d^3p_i\; d^3p_j,\\
&= \sum_{j} t_1 \frac{1}{(4\pi L)^{3/2}} e^{-(\mathbf{r}_i-\mathbf{r}_j)^2/4L},\\
&= t_1 \sum_{j;i\neq j} \rho_{ij}. \qquad (2.18)
\end{aligned}$$

where

$$\rho_{ij} = \int d^3\mathbf{r}\ \rho_i(\mathbf{r})\ \rho_j(\mathbf{r}) = \frac{1}{(4\pi L)^{3/4}} e^{-(\mathbf{r}_i-\mathbf{r}_j)^2/4L}. \tag{2.19}$$

The three-body interactions can be calculated as follows:

$$\begin{aligned}
\sum_{j,k;i\neq j\neq k} V^{(3)}_{ijk} &= \sum_{j,k;i\neq j\neq k} \int f_i(\mathbf{r}_i,\mathbf{p}_i,t)\ f_j(\mathbf{r}_j,\mathbf{p}_j,t)\ f_k(\mathbf{r}_k,\mathbf{p}_k,t)\ V(\mathbf{r}_i,\mathbf{r}_j,\mathbf{r}_k) \\
&\quad \times d^3r_i\ d^3r_j\ d^3r_k\ d^3p_i\ d^3p_j\ d^3p_k, \\
&= \sum_{j,k;i\neq j\neq k} \int f_i(\mathbf{r}_i,\mathbf{p}_i,t)\ f_j(\mathbf{r}_j,\mathbf{p}_j,t)\ f_k(\mathbf{r}_k,\mathbf{p}_k,t)\ t_2 \\
&\quad \times\delta(\mathbf{r}_i-\mathbf{r_j})\ \delta(\mathbf{r}_i-\mathbf{r}_k) d^3r_i\ d^3r_j\ d^3r_k\ d^3p_i\ d^3p_j\ d^3p_k, \\
&= \frac{t_2}{(2\pi L)^3\cdot 3^{3/2}} \sum_{j,k;i\neq j\neq k} e^{-\left[(\mathbf{r}_i-\mathbf{r}_j)^2+(\mathbf{r}_i-\mathbf{r}_k)^2+(\mathbf{r}_k-\mathbf{r}_j)^2\right]/6L}, \\
&= \frac{t_2}{(2\pi L)^3 3^{3/2}} \sum_{j,k;i\neq j\neq k} e^{-\left[(\mathbf{r}_i-\mathbf{r}_j)^2+(\mathbf{r}_i-\mathbf{r}_k)^2\right]/6L\times\frac{3}{2}}, \\
&= \frac{t_2\ (4\pi L)^{3/2\times 2}}{(2\pi L)^3\cdot 3^{3/2}} \left[\sum_{j\neq i} \frac{1}{(4\pi L)^{3/2}} e^{-(\mathbf{r}_i-\mathbf{r}_j)^2/4L}\right]^2, \\
&= \frac{t_2\ 2^3}{3^{3/2}} \left[\sum_{j\neq i} \rho_{ij}\right]^2.
\end{aligned} \tag{2.20}$$

From above derivation, we see that for three-body interactions, the mean field can be written as $[\sum_{j\neq i}\rho_{ij}]^2$. The total momentum in IQMD is conserved because the Hamiltonian is well defined for the whole system. A heavy-ion reaction should be followed with the help of G-matrix, where the real part corresponds to the propagation and imaginary part is responsible for the collision. In the simulations, however, one always use different parameterized forms for describing both real and imaginary parts of G-matrix. The real part of G-matrix along with the Coulomb interaction V_{ij}^{Coul} signifies the baryon potential. The former can further be subdivided into a Skyrme type interaction V_{ij}^{loc}, a finite range Yukawa interaction V_{ij}^{Yuk} and a momentum dependent component V_{ij}^{mdi}. The total potential reads as:

$$V^{ij}\ =\ V_{ij}^{loc}\ +\ V_{ij}^{Yuk}\ +\ V_{ij}^{Coul}\ +\ V_{ij}^{mdi}, \tag{2.21}$$

In addition to the above mentioned components of interaction potential, the isospin effects should also be incorporated in the IQMD model with proper care and the same can be included via Coulomb interaction and symmetry potential. In this model, we use real charge i.e. $Z_{proton} = 1$ and $Z_{neutron} = 0$ to include the isospin dependence of Coulomb potential. Introducing the symmetry potential, the total interaction potential takes the form:

$$V^{ij} = V_{ij}^{loc} + V_{ij}^{Yuk} + V_{ij}^{Coul} + V_{ij}^{mdi} + V_{ij}^{sym}, \tag{2.22}$$

The general form of V_{loc}, V_{Yuk}, V_{Coul} and V_{sym} and their characteristic behaviour is shown in Fig. 2.1.

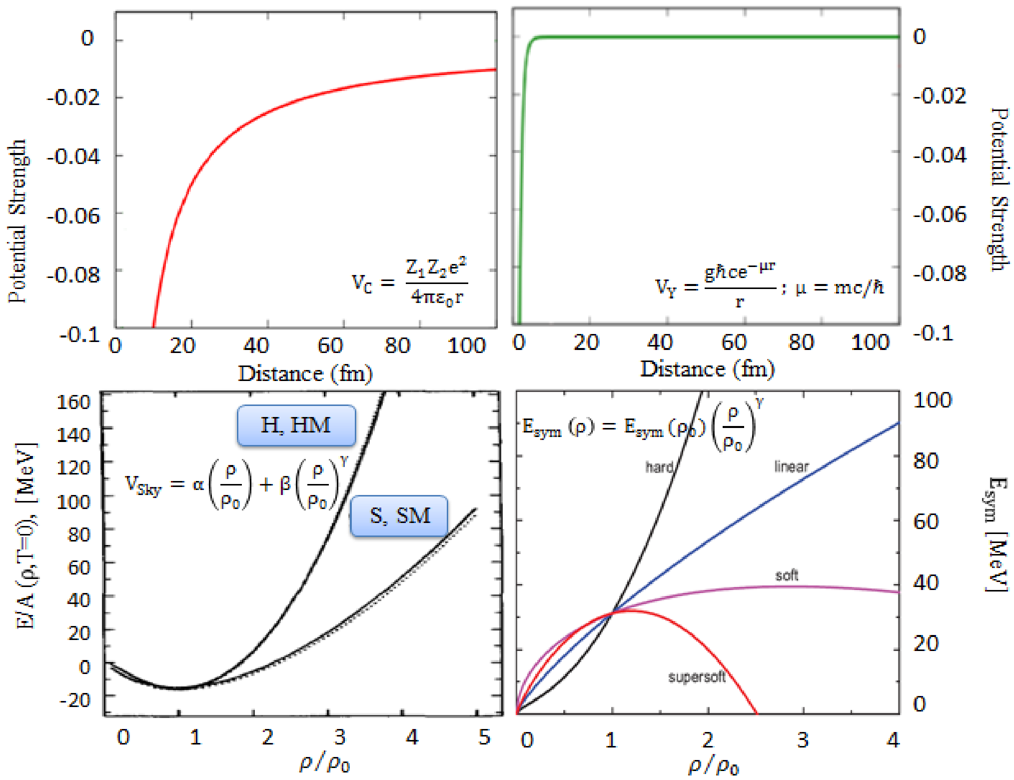

Figure 2.1: The characteristic behaviour of various components of nuclear potential. Figure is taken from Ref. [10, 18].

In the following, each of these potentials along with the parameterized forms to be implemented within the IQMD model is described in detail.

Skyrme Potential:

In nuclear matter where the density is constant, the interaction density coincides with the single particle density, and $V_{loc}^{(2)}$ as well as $V_{Yuk}^{(2)}$ are directly proportional to $(\frac{\rho}{\rho_o})$. The three-body part $V_{loc}^{(3)}$ of the interaction is proportional to $(\frac{\rho}{\rho_o})^2$. In nuclear matter, the local potential energy has the form

$$V^{loc} = \frac{\alpha}{2}(\frac{\rho}{\rho_o}) + \frac{\beta}{\gamma+1}(\frac{\rho}{\rho_o})^2. \tag{2.23}$$

Table 2.1: Parameters of static potentials [10]

K(MeV)	$\alpha(MeV)$	$\beta(MeV)$	γ	EOS
200	-356	303	1.17	S
380	-124	70.5	2	H

The potential has two free (α and β) parameters, which can be fixed by the requirement that at normal nuclear matter density, the average binding energy should be -15.75 MeV and total energy should have a minimum at ρ_o. In order to investigate the influence of different compressibilities, one can generalize the above potential energy to

$$V^{loc} = \frac{\alpha}{2}(\frac{\rho}{\rho_o}) + \frac{\beta}{\gamma+1}(\frac{\rho}{\rho_o})^{\gamma}. \tag{2.24}$$

Depending upon different values of these degrees of freedom, the above equation leads to various equation of state. The set of parameters and compressibilities corresponding to different equation of state is listed below in Table 2.1.

In the study of heavy-ion collisions, one usually has the so-called Skyrme parameterization of nuclear equation of state, which contains two sets of parameter giving the same correct binding energy and saturation density, but, two different incompressibility K (one corresponds to soft EOS with $K = 200$ MeV (at smaller value of γ), another corresponds to hard EOS with $K = 380$ MeV (at larger value of γ)). The total Skyrme potential then can be written as

$$V^{Skyrme} = \sum_{j;i\neq j} t_1\delta(\mathbf{r_i} - \mathbf{r_j}) + t_2\delta(\mathbf{r_i} - \mathbf{r_j})\rho^{\acute{\gamma}-1}((\mathbf{r_i} + \mathbf{r_j})/2). \tag{2.25}$$

Other values of α, β and γ are also available in the literature, e.g. super-stiff and super-soft EOS. However, the studies carried out by theoretical groups have established the fact that hadronic matter is soft in nature [19, 20].

Yukawa Potential:

The finite-range Yukawa potential proposed by Hideki Yukawa is added to stabilise the surface of finite nucleus [21]. The attractive Yukawa potential increases the interaction range compared to the δ-like Skyrme potential. The addition of Yukawa potential also reduces the fluctuations produced due to lack of pressure build up by the Fermi momentum.

The impact of Yukawa potential on the nuclear surface is studied by analyzing the radial density distribution of gold nucleus [10]. It was shown that the degree of preservation of nuclear surface is quite different for the two Yukawa parameters considered. However, the results of r.m.s. radius and nuclear binding energy do not differ much. The parameterized form of Yukawa potential is given by:

$$V_{ij}^{Yuk} \;=\; t_3 \frac{exp\{-|\mathbf{r}_i - \mathbf{r}_j|\}/\mu}{|\mathbf{r}_i - \mathbf{r}_j|/\mu}, \tag{2.26}$$

Here, with $\mu = 0.4$ fm and t_3= -6.66 MeV.

Coulomb Potential:

The Coulomb interaction among the nucleons plays a significant role in the study of heavy-ion collisions. It is an important asymmetry term that can be used to understand the isospin effects at intermediate energies. The Coulomb potential is represented as:

$$V_{ij}^{Coul} \;=\; \frac{Z_{eff}^2\ e^2}{|\mathbf{r}_i - \mathbf{r}_j|}. \tag{2.27}$$

Momentum dependent interactions:

An adequate explanation of the heavy-ion collisions require profound knowledge of momentum dependent interactions. A simple static equation of state, which is a function of density alone, is not sufficient to explain the dynamics of reaction at intermediate energies. The momentum dependent interactions adds additional repulsion between the nucleons of projectile and target. Therefore, the momentum dependent interactions has to be involved in the numerical realization of total potential with proper care. The momentum dependence of real part of optical potential is parameterized as follow:

$$V_{ij}^{mdi} \;=\; t_4 ln^2[t_5(\vec{p_i}' - \vec{p_j})^2 + 1]\delta(\vec{r_i} - \vec{r_j}). \tag{2.28}$$

Here t_4 = 1.57 MeV and $t_5 = 5 \times 10^{-4}\ MeV^{-2}$ are fitted to the experimental data [22]. The momentum dependence of nucleon-nucleon interaction may optionally be used in IQMD. However, introducing the momentum dependence in IQMD, one has to readjust the parameters of the Skyrme force to have correct saturation properties for normal nuclear matter and the same incompressibilities as those of the soft and hard EOS. This

Table 2.2: Parameters of the momentum dependent potentials [10]

K(MeV)	$\alpha(MeV)$	$\beta(MeV)$	γ	δ	ϵ	EOS
200	-390	320	1.14	1.57	21.54	SMD
380	-130	59	2.09	1.57	21.54	HMD

give rise to new equations of state, i.e. Hard Momentum Dependent (HMD) and Soft Momentum Dependent (SMD). Now, the static equation of state along with the momentum dependence takes the form:

$$U = \alpha\left(\frac{\rho}{\rho_0}\right) + \beta\left(\frac{\rho}{\rho_0}\right)^{\gamma} + \delta \cdot \ln^2\left(\epsilon \cdot (\Delta\vec{p})^2 + 1\right) \cdot \left(\frac{\rho}{\rho_0}\right). \qquad (2.2$$

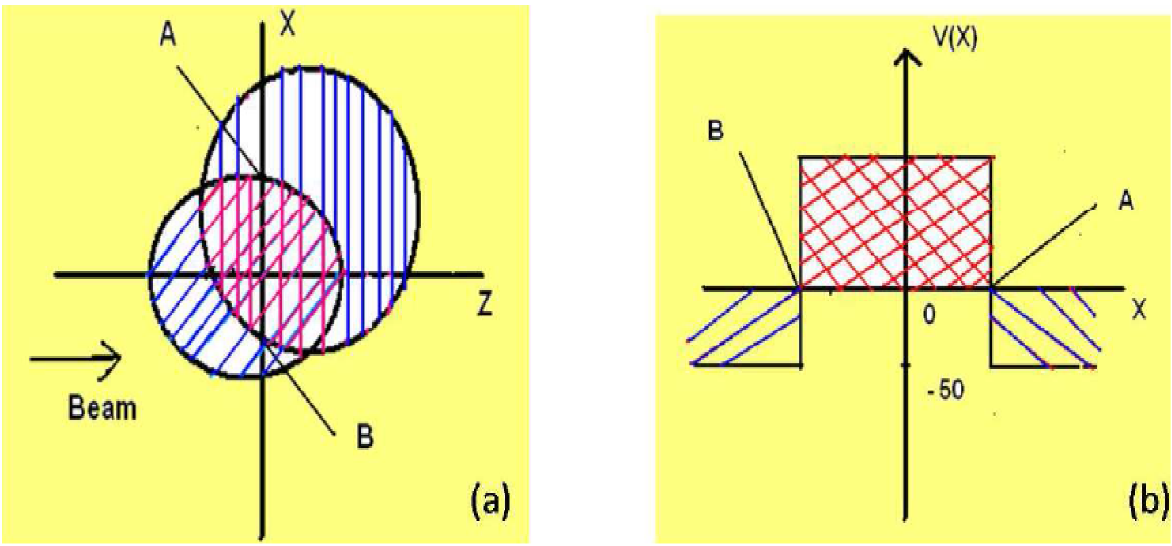

Figure 2.2: Graphical representation of transverse momentum caused by momentum dependent interaction. (a) Semi-peripheral collision between projectile and target in the reaction (Z-X) plane. (b) The potential along the X-axis. A strong repulsive potential in the participant/overlapping zone and an attractive potential in the outside region. Figure is taken from Ref. [10].

It is worth noting that the momentum dependent interactions play a significant role as long as the projectile and target overlap with each other. This can better be understood with the help of Fig. 2.2. In case, when the target and projectile do not overlap, the relative momentum between the interacting nucleons is quite small. Thus, the momentum dependent interactions do not make any difference. However, once the projectile hits the target at semi-peripheral colliding geometry, the overlapped nuclei with large relative momentum are placed closely in the configuration space (Fig. 2.2(a)). In the overlapping region, projectile (target) nucleons feel a strong repulsive potential due to neighbouring target (projectile) nucleons. Outside the overlap region, the projectile and target nucleons have no impact on each other, hence the potential is still attractive here (Fig. 2.2(b)). As a consequence, strong potential gradient is generated in the impact parameter direction. This prompts the particles to escape out of the compression zone. Consequently, a significant amount of transverse momentum transfer takes place.

Symmetry Potential:

Symmetry potential plays a significant role in the system having unequal isospin content. The difference in energy/nucleon between the pure neutron matter and symmetric nuclear matter is termed as symmetry energy. Fig. 2.3 shows the strength of symmetry energy as a function of density.

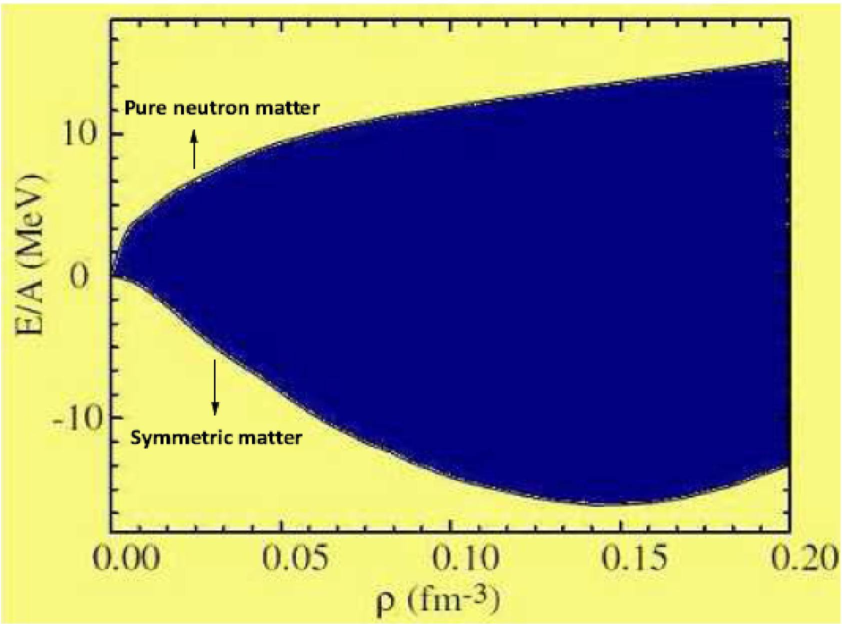

Figure 2.3: The density dependence of energy per nucleon for pure neutron matter (upper curve) and symmetric nuclear matter (lower curve). The shaded region signifies the symmetry energy. Figure is taken from Ref. [24].

Here, the upper and lower lines represent the energy per nucleon for pure neutron matter and symmetric nuclear matter. The difference between two lines indicate the estimate of energy required to convert all protons in a symmetric nuclear matter to neutrons at a particular value of density ρ. The energy per nucleon of asymmetric nuclear matter can be determined by parabolic law [23]:

$$E_{sym}(\rho, \delta_A) \;=\; E_{sym}(\rho, 0) \;+\; E_{sym}(\rho)\delta_A^2 \tag{2.30}$$

Where, $E_{sym}(\rho, 0)$ and $E_{sym}(\rho)$ are the energy per nucleon of symmetric nuclear matter and normal nuclear matter, respectively. δ_A=$(\rho_n - \rho_p)/(\rho_n + \rho_p)$ represents the isospin asymmetry of asymmetric nuclear matter. This equation validates for small values of δ only. The parameterized form of density dependence of symmetry energy is given by the relation:

$$E_{sym}(\rho) \;=\; E_{sym}(\rho_0)\left(\frac{\rho}{\rho_0}\right)^{\gamma}, \tag{2.31}$$

where, $E(\rho_0)$ = 32 MeV and is defined as symmetry energy corresponding to normal nuclear matter density ($\rho_0 = 0.17 fm^{-3}$) The value of γ describes the stiffness (or strength) of symmetry energy at densities away from the normal nuclear matter density. Usually, two different values of density dependence of symmetry energy has been observed i.e. Soft and Stiff density dependent symmetry energy. For the soft density dependent symmetry energy, the value of symmetry energy increases upto the normal nuclear matter density and then decreases for higher values of density. However, for Stiff density dependent symmetry energy, there is gradual increase in symmetry energy as a function of density. The stiff form of symmetry energy causes an early emission of nucleons from the compression zone. On the other hand, the symmetry potential is highly repulsive (attractive) for neutrons (protons) in the low density region for soft form of symmetry potential as compared to the stiff form of symmetry energy. Fig. 2.4 shows the variation of symmetry energy and symmetry potential with the density. The parameterized from of symmetry potential is given by the relation:

$$V_{ij}^{sym} \;=\; t_6\frac{1}{\varrho_0}T_3^iT_3^j\delta(\vec{r_i}' - \vec{r_j}) \tag{2.32}$$

In Eq. 2.32, t_6 = 100 MeV and T_{3i} and T_{3j} denote the isospin projection of particles i and j (being +1/2 and -1/2 for protons and neutrons, respectively).

The symmetry and Coulomb potentials are isospin dependent and remaining Skyrme, Yukawa and momentum dependent potentials are isospin independent. For a nucleus in

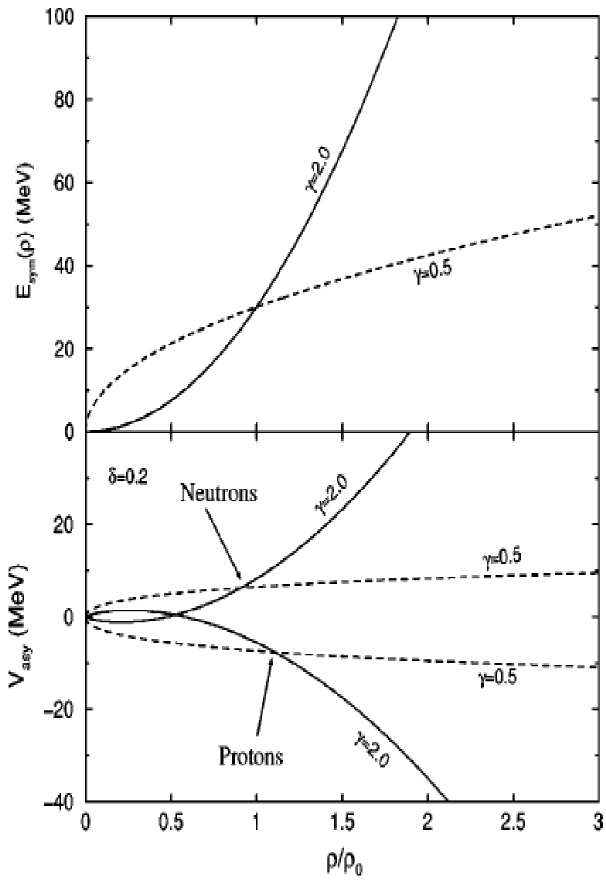

Figure 2.4: Variation of symmetry energy (upper panel) and symmetry potential (lower panel) with density for an isospin asymmetry $\delta = 0.2$ and γ =0.5 and 2.0. Figure is taken from Ref. [25].

its ground state, the expectation value of the total Hamiltonian correspond to its total binding energy. When comparing to the Bethe-Weizsäcker mass formula, the kinetic energy, the Skyrme interaction and the momentum-dependent interactions contribute to the volume energy, the Yukawa interaction to the surface and the volume energy, and the symmetry interactions to the volume symmetry energy. There is no term corresponding to the pairing energy since it corresponds to a global property of the nucleus which would be difficult to model by microscopic local forces. Therefore, the total baryon-baryon potential in IQMD model can be written as:

$$\begin{aligned} V_{ij} &= V_{ij}^{Skyrme} + V_{ij}^{Yukawa} + V_{ij}^{Coul} + V_{ij}^{MDI} + V_{ij}^{Sym} \\ &= \left(t_1\delta(\mathbf{r_i} - \mathbf{r_j}) + t_2\delta(\mathbf{r_i} - \mathbf{r_j})\rho^{\zeta-1}\left(\frac{\mathbf{r_i}+\mathbf{r_j}}{2}\right)\right) \\ &+ t_3\frac{exp(|\mathbf{r_i}-\mathbf{r_j}|/\mu)}{(|\mathbf{r_i}-\mathbf{r_j}|/\mu)} + \frac{Z_iZ_je^2}{|\mathbf{r_i}-\mathbf{r_j}|} \\ &+t_4\ln^2[t_5(\mathbf{p_i}-\mathbf{p_j})^2+1]\delta(\mathbf{r_i}-\mathbf{r_j}) \\ &+t_6\frac{1}{\varrho_0}T_{3i}T_{3j}\delta(\mathbf{r_i}-\mathbf{r_j}). \end{aligned} \tag{2.33}$$

It is worth mentioning that all these components of nuclear potential are independent of each other, that is the reason why the order of adding these potentials do not influence the results. In addition, the Skyrme and Yukawa being the elementary potentials, can't be separated.

2.2.3 The nucleon-nucleon collisions

The nucleon-nucleon collisions are included in $IQMD$ model by employing the collision terms of the well-known VUU-BUU equations [3,26]. The NN collisions are done stochastically in analogy with all cascade models [2,27]. In the case of $IQMD$, parameterizations of VerWest and Arndt have been taken [26]. A common description is used for describing the collision term, that is, two nucleons are supposed to collide with each other, if the minimum distance between the centroids of Gaussians fulfills the requirement

$$|\mathbf{r_i}-\mathbf{r_j}| \leq \sqrt{\frac{\sigma_{tot}}{\pi}}, \quad \sigma_{tot} = \sigma(\sqrt{s}, type), \tag{2.34}$$

where σ_{tot} is the total cross section and "type" denotes the ingoing collision partners (N-N, N-Δ, N-π,....). The total cross section is the sum of elastic and all inelastic cross sections.

$$\sigma_{tot} = \sigma_{el} + \sigma_{inel} = \sigma_{el} + \sum_{channels} \sigma_i. \tag{2.35}$$

In addition to nucleons, delta resonances are also produced in IQMD model, which further decay into pions. The following inelastic channels are explicitly taken into account and constitute the imaginary part of the pion optical potential

$$N\ N \rightarrow\ \Delta\ N \qquad (a),$$
$$\Delta \rightarrow\ N\ \pi \qquad (b),$$
$$\Delta\ N \rightarrow\ N\ N \qquad (c),$$
$$N\ \pi \rightarrow\ \Delta \qquad (d).$$

Elastic $\pi-\pi$, $\pi-N$, $\pi-\Delta$, $\Delta-\Delta$, $\Delta-N$ scatterings are not taken into account. Experimental cross sections are used for the processes (a) and (d) [26], as well as for the elastic nucleon-nucleon cross sections. Experimentally, inaccessible channels like ΔN $\rightarrow$ NN are calculated from their reverse reactions (here $NN \rightarrow \Delta N$) using modified detailed balance formula [28]. The angular distribution for the elastically scattered nucleons is given by:

$$\frac{d\sigma_{el}}{d\Omega} \sim e^{A(s)\cdot t} \tag{2.36}$$

where,

$$t = -2p^2(1-cos\theta) \quad and \quad A(s) = 6\frac{[3.65(\sqrt{s}-1.8766)]^6}{1+[3.65(\sqrt{s}-1.8766)]^6}, \tag{2.37}$$

with $\sqrt{s}$ the c.m. energy in GeV and A(s) is given in $(GeV/c)^{-2}$. The inelastic channels are treated in an analogous fashion. The parametrization suggested by Huber and Aichelin [29] is used where fitted differential cross sections are extracted from one-boson-exchange (OBE) calculations:

$$\frac{d\sigma_{in}}{d\Omega} \ \approx\ a(s)exp\left[b(s)cos\theta\right]. \tag{2.38}$$

The $a(s)$ and $b(s)$ are functions of $\sqrt{s}$ and vary in their definition for different intervals of $\sqrt{s}$ (see Table 2.3). θ is the polar angle.

Table 2.3: a(s) and b(s) as a function of the c.m. energy.

$\acute{x} = \sqrt{s}\ (GeV)$	$a\ (fm)$	b
2.104 - 2.12	$294.6(\acute{x}-2.014)^{2.578}$	$19.71(\acute{x}-2.014)^{1.551}$
2.12 - 2.43	$\frac{0.01224}{(\acute{x}-2.225)^2\ +\ 0.004112}$	$19.71(\acute{x}-2.014)^{1.551}$
2.43 - 4.50	$\left(\frac{2.343}{\acute{x}}\right)^{43.17}$	$33.14\ arctan(0.5404(\acute{x}-2.146)^{0.9784})$

2.2.4 Pauli blocking

Pauli blocking is a delicate quantum feature that need to be implemented within the semi classical theory (IQMD model) for the better understanding of reaction dynamics with large precision. There are mainly two methods mentioned in the literature to involve the Pauli exclusion principle within a transport model simulation. One is to introduce the Pauli potential corresponding to short range repulsion between the neighboring nucleons in the phase space. Second is by blocking the collisions and hence preventing the nucleons from being in an overpopulated state of phase space. This method is highly recommended method to be used for the study of heavy-ion reactions as the former method involve the formation of highly excited and big fragments. Therefore, additional statistical break-up (afterburner) has to be used to get exact fragment multiplicities. To avoid such inconvenience, second method is adopted for the present study. The phase space around the scattered nucleons is checked during the course of reaction. The collisions among the nucleons are blocked if the scattered nucleons are found to enter an already occupied (fully or partially) state in the phase space region. For the sake of simplicity, we assume that each nucleon occupies a sphere in coordinate and momentum space whereas two spheres are not allowed to overlap in accordance with the Pauli exclusion principle. This trick yields the same Pauli blocking ratio as obtained by an exact calculation of the overlap of the Gaussians. We calculate the fractions P_1 and P_2 of final phase spaces for each of the two scattering partners that is already occupied by other nucleons. The collision is blocked with a probability

$$P_{block} = 1 - [1 - min(P_1, 1)]\,[1 - min(P_2, 1)]\,, \tag{2.39}$$

and, correspondingly, is allowed with probability $1 - P_{block}$. For a nucleus in its ground state, we obtain an average blocking probability $< P_{block} >$ of 0.96. For absolute blocking, this factor should be one. From above description, it is clear that the Pauli factor will be zero or one depending whether the final phase-space is occupied or not. This sharp occupancy is valid for the cold nuclear matter only. Faessler *et al.* [30] were the first to include the temperature by smearing the Fermi spheres for Pauli-operator. Interestingly, the effect of this exercise was not drastic and one can neglect the temperature dependence of the Pauli-operator.

2.3 Numerical test

The basic requirement of a transport model to be used for the investigation of heavy-ion collision is to justify the ground state properties (e.g. stability) of nuclei on a time scale which is comparable to the time required for a nucleon-nucleon collision. Numerous number of numerical tests have been performed by various groups to validate the well established IQMD model over a wide range of atomic nuclei. Many of these are Heidelberg-Nantes-Frankfurt-Tübingen-Chandigarh. It is well established that the nucleon inside the nucleus moves under the influence of mean field potential generated by other nucleons and covers a significant distance during its motion upto 200 fm/c. Whenever the nucleon tries to approach the surface, it is pulled back by the other nucleons to keep it confined within a sphere of radius R.

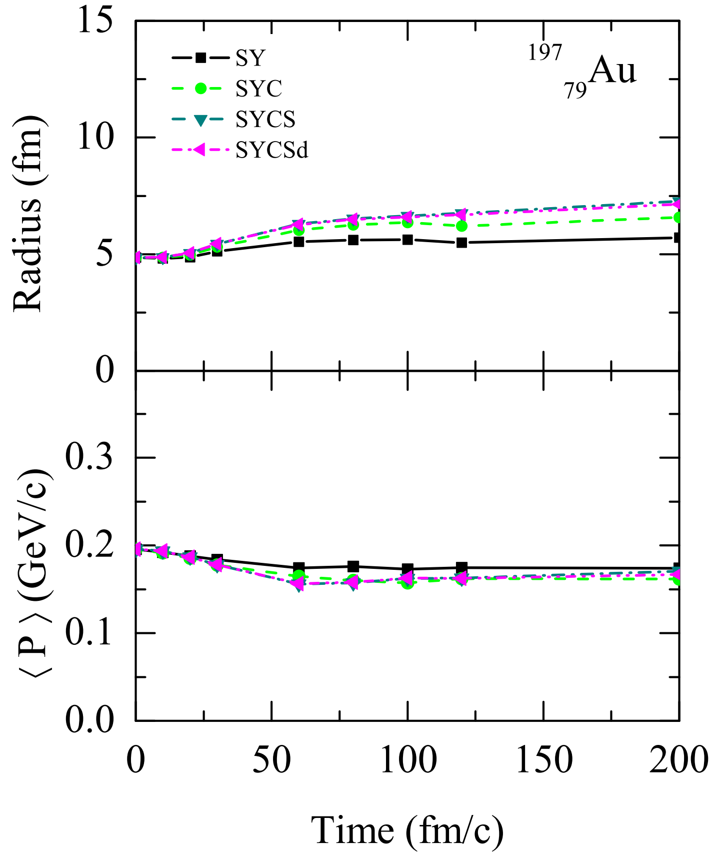

Figure 2.5: Time evolution of r.m.s. radius of $^{197}_{79}$Au nucleus and average momentum ($\langle P \rangle$) of nucleons under the influence of different sets of components of nuclear potential.

In the present study, various numerical tests have been performed by analyzing the ground state properties of gold nucleus under the influence of different components of nucleon-nucleon interaction potential. Fig. 2.5 shows the r.m.s. radius and momentum for $^{197}_{79}$Au nucleus under the influence of different sets of components of nuclear potential. Different acronyms used are defined as follow. SY stands for Skyrme + Yukawa potential, SYC stands for Skyrme + Yukawa + Coulomb potential, SYCS stands for Skyrme + Yukawa + Coulomb + symmetry potential, SYCSd stands for Skyrme + Yukawa + Coulomb + density dependent symmetry potential (with $\gamma = 0.66$). It is observed that

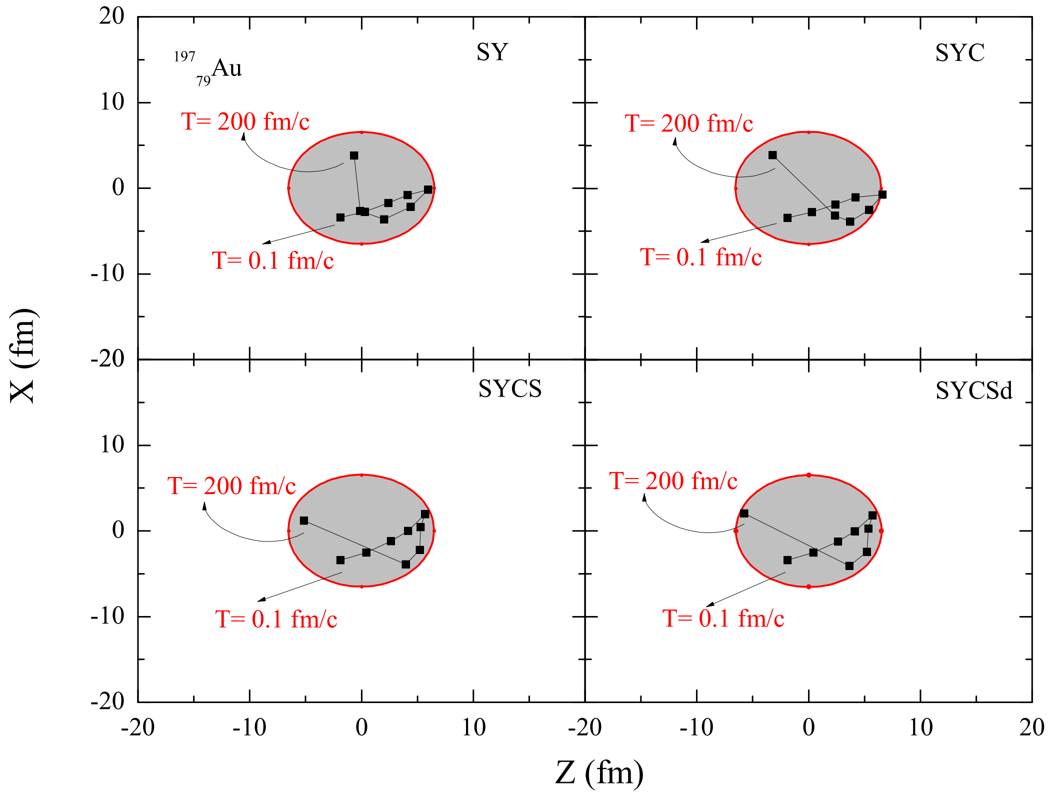

Figure 2.6: Trajectory of single nucleon under the influence of different components of nuclear potential.

for SY set of potential, the radius of nucleus and momentum of nucleons oscillates around its mean value throughout the time evolution of the reaction. However, with the addition of other components of nuclear potential such as Coulomb potential and symmetry potential, the r.m.s. radius increases. This is due to the repulsion generated in the system with the addition of these potentials. However, the particle inside the nucleus remains confined within its radius (shown in Fig. 2.6). The repulsion generated in the system with the addition of different potentials change the trajectory of nucleon. The oscillations of r.m.s.

radius and momentum around the mean value increases by including all the components of nuclear potential. This is due to the reason that for the given initialization, the potentials are not saturated. In order to achieve stability, the potential energy of the system is converted into kinetic energy and vice versa. As already mentioned in Sec. 2.2.2 that the momentum dependent potential becomes active if and only if the overlapping of projectile and target nucleons takes place. Since we are studying the ground state properties of single nucleus, hence no collisions are taking place. Therefore, the momentum dependent potential is excluded to check the stability of nucleus.

2.4 Different Methods of Clusterization

In the following subsections, the secondary models used to clusterize the phase space of nucleons are discussed.

2.4.1 Minimum Spanning Tree (MST) method

In MST [10], two nucleons share the same fragment, if their centroids are closer than a distance d_{min},

$$|\mathbf{r}_i - \mathbf{r}_j| \leq d_{min}, \tag{2.40}$$

where $\mathbf{r}_i$ and $\mathbf{r}_j$ are the spatial positions of both nucleons. The minimum distance d_{min} has been used as a free-parameter which varies between 2-4 fm. The influence of clusterization range on multi-fragmentation (at 200-300 fm/c) is reported to be small [31]. This approach (being a spatial distance approach) cannot detect different fragments which are (almost) overlapping and therefore, will give a single big fragment during the early stage of the reaction where density is quite high and the interactions among the nucleons are still active. In other words, the simple coordinate space approach cannot address the question of time scale of the fragments. To study the time of fragment formation, one needs to device a method which should be able to detect the overlapping fragments.

Modification in clusterization method has been suggested, which is discussed as follow.

2.4.2 Minimum Spanning Tree with Momentum cut (MSTM) method

In addition to spatial cut in Eq. 2.40, Kumar *et al.* [32] introduce a cut on relative momenta of two nucleon i.e.

$$|p_i - p_j| \leq p_F \tag{2.41}$$

Here, p_F is the average Fermi momentum of nucleons bound in a nucleus ($\approx$ 268 MeV/c) in its ground state. It will help to get rid of fragments that although close in space are far in momentum space. This method checks the formation of artificial and unstable fragments by excluding those nucleons having relative momenta larger than p_F. Both MST as well as MSTM method give different results at the start of a reaction. MST gives one largest cluster of size ($= A_P + A_T$), while MSTM method gives two distinct clusters of masses A_P and A_T having very large relative momenta. This algorithm identifies the largest fragment A^{max} as early as 50-60 fm/c [32].

2.4.3 Isospin-dependent Minimum Spanning Tree (isoMST) method

The isoMST method addresses the isospin dependence of cluster recognition criterion [33]. In the regular MST method, the spatial constraint between the two nucleons to share the same fragment was assumed to be fixed, irrespective of the isospin of the nucleons. However, introducing the isospin-dependence in the cluster recognition method, different values of spatial constraints are assigned depending upon the isospin of nucleon, which share the same fragment. Using this method, significant effect on heavy-ion collision observables is seen for R_0^{nn}=R_0^{np}= 6 fm and R_0^{pp}= 3 fm. The value of momentum constraint (P_0) is kept fixed as 250 MeV/c. The long range Coulomb repulsion is the reason for taking a smaller value of R_0^{pp}. However, the properties of neutron-rich nuclei, e.g. neutron skin or neutron halo effects are responsible for choosing a large value of R_0^{nn} or R_0^{np}.

2.4.4 Gemini model

The GEMINI code [34] is a statistical model based on the sequential binary decays. In this code, the excitation energy, angular momentum, charge, and mass of the hot fragment is used to calculate the decay path. A Monte Carlo technique is adopted to follow the decay chains of individual compound nuclei. The decay chain continue until we get a stable resulting product. The Hauser-Feshback formalism is used to calculate the decay width of light charged particles ($Z \leq 2$), however, the fission channel is calculated from Bohr-Wheeler formalism. The binding energy of heavy systems ($A > 12$) is calculated by using the Yukawa-plus-exponential model without including the shell and pairing correction term to calculate a series of sequential binary decays. On the other hand, the binding energy of very light system is calculated using their experimental masses. It is important to note that while using the GEMINI code to cool the hot fragments as an afterburner to a dynamic simulations some assumptions are applied such as the decay of hot nucleus is calculated by assuming it to be spherical in shape and at normal nuclear matter density. Moreover, after the decay by GEMINI the final product and their trajectories are defined and Coulomb forces or nuclear forces are not considered anymore.

Bibliography

[1] J. Cugnon, T. Mizutani, and J. Vandermeulen, Nucl. Phys. A **352**, 505 (1981).

[2] Y. Yariv and Z. Frankel, Phys. Rev. C **20**, 2227 (1979).

[3] P. Bonche, S. Koonin, and J.W. Negele, Phys. Rev. C **13**, 1226 (1976); R. Cusson and J. Maruhn, Phys. Rev. Lett. **36**, 1166 (1976).

[4] C.Y. Wong, Henry H.K. Tang, Phys. Rev. Lett. **40**, 1070 (1978)

[5] E. Suraud, Ch. Gregoire, and B. Tamain, Prog. Part. Nucl. Phys. **23**, 357 (1989)

[6] G.F. Bertsch, H. Kruse and S. Das Gupta, Phys. Rev. C **29**, 673 (1984).

[7] G.F. Bertsch, H. Kruse, and S. Das Gupta. Phys. Rev. C **29**, R673 (1984); J. Aichelin and G. Bertsch, Phys. Rev. C **31**, 1730 (1985)

[8] C. Gregoire, B. Remaud, F. Sebille, L. Vinet, and Y. Raffray, Nucl. Phys. A **465**, 317 (1987)

[9] H. Kruse, B.V. Jacak, and H. Stöcker, Phys. Rev. Lett. **54**, 289 (1985)

[10] J. Aichelin, Phys. Reports **202**, 233 (1991).

[11] C. Hartnack, R.K. Puri, J. Aichelin, J. Konopka, S.A. Bass, H. Stöcker and W. Greiner, Eur. Phys. J. A **1**, 151 (1998).

[12] M. Trefz, A. Faessler, and W.H. Dickhoff, Nucl. Phys. A **443**, 499 (1985); N. Ohtsuka, R. Linden, A. Faessler, and F.B. Malik, Nucl. Phys. A **465**, 550 (1987).

[13] H. Feldmeier, Nucl. Phys. A **515**, 147 (1990); H. Feldmeier and J. Schnack, Prog. Part. Nucl. Phys. **39**, 393 (1997).

[14] A. Ono, H. Horiuchi, T. Maruyama, and A. Ohnishi, Phys. Rev. Lett. **68**, 2898 (1992); A. Ono and H. Horiuchi, Phys. Rev. C **51**, 299 (1995); *ibid.* Prog. Part. Nucl. Phys. 53, 501 (2004).

[15] J. Molitoris, J.B. Hoffer, H. Kruse and H. Stöcker, Phys. Rev. Lett. **53**, 899 (1984).

[16] L. Wilets, Y. Yariv, and R. Chestnur, Nucl. Phys. A **301**, 359 (1978).

[17] S.M. Kiselew and Y.E. Polrowskil, Sov. Journ, Nucl. Phys. **38**, 46 (1983).

[18] Z.Q. Feng, Phys. Rev. C **85**, 014604 (2012).

[19] C. Hartnack, H. Oeschler, J. Aichelin, Phys. Rev. Lett. **96** (2006) 012302;

[20] C. Fuchs, A. Faessler, E. Zabrodin, Y.M. Zheng, Phys. Rev. Lett. **86** (2001) 1974;

[21] H. Yukawa, Phys. Rev. **76**, 300 (1949); H. Yukawa, Nobel Lecture, Dec. 12 (1949).

[22] L.G. Arnold *et al.*, Phys. Rev. C **25**, 936 (1982); G. Passatore, Nucl. Phys. A **95**, 694 (1967).

[23] B.A. Li, L.W. Chen and C.M. Ko, Phys. Rep. **464**, 113 (2008).

[24] B. A. Li, C. M. Ko, and W. Bauer, Int. J. of Mod. Phys. E **7**, 147 (1998).

[25] B. A. Li, Phys. Rev. C **69**, 034614 (2004).

[26] S.A. Bass, C. Hartnack, H. Stöcker, and W. Greiner, Phys. Rev. C **51**, 3343 (1995); B.J. VerWest and R.A. Arndt, Phys. Rev. C **25**, 1979 (1982); H. Kruse, B.V. Jacak, and H. Stöcker, Phys. Rev. Lett. **54**, 289 (1985); J.J Molitoris and H. Stöcker, Phys. Rev C **32**, R346 (1985).

[27] J. Cugnon, Phys. Rev. C **22**, 1885 (1980).

[28] P. Danielewicz and G.F. Bertsch, Nucl. Phys. A **533**, 712 (1991).

[29] S. Huber and J. Aichelin, Nucl. Phys. A **573**, 587 (1994).

[30] R.K. Puri, N. Ohtsuka, E. Lehmann, A. Faessler, M. A. Matin, Dao T. Khoa, G. Batko, and S.W. Huang, Nucl. Phys. A **575**, 733 (1994).

[31] G. Peilert, J. Konopka, H. Stöcker, W. Greiner, M. Blann, and M. G. Mustafa, Phys. Rev. C **46**, 1457 (1992).

[32] S. Kumar and R.K. Puri, Phys. Rev. C **58**, 320 (1998).

[33] Y. Zhang, Z. Li, C. Zhou, M. B. Tsang, Phys. Rev. C **85**, 051602(R) (2012).

[34] R.J. Charity, M.A. McMahan, G.J. Wozniak, R.J. McDonald, L.G. Moretto, D.G. Sarantites, L.G. Sobotka, *et al.*, Nucl. Phys. A **483**, 371 (1988).

Chapter 3

Effect of nucleon-nucleon potentials on anisotropic flow

3.1 Introduction

Reaction dynamics has always captured an important place in nuclear physics community mainly due to wider domain of the physics it caters. The measurements of collective motion [1] and, in particular, the directed transverse flow [2–4] have been predicted to provide crucial information for establishing the strength of nuclear equation of state [5–7]. It has also been used extensively over the past three decades to study the properties of hot and dense nuclear matter pinning down the nuclear matter equation of state as well as the in-medium nucleon-nucleon cross section. The dependence of directed transverse flow on the above mentioned parameters has revealed much interesting physics [1, 2, 6, 7]. In the recent years, many groups have performed experiments to study the energy dependence of directed flow and their study reveals that, there is a transition of the flow from negative scattering angles to positive scattering angles with increase in incident energy [8]. At low incident energies, the dominance of attractive mean field prompt the scattering of particles to negative deflection angles, thus producing negative flow, whereas repulsive NN collisions at higher incident energies result in the emission of particles into positive deflection angles and hence yield positive flow. At a particular beam energy, where the repulsive NN interactions balance the attractive nuclear mean field interactions, the collective transverse flow disappears. The beam energy at which this transverse flow disappears is termed as the balance energy (E_{bal}) or energy of vanishing flow (EVF) [2, 9]. The observation of balance energy has triggered intensive theoretical and experimental investigations. The balance energy is found to be sensitive towards the size of the system

[7], colliding geometry [3, 10], nuclear matter equation of state, the NN cross section [11] mass asymmetry of the reaction and isospin content [12]. Ideally, reactions can be analysed with the help of G-matrix, where real part is responsible for its propagation, whereas, imaginary part leads to nucleon-nucleon scattering. In simulations, one, however, uses separate parameterized form for both real and imaginary parts of the G-matrix. While parameterizing the potential, one starts with nuclear matter interaction represented by the Skyrme interaction and then adds additionally various components such as Coulomb, Yukawa, symmetry potentials as well as momentum dependent potential.

In other words, nucleon-nucleon interaction potential consists of Skyrme (density dependent), Yukawa (surface dependent), Coulomb, momentum dependent and density dependent symmetry components. The effect of Coulomb repulsion on balance energy (E_{bal}) has been studied for various asymmetric reactions and it has been found that sensitivity of E_{bal} increases towards the larger asymmetric reactions [12]. Momentum dependence of the EOS has also played a crucial role in heavy-ion collisions. The initial attempts with momentum dependent interactions showed a drastic effect on the collective flow as well as particle production [7, 13–15]. The particle propagating under the influence of MDI are deflected towards the transverse direction during the early phase of the reaction. As a result, transverse flow increases considerably. However, the particle production is found to be reduced drastically with the inclusion of momentum dependent interactions. On employing momentum dependent forces, the kaon production is reduced by a factor of four [13]. Puri and collaborators [7] shed light on the influence of MDI on E_{bal} and found that sensitivity of E_{bal} is different towards the lighter colliding nuclei compared to the heavier ones. Recently, symmetry potential and its density dependence has been studied and both are found to be sensitive towards collective flow [16–18]. Giant dipole resonance's (GDR) peak energy and full width at half maxima has also been studied and is found to be sensitive towards the symmetry energy [19].

Lot of experiments on balance energy/directed flow have been performed and the results are verified by various theoretical models. Many of these are, however, by using Boltzmann-Uehling-Uhlenbeck (BUU)model [20, 21]. A few of these are also reported by using quantum molecular dynamics model (QMD) [10, 13, 22]. The collective flow was measured for the first time by the Berkeley group for $^{40}Ca+^{40}Ca$ and $^{93}Nb+^{93}Nb$ at 400

MeV/nucleon using plastic ball detector at BEVALAC [23]. The first attempt to measure balance energy was made by MSU group [24]. INDRA collaboration at GANIL studied the E_{bal} as a function of impact parameter for ^{40}Ar + ^{27}Al reaction. Later on, impact parameter dependence of balance energy was studied for ^{64}Zn + ^{27}Al, ^{40}Ar + ^{45}Sc, ^{58}Ni + ^{58}Ni, ^{86}Kr + ^{93}Nb and ^{197}Au + ^{197}Au reactions respectively [21,25]. Interestingly, most of these studies take symmetric or nearly symmetric reactions into account. Experimentally, Pak *et al.* [3] studied the isospin effects on the collective flow and balance energy for central and peripheral colliding geometries and compared the results with the theoretical calculations. Liewen *et al.* [26] studied the effect of isospin degree of freedom on the collective flow and EVF using the isospin dependent QMD model. The calculated results were found to differ from the data at all colliding geometries.

In addition to this, the transverse flow (v_1) was first predicted by using fluid-dynamic model for semi-central heavy-ion collisions [27]. Soon after this, the same was observed experimentally [28]. The transverse flow was found to reach its maximum value at about 400 MeV/nucleon [29]. The dependence of transverse flow on system mass [5,30] and the isospin content [3] have also been investigated experimentally. Westfall [31] and Magestro *et al.* [32] showed that the EVF is independent of the particle type. However, Russotto *et al.* [33] have reported the energy of vanishing flow for hydrogen isotopes which is found to higher than that of helium isotopes by more than 10 MeV/nucleon. Recently, Wang *et al.* [34] studied the influence of medium-modified nucleon-nucleon elastic cross section (NNECS), isospin-dependent cluster recognition criteria and different equation of states on transverse and elliptical flow (v_2) of light charged particles by using UrQMD model. Anisotropic flows were found to be sensitive towards the NNECS, but not sensitive towards the different cluster recognition criteria. Besides the spatial constraints, however, the momentum constraints are also expected to affect the flow of light fragments.

Unfortunately, very few studies are available on the theoretical side, when we talk about the contribution of various potentials on collective flow of nucleons and the effect of various momentum constraints on fragment flow. The aim of the present chapter is atleast two fold. First is to study the contribution of various potentials towards the transverse directed flow and the balance energies for the different reactions and second is to explore the effect of isospin dependent spatial and momentum constraints on the transverse flow of light fragments.

3.2 Results and discussion

For the present study, we simulate several thousand events for the reactions of $^{58}_{26}$Fe+$^{58}_{26}$Fe, $^{58}_{28}$Ni+ $^{58}_{28}$Ni, $^{86}_{36}$Kr+ $^{93}_{41}$Nb and $^{197}_{79}$Au+ $^{197}_{79}$Au at the incident energies ranging between 60 and 140 MeV/nucleon in steps of 20 MeV/nucleon, using soft equation of state. A reduced cross section $\sigma_{red} = 0.8\sigma_{nn}^{free}$ is used in the study [35]. For the choice of impact parameter, the whole geometrical range is divided into four bins - BIN(I), BIN(II), BIN(III) and BIN(IV) i.e. $0 < \hat{b} \leq 0.28$, $0.28 < \hat{b} \leq 0.39$, $0.39 < \hat{b} \leq 0.48$, $0.48 < \hat{b} \leq 0.56$, where $\hat{b} = b/b_{max}$ with $b_{max} = 1.12(A_1^{1/3} + A_2^{1/3})$. The choice of impact parameter is based on the constraints imposed by the experimental measurements [4]. The time evolution of each reaction is followed till the transverse flow saturates. For the present heavy-ion reactions, the saturation time is kept 200 fm/c.

3.2.1 Time evolution of directed transverse flow

In Fig. 3.1, the time evolution of $\langle P_x^{dir} \rangle$ for the reaction of $^{58}_{26}$Fe+ $^{58}_{26}$Fe is displayed. The upper limit of scaled impact parameter bin for these events is $\hat{b} = 0.28$. The calculations were performed for different sets of potentials with energy varying between 60 and 140 MeV/nucleon in steps of 20 MeV/nucleon. In order to study the contribution of various components of potential towards the balance energy, we started with basic potential and then added other terms of potentials followed by resimulation of the reaction. This procedure is repeated for all sets of components of potential. The acronym SY stands for Skyrme + Yukawa potential, SYC stands for Skyrme + Yukawa + Coulomb potential, SYCM stands for Skyrme + Yukawa + Coulomb + momentum dependent potential, SYCMS stands for Skyrme + Yukawa + Coulomb + momentum dependence + symmetry potential and SYCMSd stands for Skyrme + Yukawa + Coulomb + momentum dependence + density dependent symmetry potential with $\gamma = 0.66$. The symmetry energy varies with the density according to the Eq. 2.31. From Fig. 3.1, it is clear that

1. During the initial phase of the reaction, transverse directed flow always attains a negative value pointing towards the dominance of attractive interaction between colliding nucleons. With the passage of the time, the transverse flow becomes less

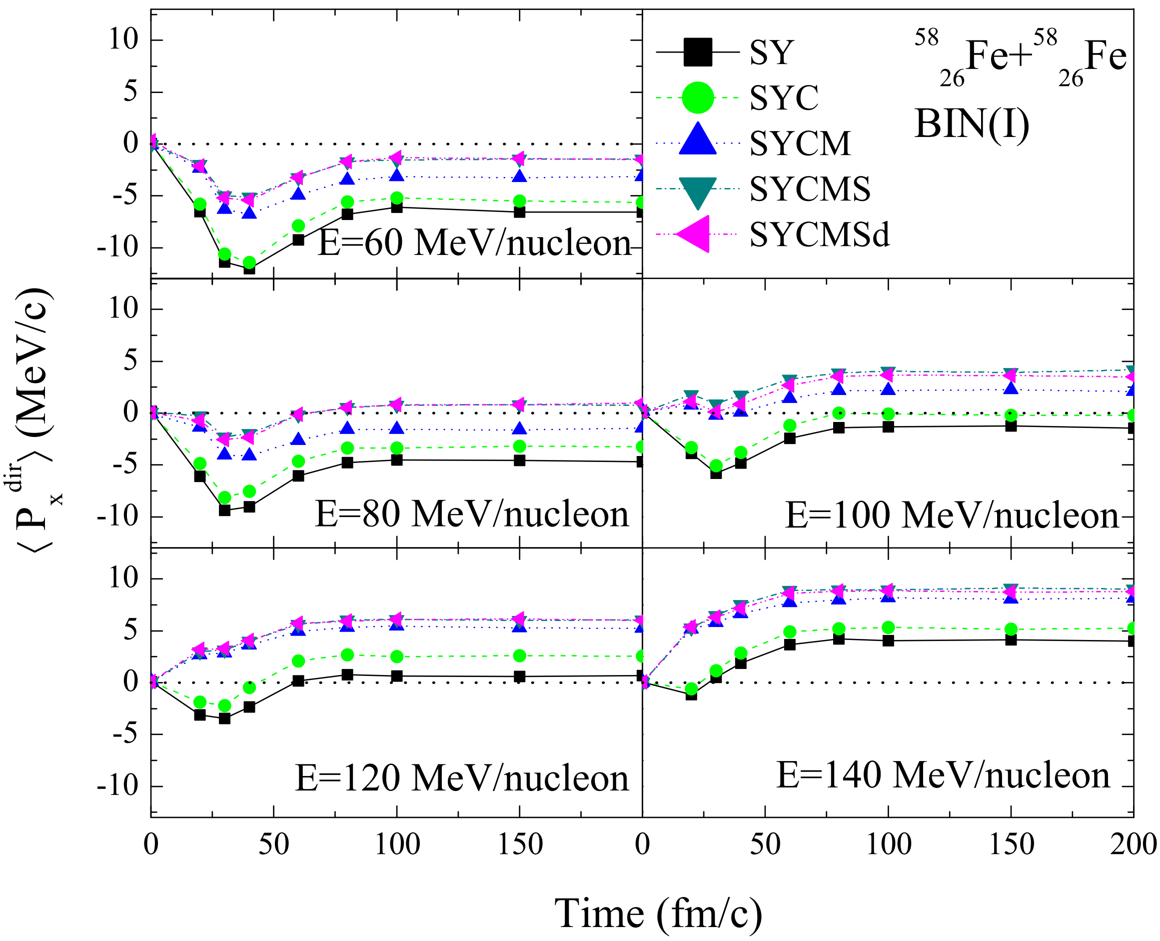

Figure 3.1: Time evolution of $\langle P_x^{dir} \rangle$ at incident energies 60, 80, 100, 120, 140 MeV/nucleon for different set of potentials. Various acronyms (SY, SYC, SYCM, SYCMS, SYCMSd) are explained in the text.

negative and ultimately saturates at about 100 fm/c. This saturation time changes with increase in the incident energy as nucleons collide at faster speed. With the increase in the incident energy, the high dense phase is created much earlier during the course of the reaction, that leads to early finishing of the reaction.

2. At low incident energies, the less availability of the free phase space does not allow frequent binary nucleon-nucleon collisions; therefore, interactions remain attractive at these incident energies. However, at higher incident energies one has frequent nucleon-nucleon binary collisions responsible for the repulsive behavior of the net

nuclear interactions.

3. Moreover, transverse directed flow becomes more positive or less negative with the increase in the incident energy as well as with the addition of various components of potentials. The gradual contribution of various potentials impart additional repulsion to the colliding partners. Due to this reason, the net transverse flow becomes more positive.

3.2.2 Rapidity dependence of $\langle P_x/A \rangle$

Figs. 3.2 and 3.3, display the directed flow in terms of final state transverse momentum ($\langle P_x/A \rangle$) as a function of rapidity distribution for the reactions ${}^{58}_{28}$Ni+ ${}^{58}_{28}$Ni and ${}^{58}_{26}$Fe+ ${}^{58}_{26}$Fe, respectively. The displayed results are for scaled impact parameter BIN(I) and different

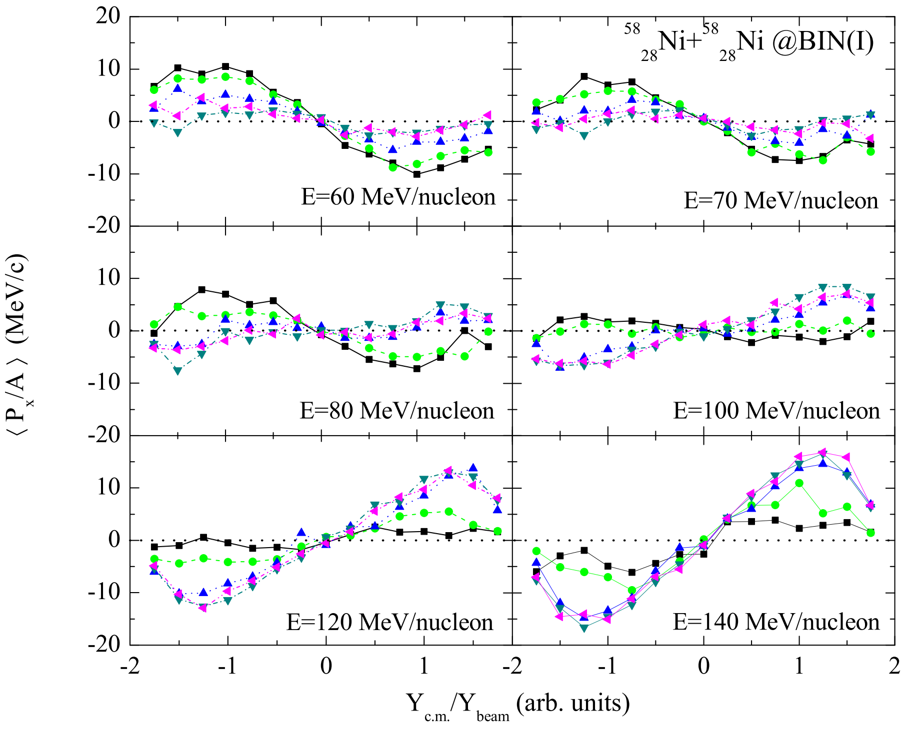

Figure 3.2: Rapidity distribution of $\langle P_x/A \rangle$ for the reaction ${}^{58}_{28}$Ni+${}^{58}_{28}$Ni at E = 60, 70, 80, 100, 120, 140 MeV/nucleon for different set of potentials at reduced impact parameter bin= BIN(I). Various acronyms have the same meaning as in Fig. 3.1.

panels indicate the results plotted at various incident energies. Each line corresponds to different sets of components of nuclear potential. One can clearly see that the nuclear flow depicts a well known behaviour. In Fig. 3.2, the effect of isospin is seen due to slight difference in the number of neutrons. The slope of $\langle P_x/A \rangle$ plot is used to extract the information about the balance energy. In all cases, we take the slope of these plots at various energies. The slope is negative at lower incident energies which changes to positive value at higher incident energies. Between these two limits, the slope becomes nearly flat and the energy at which this occurs is regarded as the balance energy. The experimental value of balance energy for the system $^{58}_{28}Ni + ^{58}_{28}Ni$ is 69 ± 3 MeV/nucleon for BIN(I) [3], and theoretically, the simulations including all the components of interaction potential, predict balance energy at around 70 MeV/nucleon. One also notices that the nuclear

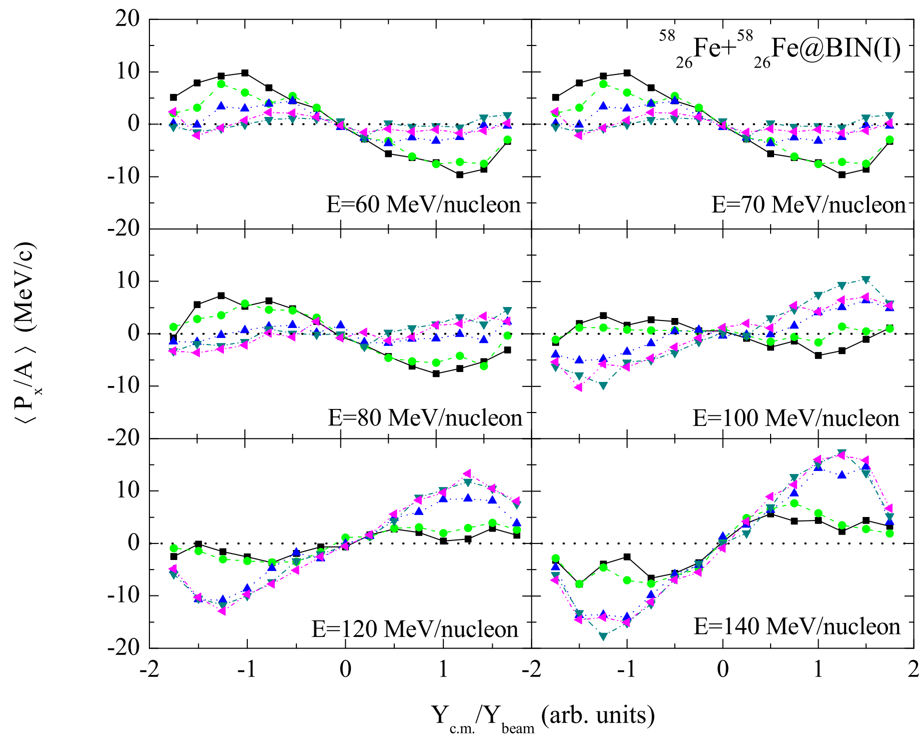

Figure 3.3: Same as Fig. 3.2, but for the system $^{58}_{26}$Fe+$^{58}_{26}$Fe.

flow attains a more positive value with the addition of various potentials. Although, the values of $\langle P_x/A \rangle$ corresponding to the SYCM and SYCMS potentials do not differ much compared to those of the SYCMSd, there is a visible difference for SY and SYC compared to SYCM at all the incident beam energies. This difference between the various sets of potentials shed light on the significance of Coulomb and momentum dependent interactions in heavy-ion collisions.

This method ($\langle P_x/A\rangle$) offers a rather complicated way to study the directed transverse flow in comparison to the $\langle P_x^{dir}\rangle$. Therefore, to further explore the contribution of specific potential, results are elaborated in the following figures by using $\langle P_x^{dir}\rangle$ as an observable.

3.2.3 The transverse directed flow as a function of incident energy for various impact parameter bins

Figs. 3.4 and 3.5 represent the variation of $\langle P_x^{dir}\rangle$ as a function of incident energy of colliding partners for the reactions of $^{58}_{28}$Ni+ $^{58}_{28}$Ni and $^{58}_{26}$Fe+ $^{58}_{26}$Fe, respectively. The results are calculated using four different reduced impact parameter bins. The data points [3] are represented by stars and a horizontal line on the data point indicates experimental errors. Experimental values of the balance energy for the reactions of $^{58}_{28}$Ni+ $^{58}_{28}$Ni are $69 \pm 3, 72 \pm 3, 80{\pm}3, 84{\pm}5$ MeV/nucleon, for the BIN(I), BIN(II), BIN(III), and BIN(IV), respectively, whereas the simulations, including all the components of interaction potential has balance energy at 77, 78, 80 and 85 MeV/nucleon, respectively for the BIN(I), BIN(II), BIN(III) and BIN(IV). Although, the values of $\langle P_x^{dir}\rangle$ corresponding to SYCM and SYCMS sets of potentials do not differ much compared to SYCMSd set of potentials, there is a visible difference for SY and SYC compared to SYCM at all impact parameter bins.

This difference in the balance energy due to various sets of potentials shed light on the significance of the Coulomb potential, momentum dependent interactions and symmetry potential in heavy-ion collisions. One can clearly see that:

1. Transverse directed flow increases with the increase in the incident energy and there is a transition of the nuclear flow from negative to positive value with increase in the incident energy. This is true at all the impact parameter bins as well as for all sets of the potentials. The value of the incident energy corresponding to the net zero flow is the balance energy of the transverse directed flow. At this incident energy, the two opposing forces (attractive mean field at low energies and repulsive nucleon-nucleon collisions at high energies) counter-balance each other and ceases the net motion of the compressed nuclear matter.

2. As mentioned earlier, the value of $\langle P_x^{dir}\rangle$ becomes more positive with the participa-

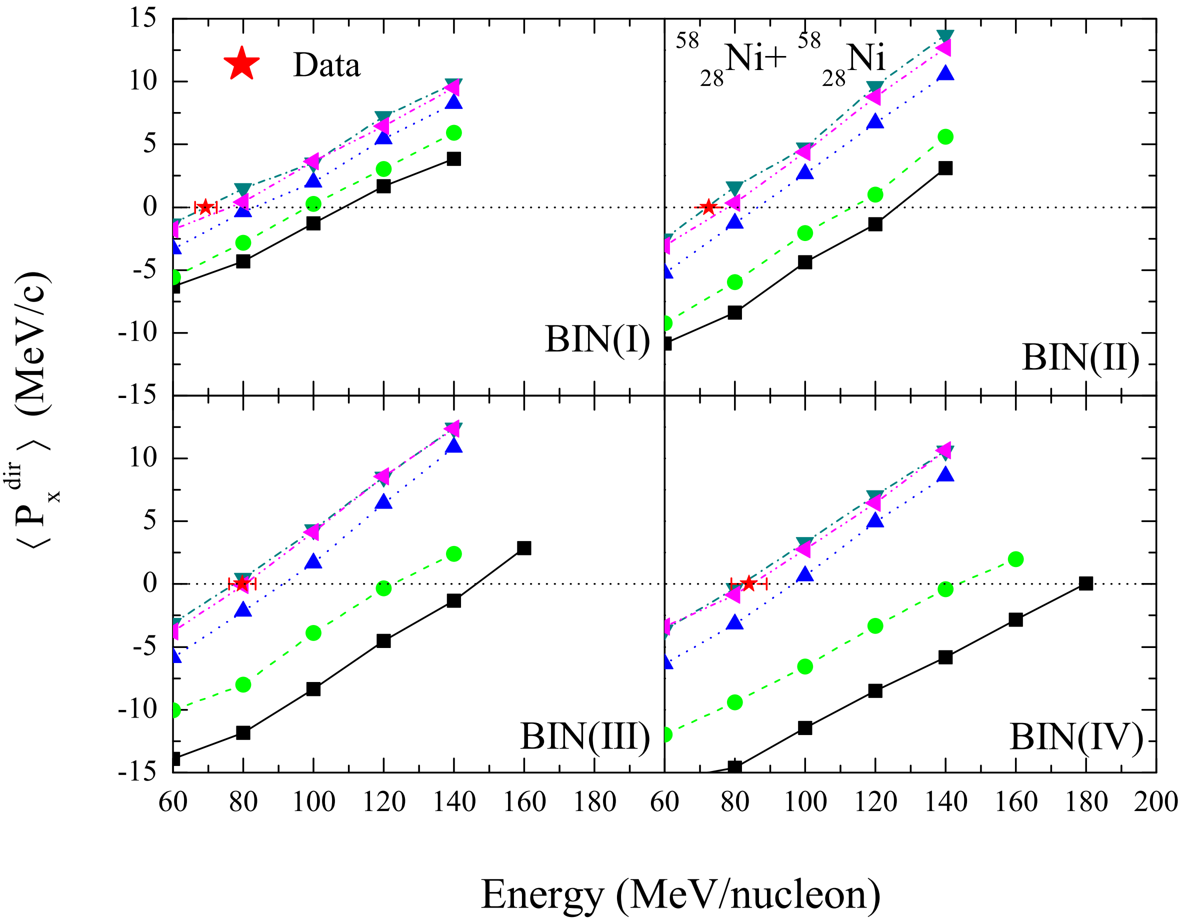

Figure 3.4: Incident energy dependence of the final stage directed flow $\langle P_x^{dir} \rangle$ for the reaction of $^{58}_{28}$Ni+ $^{58}_{28}$Ni at different impact parameter bins. Different symbols have the same meaning as in Fig. 3.1.

tion of Coulomb potential, followed by the momentum dependent interactions, the symmetry potential further add to the repulsion. However, the density dependence of the symmetry potential does not play a significant role. The participation of these potentials provide extra repulsion to the colliding matter, thereby increasing the transverse directed flow. Although the contribution of symmetry potential is quite small, it is still noticeable. The minor contribution of the symmetry potential is primarily attributed to the increase in the neutron content.

3. As one moves from lower to higher impact parameter bins, the dominance of the

Coulomb potential and MDI decreases considerably due to the decrease in the participant zone. As a result, there is a net reduction in the number of binary nucleon-nucleon collisions and hence transverse directed flow.

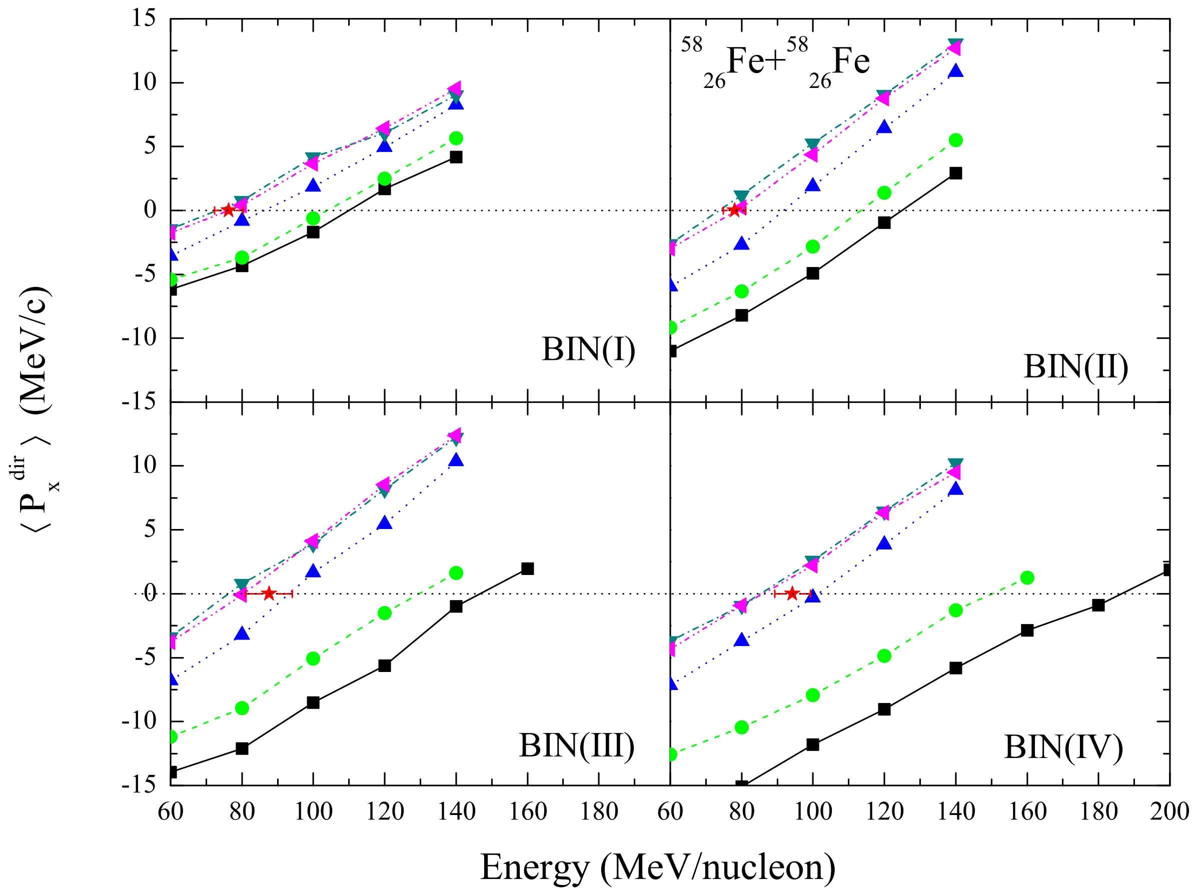

Figure 3.5: Same as in Fig. 3.4, but for the reaction of $^{58}_{26}$Fe+ $^{58}_{26}$Fe.

Further, to explore the isospin dependence of directed transverse flow, in Fig. 3.5, the $\langle P_x^{dir} \rangle$ as a function of beam energy for the reactions of $^{58}_{26}$Fe+$^{58}_{26}$Fe is displayed. The calculated values of balance energy for this reaction are 77, 79, 81 and 86 MeV/nucleon for BIN(I), BIN(II), BIN(III) and BIN(IV) respectively, whereas the experimentally observed values corresponding to these impact parameter bins are $76 \pm 4, 78 \pm 3, 88 \pm 6$ and 94 ± 4 MeV/nucleon. Interestingly, we find that with the increase in the neutron content, the balance energy shifts towards the higher end. This has been attributed to the fact that neutron-neutron (σ_{nn}) and proton-proton (σ_{pp}) cross section is a factor 3 times smaller than the neutron-proton (σ_{np}) cross section. Due to this reason, collective flow becomes less repulsive and results in net increase in the energy of disappearance of flow.

3.2.4 The impact parameter dependence of energy of vanishing flow

To further explore the contribution of various potentials on the balance energy, in Fig. 3.6, the E_{bal} as a function of scaled impact parameter $\hat{b} = b/b_{max}$ is displayed, where b_{max} represents the largest estimated impact parameter for a simulated event, for the system $^{58}_{26}Fe +^{58}_{26} Fe$ (a), $^{58}_{28}$Ni+ $^{58}_{28}$Ni (b), $^{86}_{36}$Kr+ $^{93}_{41}$Nb (c) and $^{197}_{79}$Au+ $^{197}_{79}$Au (d), using soft EOS. The calculated values of E_{bal} are plotted at the upper limit of each impact parameter bin. Stars represents experimental data [3, 21] and vertical line on data points indicate experimental error. A careful look at Fig. 3.6 reveals that:

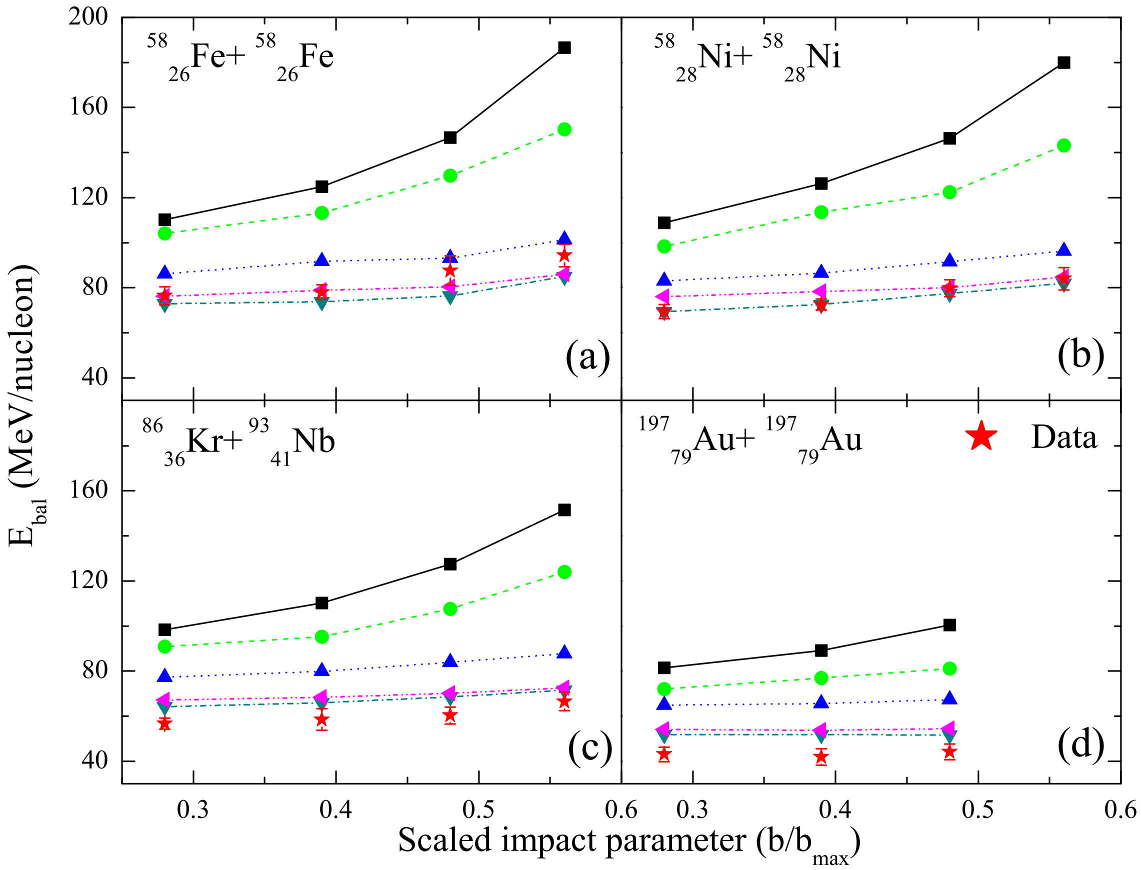

Figure 3.6: E_{bal} as a function of scaled impact parameter for the reaction of $^{58}_{26}$Fe+ $^{58}_{26}$Fe (a), $^{58}_{28}$Ni+ $^{58}_{28}$Ni (b), $^{86}_{36}$Kr+ $^{93}_{41}$Nb (c) and $^{197}_{79}$Au+ $^{197}_{79}$Au (d).

1. E_{bal} increases as a function of scaled impact parameter for all sets of potentials, which is in agreement with the findings of Pak *et al.* [3]. The cause of this behavior lies in the fact that with increase in the impact parameter, fewer nucleon-nucleon collisions yield reduced repulsive forces. As a result, mean field dominates. To conquer this effect, high value of incident energy is required to get net zero flow value. But, here we are able to more definitely extract the role of various potentials towards the E_{bal}. These results are also in agreement with Puri and collaborators [7].

2. In agreement with the results displayed in Figs. 3.4 and 3.5, E_{bal} decreases with the addition of Coulomb potential, momentum dependent potential and symmetry potential. The decrease due to Coulomb potential has been attributed to the repulsive behavior of the Coulomb forces. One notices that inclusion of MDI enhances the collective flow, therefore decreasing the balance energy. This decrease in the balance energy is due to the fact that MDI suppress the number of binary nucleon-nucleon collisions. Moreover, the addition of symmetry potential further reduces the balance energy to lower values. The effect of symmetry potential towards the balance energy is more pronounced as one moves from lighter to heavier masses. The reason behind this behavior is the increased number of neutron content.

3. With the increase in the combined mass of the system, the disappearance of flow occurs at relatively low values of incident energy. This happens due to frequent nucleon-nucleon collisions with increase in combined mass of the system.

Further, for the lighter systems, we are able to reproduce the balance energy close to the experimental data. However, for heavier systems the calculated values of balance energy lags behind the experimental values. This could be due to repulsive behaviour of the symmetry energy with increase in the number of neutrons. We also see a weaker dependence of the balance energy on the scaled impact parameter for heavier systems, when we considered SYCMSd interaction potential. This is in agreement with the findings of Magestro *et al.* [21].

Fig. 3.7 shows the tendency of single potential to pull down the balance energy for the reaction of $^{58}_{28}$Ni+ $^{58}_{28}$Ni at different colliding geometries with Coul= SY-SYC (Coul represent the change in the balance energy due to Coulomb interaction) , MDI = SYC-

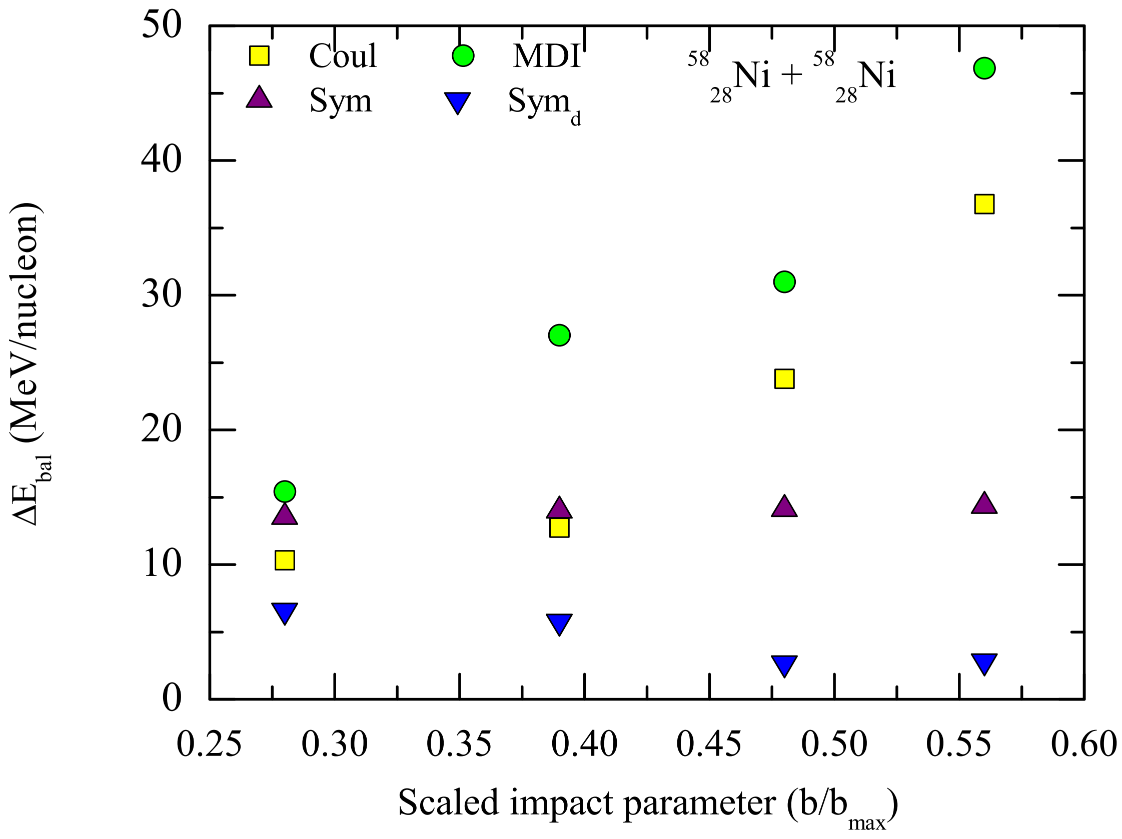

Figure 3.7: ΔE_{bal} as a function of scaled impact parameter for the reaction $^{58}_{28}$Ni+ $^{58}_{28}$Ni.

SYCM, Sym = SYCM-SYCMS and Sym_d = SYCMS-SYCMSd. The absolute value of ΔE_{bal} is plotted as a function of the scaled impact parameter. It is clear from the figure that the maximum change in the balance energy is observed due to the momentum dependent interactions followed by the Coulomb repulsion, symmetry potential and finally by the density dependent symmetry potential. The inclusion of MDI reduces the number of collisions at all colliding geometries by breaking the initial correlations among the nucleons and pushing the energy of vanishing flow towards lower energies. Moreover, the effect is enhanced at peripheral collisions. Coulomb interactions also play an important role at peripheral geometries. This is due to the repulsive nature of Coulomb interactions. In central collisions, the repulsion produced due to large number of charge particles in the participant zone, is stronger compared to peripheral collisions. However, symmetry potential corresponding to normal nuclear matter density reduces the change in the balance energy by a same amount at all impact parameters. However, if we take the density dependence of the symmetry energy into account the change in the balance energy with impact parameter decreases. It is observed that the results obtained are true for the entire mass range.

3.2.5 Effect of spatial and momentum constraints on transverse flow

The effect of spatial and momentum constraints have been carried out under the influence of all components of NN potential. Minimum spanning tree is the fastest method to construct the fragments by putting constraint on space coordinates of nucleons at the saturation time of a heavy-ion reaction. Studies have been carried out by putting constraints on momentum space also [36]. Since IQMD is capable of distinguishing between proton and neutron. Recently, it has been suggested that constraints in spatial and momentum coordinates of nucleons based on the isospin can give better configuration of fragments formed [37]. This method is well known as isoMST. In the present section, author has attempted to optimize the constraints among proton-proton, neutron-neutron and neutron-proton. The idea behind this attempt is that the proton-proton interaction is repulsive in contrast to the neutron-neutron and neutron-proton interaction. The isospin-dependent spatial and momentum constraints are supposed to give more stable fragment configurations. Adopting this procedure, the multiplicity of different mass fragments as well as free nucleons are affected.

In the present study, twenty thousand events were simulated for the reaction $^{197}_{79}$Au + $^{197}_{79}$Au using soft equation of state. In order to compare the results with the experimental data, we have used a reduced isospin and energy dependent cross section $\sigma_{red} = 0.8\sigma_{nn}^{free}$ [35]. The reaction is followed till the saturation time of the reaction (i.e. 200 fm/c). The geometrical impact parameters interval presented here is, 1.9 to 6.2 fm. This is because the transverse flow exhibits a maxima at the semi-central colliding geometry [30]. In order to investigate the effect of isospin-dependent spatial and momentum constraints, different combinations of spatial and momentum constraints (relative distance between nucleons) for p-p and n-p or n-n has been applied. The momentum constraints used in the present study is 250 MeV/c for p-p and 150 MeV/c for n-n or n-p, respectively. These

Table 3.1: Different isoMSTP parameters.

isoMSTP(N)	r^{pp}_{min} (fm)	$r^{nn/np}_{min}$ (fm)	isoMSTP(N)	r^{pp}_{min} (fm)	$r^{nn/np}_{min}$ (fm)
isoMSTP(I)	3	3	isoMSTP(V)	4	3
isoMSTP(II)	3	4	isoMSTP(VI)	4	4
isoMSTP(III)	3	5	isoMSTP(VII)	4	5
isoMSTP(IV)	3	6	isoMSTP(VIII)	4	6

combinations are abbreviated as isoMSTP(N) in the text. The complete description of different combinations used is mentioned in the Table 3.1.

Fig. 3.8 shows the rapidity distribution of the coefficient of transverse flow (v_1) [38] for fragments ranging from Z=1 to Z=4 at an incident energy 250 MeV/nucleon. The results are displayed for different values of isospin dependent cluster recognition criteria in the projectile rapidity region. To compare our results with the experimental data as well as to compare different particle species, we use normalized transverse momentum and rapidity, defined as [28]:

$$p_t^{(0)} = (p_t/A)/(p_P^{c.m.}/A_P) \quad ; \quad Y^{(0)} = (Y/Y_P)^{c.m.} \tag{3.1}$$

where p_t, p_P and Y_P denotes the transverse momentum, projectile momentum and projectile rapidity respectively. Rapidity is defined in Eq. 1.3. It is observed that the transverse flow is larger in case of heavier fragments compared to the lighter ones. This is due to the significant contribution of collective momentum of nucleons for the heavier fragments. With increase in charge of fragment, the shape of v_1 also changes. A closer look at Fig. 3.8 reveals that increasing the value of r^{pp}_{min} and $r^{nn/np}_{min}$ transverse flow decreases.

Different constraints used in isoMSTP indicate different values of spatial and momentum constraints for p-p and n-p (or n-n) to share the same fragment. It is observed that for light clusters, the transverse flow increases as one moves from the mid-rapidity region towards the projectile rapidity region almost linearly for all fragment species. The reason for the increase in transverse flow is the compression generated in the mid-rapidity region. As a result, the particles with large relative momenta are repelled along the in-plane transverse direction. At peripheral rapidities, however, the flow of LCP (Z=1, Z=2) increases in contrast to the transverse flow of IMF (Z=3, Z=4). The LCPs originate from the highly compressed participant zone and therefore, feels the repulsion to a greater ex-

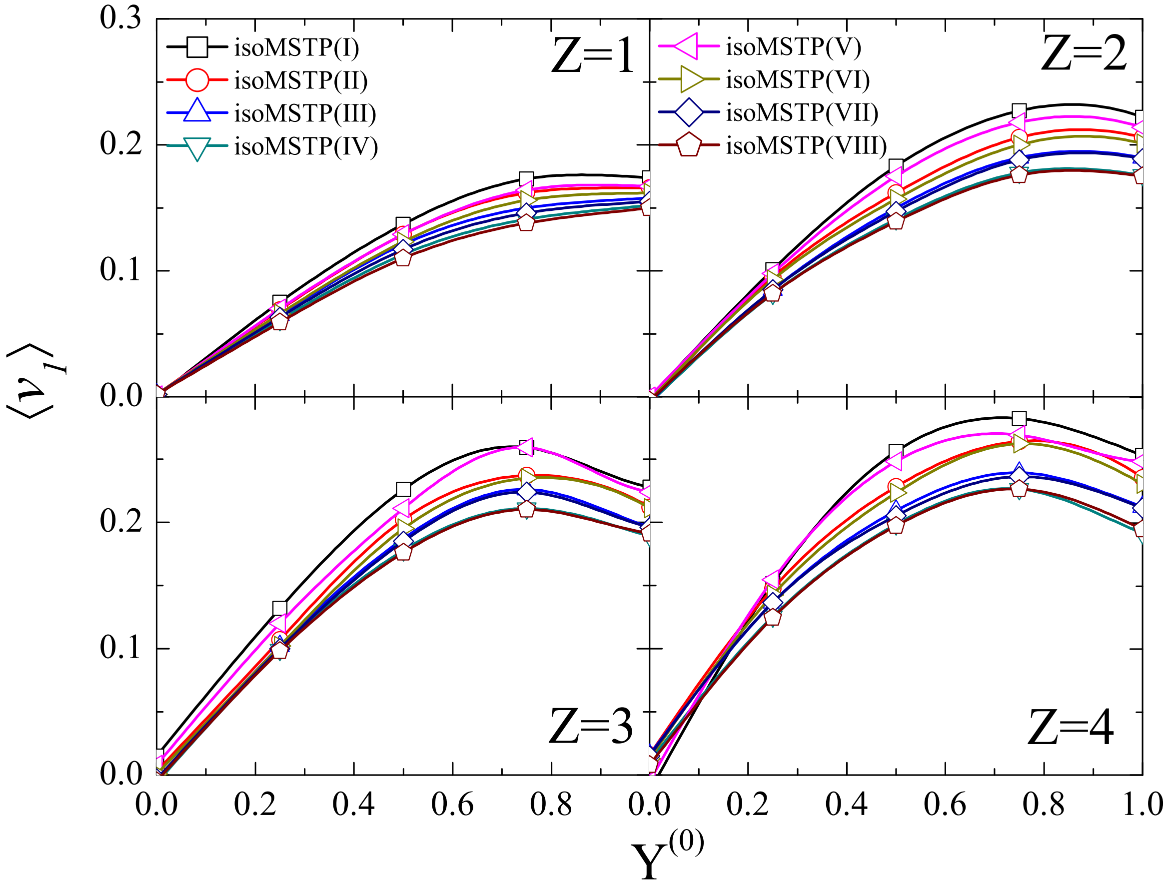

Figure 3.8: Rapidity dependence of transverse flow ($\langle v_1 \rangle$) of charged fragments with Z=1 to Z=4 for different isoMSTP combinations at incident energy 250 MeV/nucleon for the reaction $^{197}_{79}$Au+$^{197}_{79}$Au.

tent. While, the lesser number of heavy fragments in the peripheral rapidity region is the cause for reduced transverse flow of heavy fragments in peripheral rapidities.

In addition, Fig. 3.8 also reveals that for a particular fragment, with increase in minimum distance required to share a fragment the transverse flow decreases. This happens because as the value of r^{pp}_{min} or $r^{nn/np}_{min}$ increases, number of nucleons within a fragment increases. As a result, lesser number of particles are produced and hence the corresponding value of transverse flow decreases. One can also observe that the transverse flow for all fragment species is maximum in the rapidity region $0.5 \leq Y^0 \leq$0.7.

In order to elaborate our results, in Fig. 3.9 the transverse momentum ($p_t^{(0)}$) dependence of transverse flow in a specific rapidity domain i.e. $0.5 \leq Y^{(0)} \leq 0.7$ is shown. The reason for selecting this rapidity domain is the availability of experimental data [29].

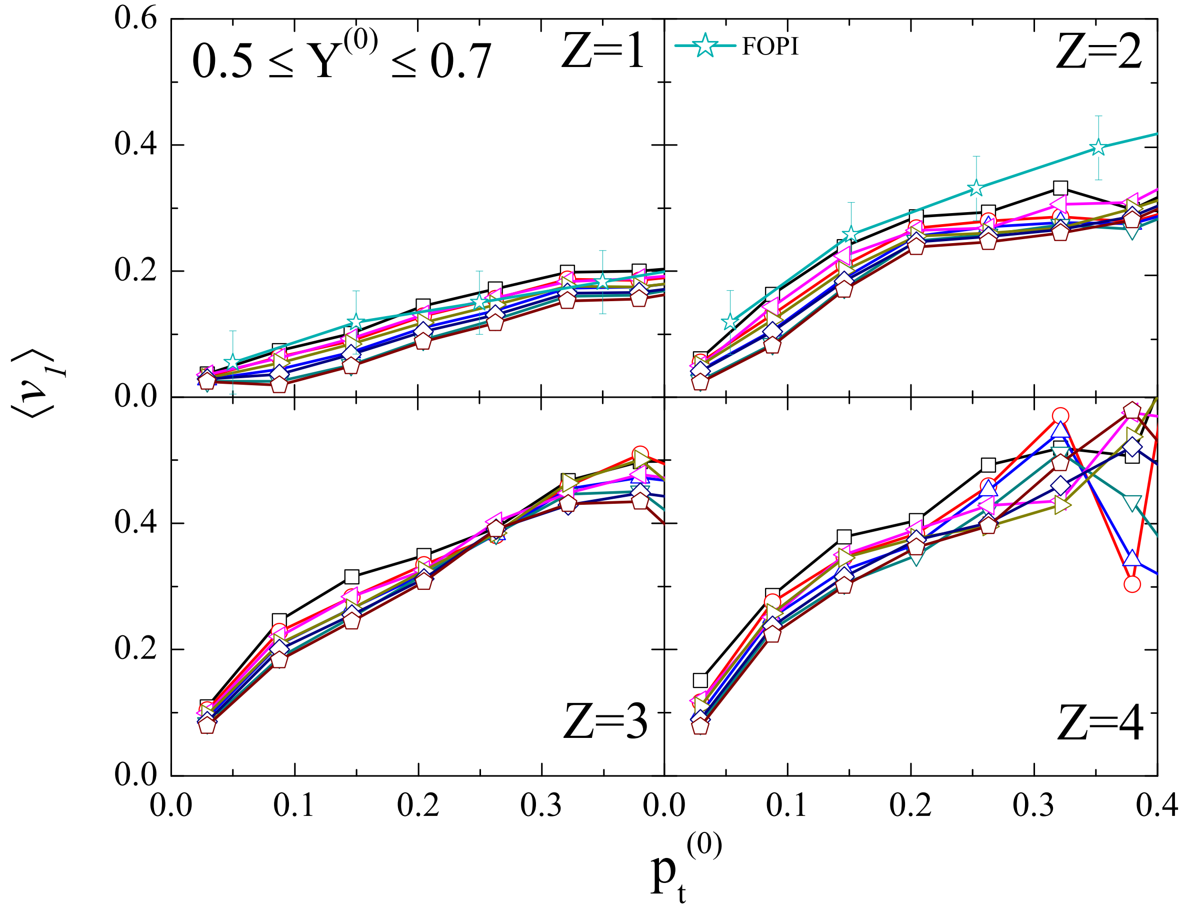

Figure 3.9: Transverse flow of charged fragments as a function of normalized transverse momentum extracted in the rapidity domain $0.5 \le Y^{(0)} \le 0.7$ at 250 MeV/nucleon. Different lines have the same meaning as in Fig. 3.8 .

The results are displayed for charged fragments with Z=1 to Z=4 for different isoMSTP constraints explained in Table 3.1. It is observed that, the low p_t particles are subjected to a reduced repulsion along the impact parameter direction. While, the high p_t particles due to the enhanced repulsion generated in the system give rise to large transverse flow (v_1)for all fragment species. As we increase the distance r_{min}^{pp} or $r_{min}^{nn/np}$, the transverse flow decreases for all p_t particles. As the fragment charge increases, lesser number of particles are available with large value of transverse momenta associated with them. Due to this reason, fluctuation in v_1 is observed for the high p_t particles associated with heavy fragments.

The comparison of our results for transverse flow of charged fragments Z=1 and Z=2 with the experimental data show that the transverse flow obtained by using the isoMSTP with r_{min}^{pp}=3 fm and $r_{min}^{nn/np}$ = 6 fm is in close agreement with the data of Andronic *et al.* [29]. Therefore, the further analysis is carried out by using this particular combination.

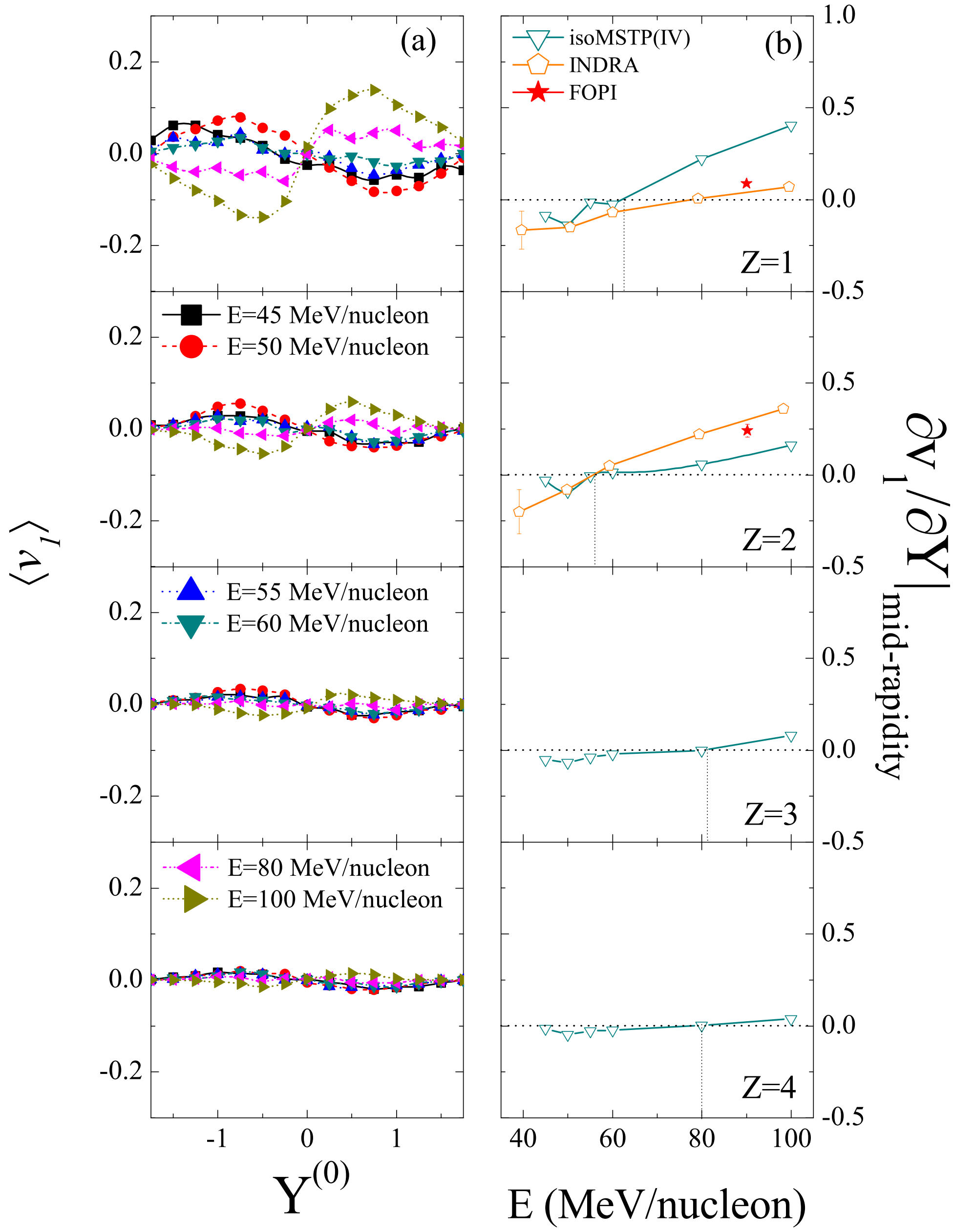

Figure 3.10: Rapidity dependence of transverse flow (a) and energy dependence of slope of transverse flow (b) for charge fragments Z=1 to Z=4 (top to bottom panels) for isoMSTP(IV) combination.

Fig. 3.10(a) displays the rapidity dependence of transverse flow at incident energies between 40 and 100 MeV/nucleon. The slopes of the curves of Fig. 3.10(a) are obtained from the mid-rapidity region ($|Y^{(0)}| \leq 0.25$) and is represented in Fig. 3.10(b). It is observed that the slope of the transverse flow changes from negative to positive with increase in incident energy. At low incident energies, the dominance of attractive mean field results in negative flow values. While, the opposite is true at higher incident energies, where, the repulsion created due to violent nucleon-nucleon collisions dominates. At the energy of vanishing flow, these two opposing forces (attractive and repulsive) counter balance each other and the net flow vanishes. The trend of the slope obtained by using isoMSTP(IV) is in agreement with the INDRA [39] and FOPI [29] results. A closer look at Fig. 3.10(b) reveals that the EVF for Z=1 fragments is higher compared to the Z=2 fragments. Similar results were also obtained by Russotto *et al.* [33]. However, the EVF for heavier fragments (Z $\geq$ 3) fragments is found to be higher, which may be due to reason that these fragments originate from the spectator region. While, the EVF is a phenomenon that arises from the mid-rapidity participant region. Therefore, no specific conclusion can be drawn for the EVF of heavier fragments.

3.3 Summary

We have studied the contribution of different components of potential on the disappearance of flow. The impact parameter dependence of balance energy for the reactions $^{58}_{26}$Fe+ $^{58}_{26}$Fe, $^{58}_{28}$Ni+ $^{58}_{28}$Ni, $^{86}_{36}$Kr+ $^{93}_{41}$Nb and $^{197}_{79}$Au+ $^{197}_{79}$Au has been studied in detail. Our calculations for the considered energy range clearly demonstrate the dominance of Coulomb potential and momentum dependent interactions over the other components of the potential for lighter colliding systems. However, the contribution of symmetry potential also become significant in the collision of heavier nuclei. In addition, the cluster recognition criteria is optimized by studying the transverse flow of charged fragments with Z= 1, 2, 3 and 4. The simple MST method is modified by including the isospin dependence in spatial and momentum constraints. The comparison of our results with the experimental data shows that the light fragments produced by using isoMSTP(IV), are able to explain the experimental data. In addition, the energy of vanishing flow of charge fragments has also been explored and is found to be sensitive towards the charge of the fragment. The energy of vanishing flow of Z=1 fragments is found to be higher than the Z=2 fragments, which is in agreement with the previous studies. However, no specific conclusion can be drawn for the energy of vanishing flow of heavier fragments (Z $\geq$ 3).

Bibliography

[1] P.Danielewicz, R.A. Lacey, P.B. Gossiaux, C. Pinkenburg, P. Chung, J.M. Alexander, and R.L. McGrath, Phys. Rev. Lett. **81**, 2438 (1998); Q. Pan and P. Danielewicz, Phys. Rev. Lett **70**, 2062 (1993).

[2] D. Krofcheck, *et al.*, Phys. Rev. Lett. **63**, 2028 (1989); D. Krofcheck, *et al.*, Phys. Rev. C **46**, 1416 (1992).

[3] R. Pak, *et al.*, Phys. Rev. Lett. **78**, 1022 (1997); R. Pak, *et al.*, Phys. Rev. Lett. **78**, 1026 (1997).

[4] R. Pak, *et al.*, Phys. Rev. C **53**, R1469 (1996).

[5] K.G.R. Doss, *et al.*, Phys. Rev. Lett. **57**, 302 (1986).

[6] A. Bonasera, F. Gulminelli, and J. Molitoris, Phys. Rep. **243**, 1 (1994).

[7] A.D. Sood, R.K. Puri, J. Aichelin, Phys. Lett. B **594**, 260 (2004); A.D. Sood, R. K. Puri, Eur. Phys. A **30**, 571 (2006); A.D. Sood, R.K. Puri, Phys. Rev. C **69**, 054612 (2004).

[8] J.P. Sullivan, *et al.*, Phys. Lett. B **249**, 8 (1990); C.A. Ogilvie *et al.*, Phys. Rev. C **42**, R10 (1990); J. Peter, Nucl. Phys. A **545**, 173c (1992).

[9] A. Bonasera and L.P. Csernai, Phys. Rev. Lett. **59**, 630 (1987); A. Bonasera, L.P. Csernai, and B. Schurmann, Nucl. Phys. A **476**, 159 (1988).

[10] S. Soff, S.A. Bass, C. Hartnack, H. Stocker, and W. Greiner, Phys. Rev. C **51**, 3320 (1995); R. Chugh and R.K. Puri, Int. J. Mod. Phys. E, **19**, 2009 (2010); S. Kumar, M.K. Sharma, R.K. Puri, K.P. Singh, and I.M. Govil, Phys. Rev. C **58**, 3494 (1998); R. Chugh and R.K. Puri, Phys. Rev. C **82**, 14603 (2010).

[11] S. Kumar, Rajni and S. Kumar, Phys. Rev. C **82**, 024610 (2010).

[12] S. Goyal and R.K. Puri, Nucl. Phys. A **853**, 164 (2011).

[13] J. Aichelin, Phys. Rep. **202**, 233 (1991).

[14] J. Aichelin, A. Rosenhaur, G. Peilert , H. Stöcker, and W. Greiner, Phys. Rev. Lett. **58**, 1926 (1987).

[15] C. Hartnack, R.K. Puri, J. Aichelin, J. Konopka, S.A. Bass, H. Stocker, and W. Greiner, Eur. Phys. J. A **1**, 151 (1998); C. Hartnack, H. Oeschler, Y. Leifels, E.L. Bratkovskaya, and J. Aichelin, Phys. Rep. **510**, 119 (2012).

[16] K.S. Vinayak, S. Kumar, Eur. Phys. J. A **47**, 144 (2011).

[17] S. Gautam, A.D. Sood, R.K. Puri and J. Aichelin, Phys. Rev. C **83**, 034606 (2011).

[18] B.A. Li, Phys. Rev. Lett. **85**, 4221 (2000); B.A. Li, L.W. Chen and C.M. Ko, Phys. Rep. **464**, 113 (2008); D.V. Shetty, S.J. Yennello, G.A. Souliotis, Phys. Rev. C **76**, 024606 (2007).

[19] C. Tao, Y.G. Ma, G.Q. Zhang, X.G. Cao, D.Q. Fang, and H.W. Wang, Phys. Rev. C **87**, 014621 (2013); L. Trippa, G. Colo, and E. Vigezzi, Phys. Rev. C **77**, 061304(R) (2008); C.L. Gang, MA Z. Yu, Chin. Phys. Lett. **25**, 1625 (2008).

[20] B.A. Li, Phys. Rev. C **48**, 2415 (1993).

[21] D.J. Magestro, W. Bauer, G.D. Westfall, Phys. Rev. C. **62**, 041603(R) (2000).

[22] E. Lehmann, R.K. Puri, A. Fessler, G. Batko, S.W. Huang, Phys. Rev. C **51**, 2113 (1995); E. Lehmann, *et al.*, Prog. Part. Nucl. Phys. **30**, 219 (1993); S. Goyal, R.K. Puri, Phys. Rev. C **83**, 047601 (2011).

[23] H.A. Gustafsson, *et al.*, Phys. Rev. Lett. **52**, 1590 (1984).

[24] G.F. Bertsch, W.G. Lynch, M.B. Tsang, Phys. Lett. B **189**, 384 (1987).

[25] Z.Y. He, *et al.*, Nucl. Phys. A **598**, 248 (1996).

[26] C. Liewen, Z. Fengshou and J. Genming, Phys. Rev. C **58**, 2283 (1998).

[27] H. Stöcker, J.A. Maruhn, W. Greiner, Phys. Rev. Lett. **44**, 725 (1980).

[28] A. Andronic, *et al.*, Phys. Rev. C **67**, 034907 (2003) .

[29] A. Andronic, *et al.*, FOPI collaboration, Phys. Rev. C **64**, 041604 (2001) .

[30] F. Rami, *et al.*, Nucl. Phys. A **646**, 367 (1999).

[31] G.D. Westfall, *et al.*, Phys. Rev. Lett. **71**, 1986 (1993).

[32] D.J. Magestro, *et al.*, Phys. Rev. C **61**, 021602 (2000).

[33] P. Russotto, M.D. Cozma, A. Le Fèvre, Y. Leifels, R. Lemmon, Q. Li, J. Łukasik, W. Trautmann, Eur. Phys. J. A **50**, 38 (2014).

[34] Y. Wang, C. Guo, Q. Li, H. Zhang, Z. Li, W. Trautmann, Phys. Rev. C **89**, 034606 (2014) .

[35] S. Gautam, J. Phys. G. **37**, 085102 (2010); S. Gautam, A. D. Sood, R.K. Puri, J. Aichelin, Phys. Rev. C **83**, 014603 (2011).

[36] S. Kumar and R.K. Puri, Phys. Rev. C **58**, 320 (1998).

[37] Y. Zhang, Z. Li, C. Zhou, M.B. Tsang, Phys. Rev. C **85**, 051602(R) (2012).

[38] S. Voloshin, Y. Zhang, Z. Phys. C **70**,665 (1996).

[39] J. Łukasik *et al.*, Phys. Lett. B **608**, 223-230 (2005).

Chapter 4

Influence of various components of interaction potential on global nuclear stopping

4.1 Introduction

It is well established that central heavy-ion collisions at intermediate energies provide precious information about the nuclear EOS, which virtually reflects the properties of hot and dense nuclear matter under the extreme conditions of temperature, pressure and density. The detailed information about these parameters is helpful for determining the degree of thermalization achieved in a dynamical process during the collision of heavy-ions, which in turn is useful for understanding the collapse of supernova and formation of neutron stars [1,2]. Theoretically, the time evolution of a reaction can be followed within the G-matrix; real part (represented by the mean field) signifies the propagation and imaginary part (nucleon-nucleon scattering) looking after the two body binary collisions. The real part of the G-matrix is also linked with nuclear equation of state. The hot and dense nuclear matter formed in a reaction has also been linked with the nuclear equation of state and with the binary collisions [3]. The degree (or extent) of stopping of nucleons of projectile and target is influenced by both binary collisions as well as by the in-medium effects such as Fermi momentum and Pauli blocking. Several different experimental and theoretical observables have been proposed in the literature as a sensitive probe to study various aspects of nuclear matter at intermediate energies. One of the essential observables, which is necessary to understand the basic reaction dynamics is the nuclear stopping: a prime source of information for analysing the energy spectra as well as the particle densities of the compressed nuclear matter during the early phase of a reaction when fireball is formed by the participant nucleons [4].

It is worth mentioning that nuclear stopping also depicts the quantity of dissipated energy and amplitude of collective motion and controls the reaction mechanism such as deep inelastic scattering and neck formation. Moreover, higher the temperature (and matter density), larger is the nuclear stopping [5–7]. In other words, full stopping corresponds to nearly complete equilibrium (or thermalization) reached in a reaction.

It should also be kept into mind that the degree of equilibration between the nucleons of target and projectile is crucial for understanding the complex reaction mechanism associated with a reaction. A great deal of experiments has been performed to understand the properties of hot and dense nuclear matter formed in a reaction [1, 2, 8, 9]. Equal number of theoretical approaches has also been developed to follow the reaction [10–13]. First study on nuclear stopping has been carried out by Renfordt *et al.* [3] for the reaction of ${}^{40}_{18}$Ar+${}^{207}_{82}$Pb and nearly complete nuclear stopping (and isotropy) has been reported for head on collisions. In 1988, Bauer [14] has predicted that the nuclear stopping can be used for nuclear equilibration. Following this, Hong *et al.* [15] have studied the proton and deuteron rapidity spectra for the central collisions of ${}^{58}_{28}$Ni+${}^{58}_{28}$Ni and ${}^{197}_{79}$Au+${}^{197}_{79}$Au at beam energies between 1 and 2 GeV/nucleon. This study has linked degree of stopping with the size of interacting matter. Similarly, same conclusions have also been drawn when system size dependence of nuclear stopping has been explored for hydrogen isotopes by Reisdorf *et al.* [16]. This study is further advanced by Yang, Liu, and Li *et al.* [17–21] who have analyzed the role of various isospin ingredients such as symmetry energy, in-medium nucleon-nucleon cross section and Coulomb interactions etc. on nuclear stopping. Interestingly, stopping has been found to be sensitive towards the in-medium NN cross section; however, no sensitivity has been reported for symmetry energy. At the same time, induction of Coulomb interaction is found to reduce nuclear stopping irrespective of system, geometry and beam energy. A careful analysis of literature reveals that number of attempts have been made where determination of different model ingredients such as equation of state, nucleon-nucleon cross sections, etc. have been done using nuclear stopping and their role has been reported [8, 22–26]. Even stopping has been studied in terms of memory loss [27, 28]. Interestingly, momentum distribution of the fragments has rarely been studied, though it can shed light on the reaction mechanism. Peilert *et al.* [29] did investigate the equilibration of the incident longitudinal momentum in NN collisions and found that just after the stage of the maximum compression, the matter flows out of the central zone and causes the degradation of the longitudinal momenta into transverse degree of freedom. They also pointed out that for achieving a better thermalization, one should consider the participant region only. Ono *et al.* [30] have studied the momentum distribution of the fragments produced in the reaction of $^{12}_{6}C+^{12}_{6}C$ at an incident energy 28.7 MeV/nucleon by considering several cases of stochastic collisions. They found that the momentum distribution is sensitive to the stochastic collision process. They also found that collective flow of low momentum particles (such as α particles) seem to reflect the effective interactions compared to the flow of free nucleons alone. Chung *et al.* [31] have studied the effect of various momentum constraints on elliptic flow of protons for the reaction $^{197}_{79}Au + ^{197}_{79}Au$. These constraints are found to provide a better understanding of the interplay between hot and compressed nuclear matter. In all above studies, few gaps still remain: For example: above studies are for scattered reactions, no systematic is available. Secondly, there are further ambiguities associated with the nuclear equation of state and no clear rules were applied. This being the case, it is important to constraint the specific observables to limit the uncertainties in the nuclear equation of state. Therefore, it would be of great interest to investigate the nuclear stopping associated with the nucleons having different momentum. In this chapter, we plan to investigate the following:

1. The role of various potentials towards the global nuclear stopping. In addition, the isospin sensitivity will also be examined in nuclear stopping.

2. Here, which momentum range of the particles is contributing significantly towards nuclear stopping at a particular energy and impact parameter.

4.2 Results and discussion

It is worth mentioning that various observables have been mentioned in the literature to probe the nuclear stopping [8, 16]. One of these observables involve the ratio of the transverse to longitudinal component of the momentum has been used. This quantity is represented by the anisotropic ratio (R) [3].

$$\langle R \rangle = \frac{2}{\pi} \frac{(\sum_i P_\perp(i))}{(\sum_i P_\parallel(i))}, \tag{4.1}$$

where, $P_\perp(i) = \sqrt{P_x^2(i) + P_y^2(i)}$ and $P_\parallel(i) = P_z(i)$. For a complete stopping, the value of R is expected to be unity.

One can also define the nuclear stopping in terms of ratio of variances of transverse rapidity distribution to the longitudinal rapidity distribution, denoted by: VARXZ, where, the longitudinal rapidity distribution is given by the Eq. 1.3. In order to get the transverse rapidity distribution, the longitudinal component of momentum (P_z) is replaced by the transverse component of momentum (P_x).

Now, the stopping observable, VARXZ, is the ratio of variances of transverse (VARX or $\sigma^2(x)$) relative to the longitudinal (VARZ or $\sigma^2(z)$) rapidity distribution.

$$VARXZ = \frac{\sigma^2(x)}{\sigma^2(z)} \quad ; \quad \sigma^2(x) = (FWHM/2.36)^2 \tag{4.2}$$

Here, FWHM is the full width at half maxima of rapidity distribution.

4.2.1 Energy dependence of nuclear stopping

For the present analysis, several thousand events have been generated for the reaction of $^{120}_{50}$Sn + $^{120}_{50}$Sn at incident energies between 30 and 1200 MeV/nucleon covering entire colliding geometry. A soft equation of state along with isospin and energy dependent cross section (σ_{iso}) have also been used. The role of different components of potential has been analyzed by starting from basic potential and adding one by one all other components of the potential and then studying the stopping reached in a reaction. Different acronyms have the same meaning as described in Chapter 3. It is worth mentioning here that different forms of symmetry energy (stiff/soft) do not affect the nuclear stopping significantly [32]. In Figs. 4.1 (a) and (b), the results of nuclear stopping defined by Eq. 4.1 as a function of incident energy for protons and neutrons emitted in the reaction of $^{120}_{50}$Sn+$^{120}_{50}$Sn are shown. Various lines represent different sets of components of nuclear potential. Following conclusions can be drawn from the figures:

1. At low incident energy, binary collisions are scarce due to Pauli blocking. This results in the preservation of correlations and does not allow fragmentation of the

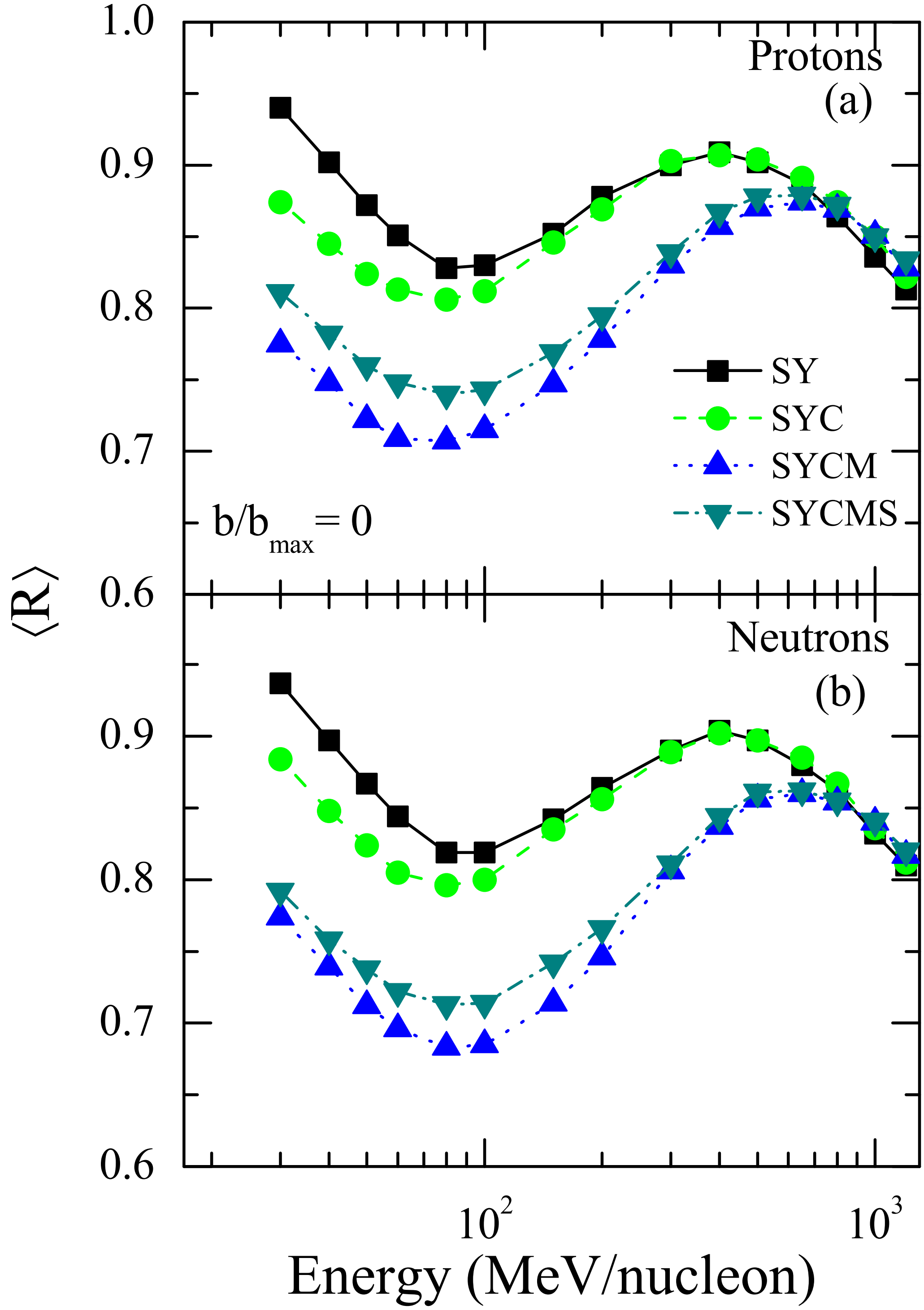

Figure 4.1: Nuclear stopping ⟨R⟩ as a function of incident energy for the central collisions of the reaction ${}^{120}_{50}$Sn+${}^{120}_{50}$Sn for protons (a) and neutrons (b). Various symbols indicate different sets of components of nuclear potential.

matter. Fragments close to target and projectile masses are then emitted [26]. These excited heavy fragments de-excite by emitting free nucleons (FN) and light fragments with the passage of time [26]. As a result, isotropic momentum distribution of the whole composite system increases with the evolution of reaction. However, near the Fermi energy, the longitudinal rapidity distribution of nucleons is broader compared to the transverse rapidity distribution. The broad shape of the longitudinal rapidity distribution preserves the entrance channel effects, even in the most central collisions. This reduces the nuclear stopping near the Fermi energy. Above the Fermi energy, two-body collisions play dominant role. Nucleons suffer more violent binary collisions and stopping reaches a maximum around 400 MeV/nucleon. At higher incident energies (around 1000 MeV/nucleon), the mean free path and reaction time between the nucleons decreases significantly. This does not allow equilibration of the longitudinal and transverse momentum, which leads towards the transparency of the matter. As a result, more will be the transparency in the matter with increase in incident energy and less will be the stopping.

2. At lower incident energies, maximum stopping is seen for SY set of the potential. The addition of other components in the potential results in reduced stopping. However, this difference diminishes with incident energies and vanishes at sufficient higher energies. The attractive behaviour of Skyrme and Yukawa potential leads to the production of heavy fragments. These heavy fragments get stabilized by emitting free nucleons and light fragments at the later stage. This leads to isotropic momentum distribution of nucleons. With the addition of other components of interaction potential, repulsion generated in the colliding matter breaks the correlations among the nucleons. This results in anisotropic emission of free nucleons and light fragments.

3. It is worth mentioning that at intermediate energies (around 400 MeV/nucleon), no significant difference is seen with the addition of Coulomb interactions. In contrast, inclusion of momentum dependent potential results in reduced stopping.

In order to further understand the above findings, we separate out the stopping due to free protons and fragments with $Z \geq 2$ (see Fig. 4.2). Here, complete potential (SYCMS) is

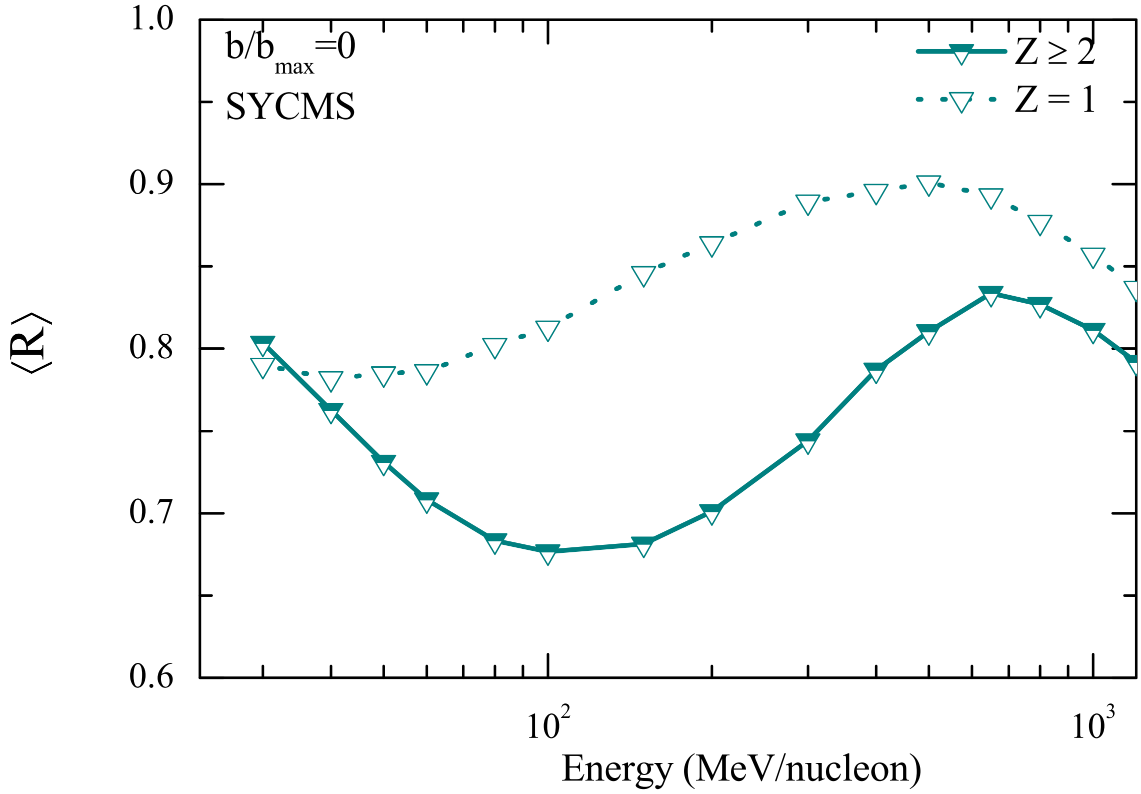

Figure 4.2: Nuclear stopping of fragments with Z≥ 2 (solid line) and free protons (dotted line) as a function of incident energy for the central collision of the reaction $^{120}_{50}$Sn+$^{120}_{50}$Sn including all the components of the interaction potential.

used for analysis. One can clearly see that at low incident energies, the nuclear stopping for the fragments with Z≥ 2 decreases, passes through a minimum and then increases again. However, only small change occurs in the case of protons. At low incident energies, most of nuclear correlations are preserved. Due to this, not enough free protons are emitted from the bounded matter. Further, the distribution of the fragments in the phase space is not isotropic irrespective of the incident energies. With the increase in incident energy and colliding geometry, multiplicity of intermediate mass fragments (IMF's) shows a rise and fall behaviour [2, 33, 34]. Due to this reason, a dip in the stopping ratio corresponds to maximal production of IMF's [23]. It is worth mentioning that the energy dependence of nuclear stopping does not have universal behaviour as a function of impact parameter. This statement is true for all combinations of potential such as SY, SYC, SYCM, and SYCMS. In order to further investigate the contribution of different components of nuclear potential near the Fermi energy as well as the isospin effects of neutron proton content, we have analyzed stopping at 50 MeV/nucleon.

4.2.2 Impact parameter dependence of nuclear stopping

Figs. 4.3 (a) and (b) show impact parameter dependence of nuclear stopping for protons and neutrons, separately. The displayed results are for different sets of components of nuclear potential. A closer look at Fig. 4.3 reveals that SY set of potential gives higher

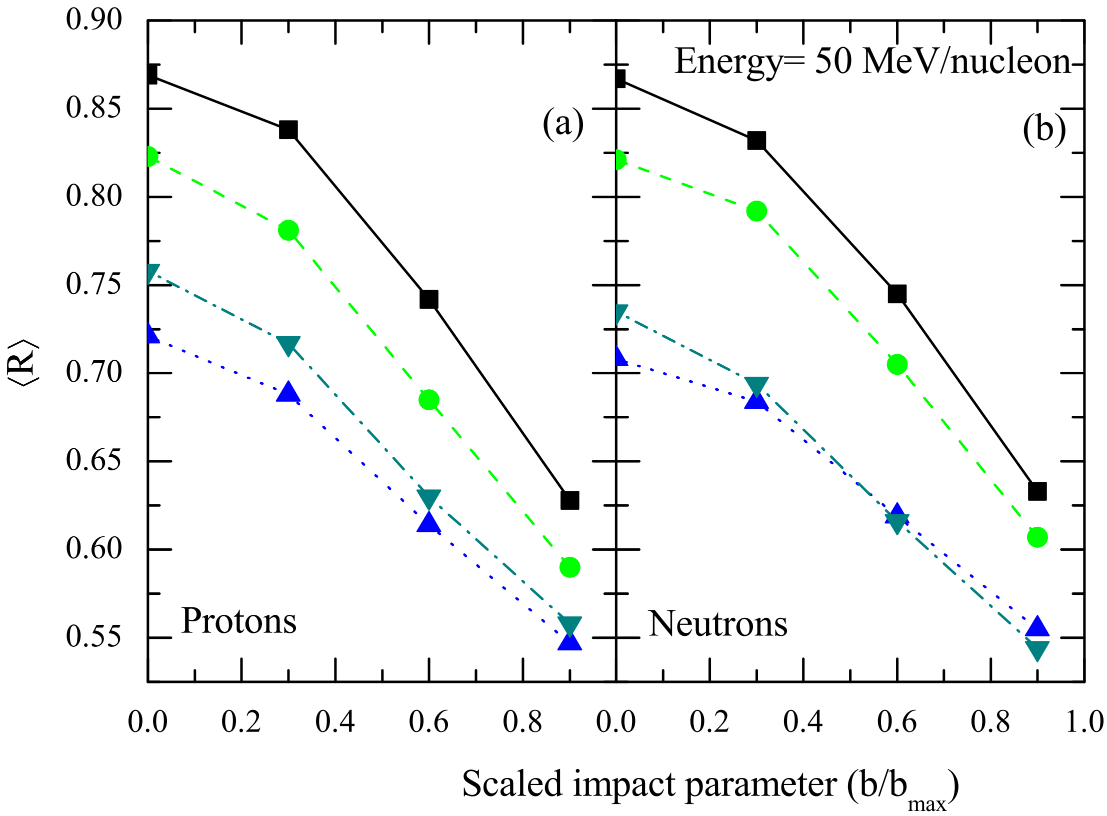

Figure 4.3: Nuclear stopping as a function of scaled impact parameter for proton (a) and neutrons (b) at incident energy 50 MeV/nucleon.

nuclear stopping at all impact parameters. The addition of Coulomb interaction and momentum dependent interactions reduce the net nuclear stopping. Due to repulsive nature of Coulomb and momentum dependent interactions, the binary collisions are suppressed to a greater extent. One also sees mild sensitivity of symmetry potential towards the nuclear stopping in central collisions. However, this sensitivity disappears at higher impact parameters (see Fig. 4.4). The mild sensitivity of symmetry potential is due to large N/Z ratio of the reaction chosen for the present study. One can also see, where the nuclear stopping of protons and neutrons is nearly the same, weak dependence of nuclear stopping on asymmetric isospin content is observed. This result is in agreement with Jain *et al.* [35]. To get precise information about the contribution of individual components of nuclear potential at a specific colliding geometry, we present in Figs. 4.4(a) and (b), the percentage change in the nuclear stopping for protons and neutrons as a function of scaled impact parameter.

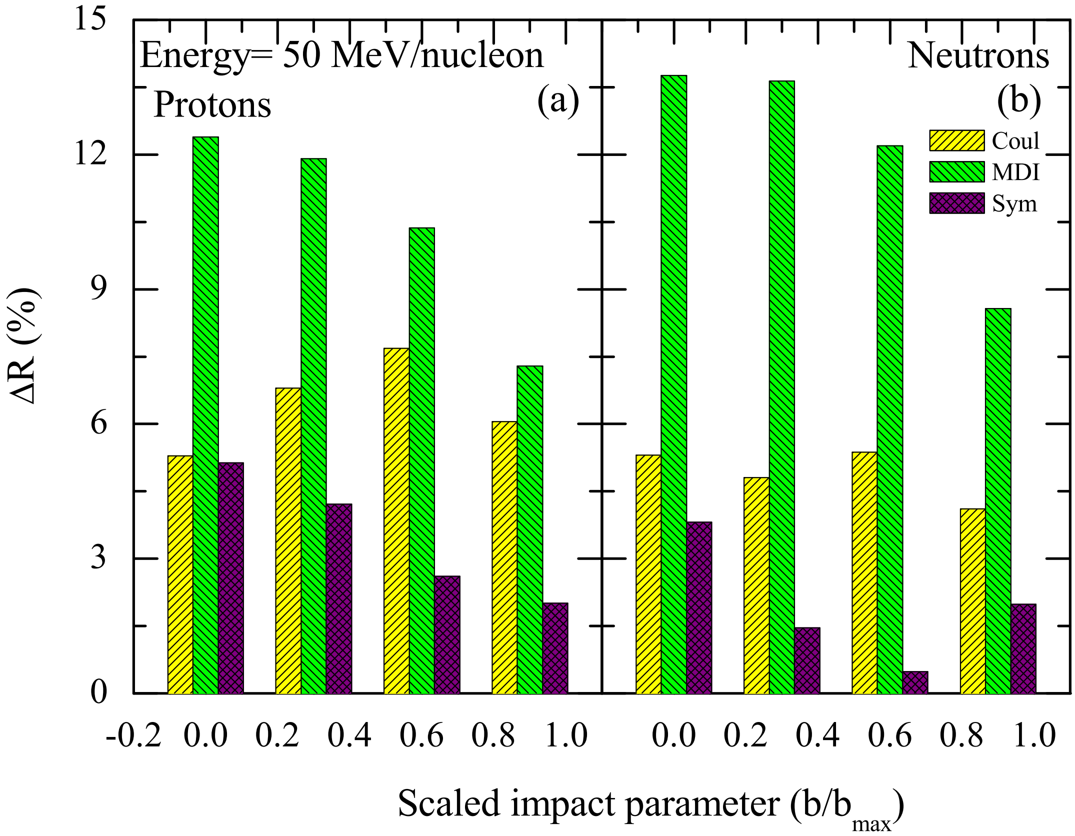

Figure 4.4: Change in nuclear stopping as a function of scaled impact parameter for protons (a) and neutrons (b) at incident energy 50 MeV/nucleon.

Following conclusions can be drawn from the figures:

1. At central collisions, momentum dependent interactions play major role for variation in the nuclear stopping of protons as well as neutrons. Momentum dependent interactions reduce the binary collisions to some extent leading to sudden decrease in the nuclear stopping. This effect enhances for neutrons, which exceeds motions in the reaction chosen for present case. Second important contribution is made by the Coulomb interaction. The repulsive behavior of Coulomb interaction results in

net reduction of the nuclear stopping. The symmetry potential has less significance towards the nuclear stopping.

2. The change in the nuclear stopping due to various components of the potential decreases as one goes towards peripheral colliding geometries. At peripheral collisions, participant matter is very small leaving behind large volume of spectator region. The momentum dependent interactions are able to even break spectator matter [22]. This results in isotropic distribution of the nucleons. Hence, lesser change in the nuclear stopping is observed. But in the case of Coulomb interactions, the situation is different. The effect of Coulomb repulsion is stronger at peripheral colliding geometries. This is due to heavier fragments produced in the peripheral collisions which produce enhanced effect of Coulomb potential.

4.2.3 Effect of isospin-dependent cross section on nuclear stopping

From the above discussion, it is evident that isospin effects are caused by three isospin-dependent components, namely, the Coulomb interactions, symmetry potential and the NN cross sections. The effect of first two components has been explained in the above discussion. The effect of isospin dependent NN cross section on nuclear stopping of protons and neutrons is shown in Figs. 4.5 (a) and (b). Here, nuclear stopping of the protons and neutrons is plotted as a function of scaled impact parameter. The results are displayed by taking into account the components of interaction potential (i.e. SYCMS) along with isospin-dependent (σ_{iso}) and independent (σ_{noiso}) NN cross section. For the isospin-independent cross section, neutron-proton cross section (σ_{np})is treated equal to the neutron-neutron and proton-proton cross section (σ_{nn} and σ_{pp}). The larger nuclear stopping is observed for protons in central impact parameters. This is due to repulsive interaction between the charged particles. The isospin-dependent cross section enhances the nuclear stopping (7 % in the case of protons and 6% in the case of neutrons). This is due to the fact that in the case of isospin dependent cross section, neutron-proton cross section is about 3 times greater than corresponding neutron-neutron and proton-proton cross sections. Moreover, the isospin-dependent cross section plays a significant role towards the nuclear stopping in central geometries.

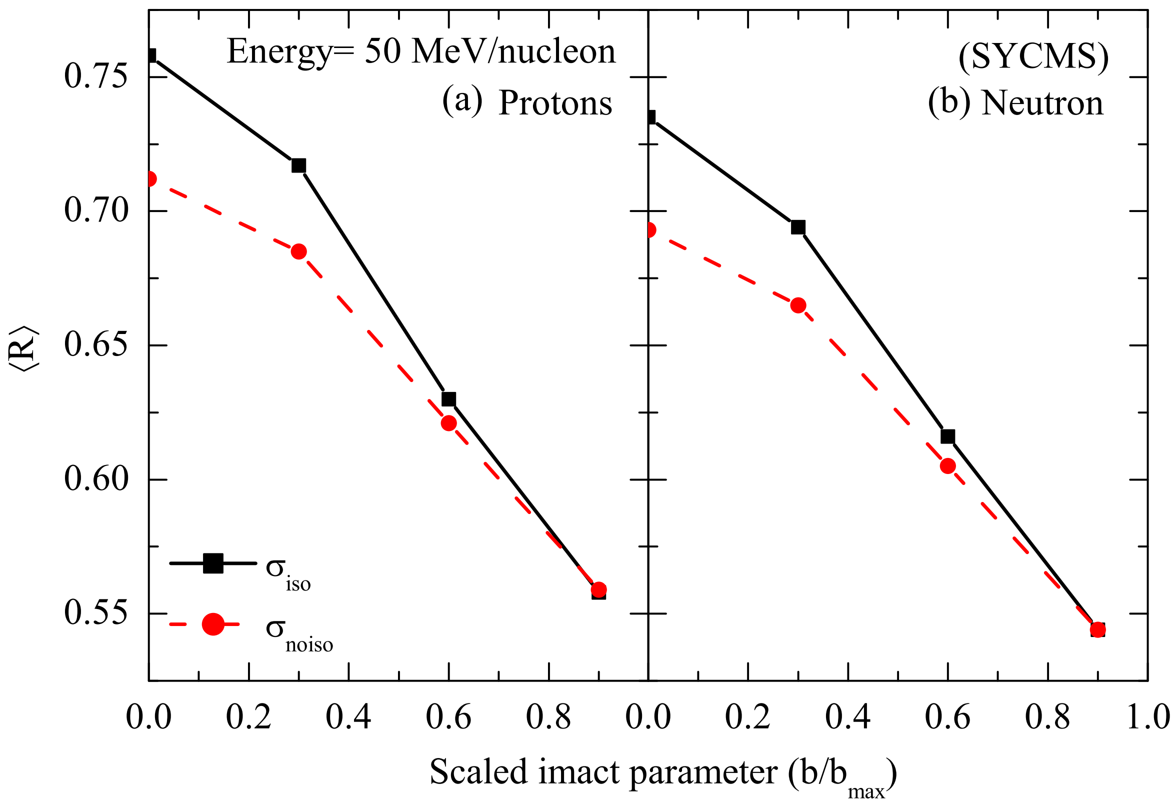

Figure 4.5: Nuclear stopping as a function of scaled impact parameter for protons (a) and neutrons (b) for isospin-dependent (σ_{iso}) and isospin-independent (σ_{noiso})NN cross section.

4.2.4 Momentum distribution of particles participating in nuclear stopping

It is well known that at peripheral collisions, the relative momentum of nucleons in the participant zone is quite large. This gives rise to various interesting observables at intermediate energy to explore nuclear matter equation of state. The nuclear matter is highly compressed in the participant zone, which equilibrate itself at the later stage of the reaction by the emission of nucleons with different momentum associated with them. However, which momentum range particles are responsible for the better equilibration of the system is still not known. Motivated by this, we checked the relative momentum of all nucleons and divide them into different bins. For the present analysis, we simulated several thousand events for the reactions of ${}^{197}_{79}Au+{}^{197}_{79}Au$ and ${}^{58}_{28}Ni+{}^{58}_{28}Ni$ at reduced impact parameter $\hat{b}$ <0.15, where $\hat{b} = b/b_{max}$ with b_{max}= 1.15($A_1^{1/3}$+$A_2^{1/3}$) with A_1 and A_2 being the masses of target and projectile, respectively. The choice of impact parameter is guided by the experimental measurements [16]. The simulations were carried out for the incident energies ranging between 50 and 1000 MeV/nucleon. A soft equation of state along with 0.8σ_{nn}^{free} has been employed that also includes the standard symmetry potential as has been described in detail by Hartnack *et al.* [12]. The reactions are followed until the saturation is reached, which in the present work is 200 fm/c. The phase space of nucleon was tested before and after binary collisions for large number of events and on an average, a change in momentum of few hundred of MeV/c was found.

In order to explore the participation of nucleons in stopping with a specific momentum, we divide whole momentum range into different bins MBIN(I), MBIN(II), MBIN(III), MBIN(IV) and MBIN(V). The momentum range of different bins is listed in Table 4.1.

Table 4.1: Ranges of momentum for different bins

BIN	MOMENTUM RANGE (MeV/c)
MBIN(I)	0< p $\leq$ 100
MBIN(II)	100< p $\leq$ 200
MBIN(III)	200< p $\leq$ 300
MBIN(IV)	300< p $\leq$ 400
MBIN(V)	p > 400

In order to study the momentum distribution of charge fragments, we display in Fig. 4.6, the momentum distribution of the particles as a function of incident energy for the central collisions of the reaction $^{197}_{79}$Au+$^{197}_{79}$Au at 200 fm/c. It is clear from the figure that the percentage of the particles lying within the lowest momentum range (MBIN(I)) is less compared to all other momentum range bins at energies $\geq$ 200 MeV/nucleon. The momentum distribution of the particles of MBIN(I) is followed by MBIN(II) and then by MBIN(III) and finally by MBIN(IV). Moreover, one can clearly see that below 400 MeV/nucleon, the momentum transferred to the particles is not uniform. For MBIN(I), and MBIN(II), it decreases with increase in the incident energy, whereas for MBIN(III) (MBIN(IV)) the number of particles increases upto 200 MeV/nucleon (400 MeV/nucleon) and then decreases with further increase in incident energy. Beyond 200 MeV/nucleon, the distribution of the particles belonging to MBIN(I) remains nearly the same, whereas,

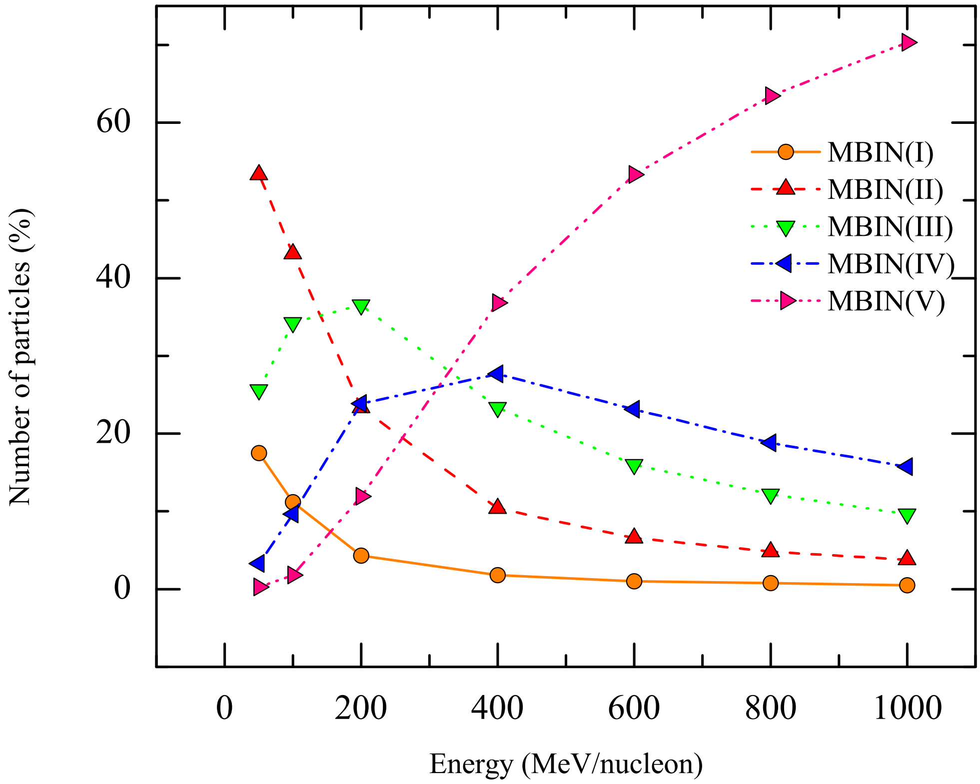

Figure 4.6: Momentum distribution of particles as a function of incident energy using various momentum cuts MBIN(I), MBIN(II), MBIN(III), MBIN(IV) and MBIN(V).

particles lying in MBIN(II) and MBIN(III), keep on decreasing with increase in the incident energy. After 400 MeV/nucleon, there is a significant increase in the number of particles in higher momentum range bins. With the increase in the incident energy, there is an increase in the binary NN collisions. Hence, the nucleons with low momenta associated with them get accelerated towards the high momentum bin and thereby creating a vacancy in the lower momentum bin. That is why with an increase in the incident energy, the number of particles in lower momentum bin decreases and those in the higher momentum bin increases simultaneously. Though, we have considered the complete range of incident energy, but the main goal of present work is confined upto 400 MeV/nucleon. Above 400 MeV/nucleon due to the complete disassembly of nuclear matter, the nuclear stopping decreases and transparency comes into picture. In the following discussion, we mainly concentrate on the results at incident energy below 400 MeV/nucleon.

4.2.5 Stopping parameter (VARXZ) as a function of fragment charge

Here we will discuss other parameter (VARXZ), which is equally important to study the nuclear stopping as that of $\langle R \rangle$. Fig. 4.7 shows the stopping parameter VARXZ as a function of Z at different incident energies for the reactions of $^{197}_{79}$Au+$^{197}_{79}$Au and $^{58}_{28}$Ni+$^{58}_{28}$Ni. It is worth mentioning that, for the calculation of VARXZ, the rapidity distribution of nucleons is fitted over the entire rapidity range (i.e. -1.75 $\leq \frac{Y_{c.m.}}{Y_{beam}} \leq$ 1.75). The nuclear stopping for the selected momentum bins are shown along with the whole range of momentum distribution (M-ALL). Following conclusions can be drawn from the figure:

1. It is clear from the figure that the nuclear stopping decreases with the increase in fragment charge. With increase in fragment charge, the longitudinal component of rapidity distribution increases compared to the transverse rapidity distribution. Due to this reason, there is anisotropic distribution of nucleons in the momentum space. Similar results are also shown in Ref. [16].

2. It can be clearly observed that stopping is maximum for MBIN(I) particles. This is due to the dominance of the participant zone. Particles with small momentum accumulate near the mid-rapidity region and yield a compressed participant zone and hence results in larger nuclear stopping. As we move towards the high momentum range associated with the particles, the dominance of the participant region start decreasing. Particles with large momentum tends to increase the longitudinal component of the rapidity compared to the transverse component. Moreover, as we consider the whole momentum range of the colliding nucleons (M-ALL), the overall nuclear stopping decreases.

3. A closer look at Fig. 4.7 shows that at low incident energies, particles with high momentum are not available to take part in the nuclear stopping. With increase in the incident energy, high momentum particles also start participating initially for the heavier fragments and then for all the fragments. In addition, for all momentum bins, the nuclear stopping does not follow a uniform trend with an increase in the charge of the fragments. There is a large variation in the nuclear stopping for

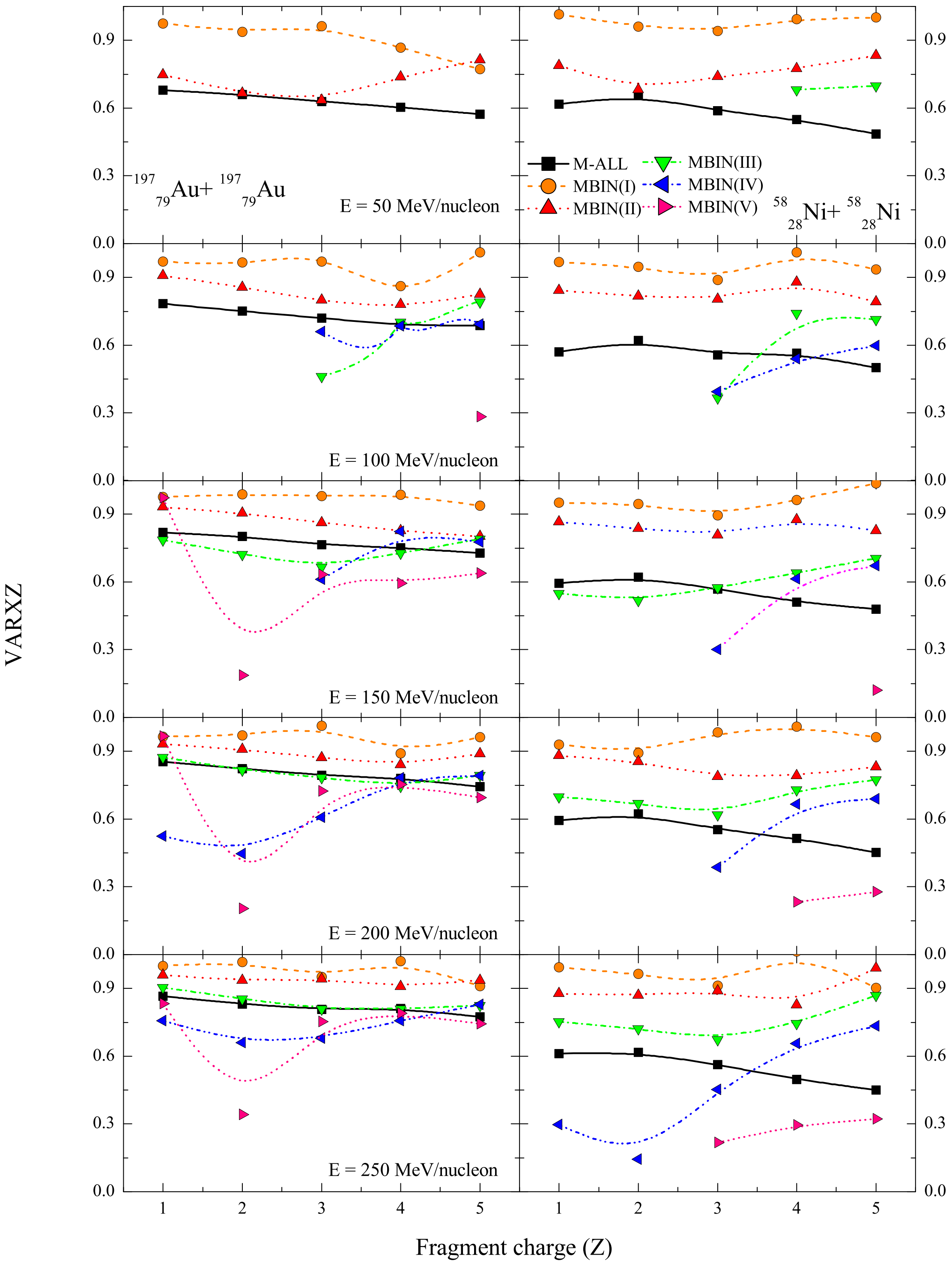

Figure 4.7: VARXZ as a function of charge of fragment (Z) for $^{197}_{79}Au+^{197}_{79}Au$ (left) and $^{58}_{28}Ni+^{58}_{28}Ni$ (right) at various incident energies and momentum bins.

the highest momentum bin (MBIN(IV)). Similar trend has also been observed for the reaction of $^{58}_{28}$Ni+$^{58}_{28}$Ni. It is worth to mention here that the high momentum of particles tends to decrease the nuclear stopping due to broader shape of longitudinal rapidity distribution. That is why a minima in stopping is observed around Z=2 fragment.

4.2.6 Stopping parameter (VARXZ) as a function of incident energy

Fig. 4.8. displays the nuclear stopping VARXZ as a function of incident energy.The momentum bins are same as discussed in Fig. 4.7 for the selected range of momentum bins. A slight increase in the nuclear stopping with increase in the incident energy is observed for all momentum bins. The statement is true for all the fragments irrespective of the reactions considered. It also confirms the previous findings that MBIN(I) particles contribute maximum towards stopping. With an increase in the incident energy, one expects a progressive increase in the nucleon-nucleon collisions at the expense of the nuclear mean field. Due to this, there will be a rapid increase in the transverse energy, that results in enhanced nuclear stopping in the longitudinal direction. For the light charge fragments, particles with large momenta are available only at high incident energies. Whereas, for the heavy charge fragments (Z $\geq$ 3) particles with large momentum exists throughout the energy range. In the comparison of results for the reactions of $^{197}_{79}$Au+$^{197}_{79}$Au with $^{58}_{28}$Ni+$^{58}_{28}$Ni, it is found that less stopping is observed for the lighter systems. This is due to the fact that stopping is governed by the participant zone only, which in turn depends on the mass of colliding nuclei and incident energy. In addition, for lighter systems, the distance between two successive collisions is comparable to the diameter of the nucleons. This results in more transparency.

4.2.7 Stopping parameter (VARXZ) as a function of momentum distribution of particles

In Fig. 4.9, the nuclear stopping as a function of momentum distribution of the particles is shown. The results are plotted at the higher limit of each momentum bin. Various symbols indicate different incident energies. Panels from the top to bottom indicate the nuclear stopping for different fragments of $^{197}_{79}$Au+$^{197}_{79}$Au (left panels)and $^{58}_{28}$Ni+$^{58}_{28}$Ni

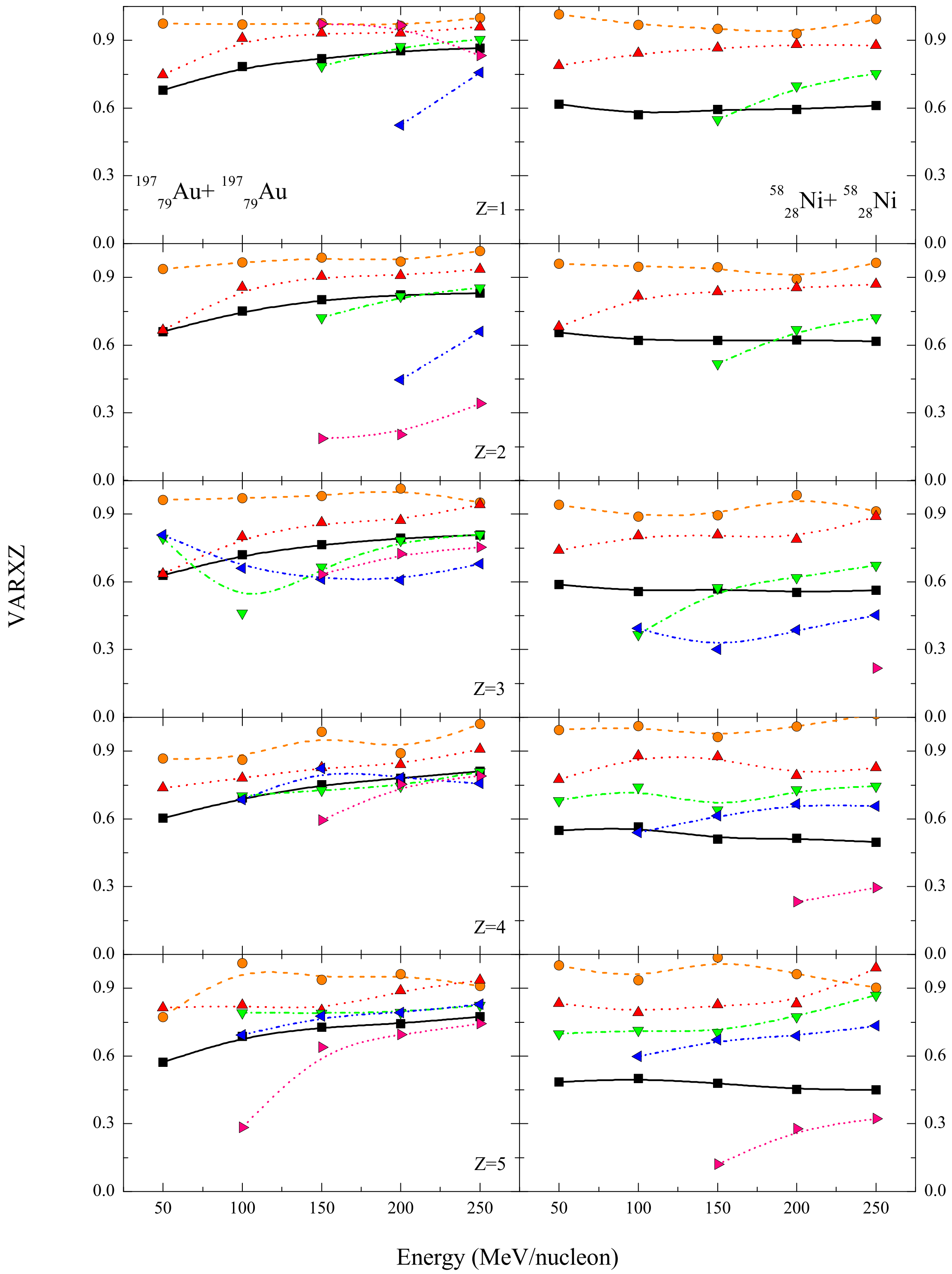

Figure 4.8: VARXZ as a function of incident energy for $^{197}_{79}$Au+$^{197}_{79}$Au and $^{58}_{28}$Ni+$^{58}_{28}$Ni for different Z and momentum bins defined in Table 4.1.

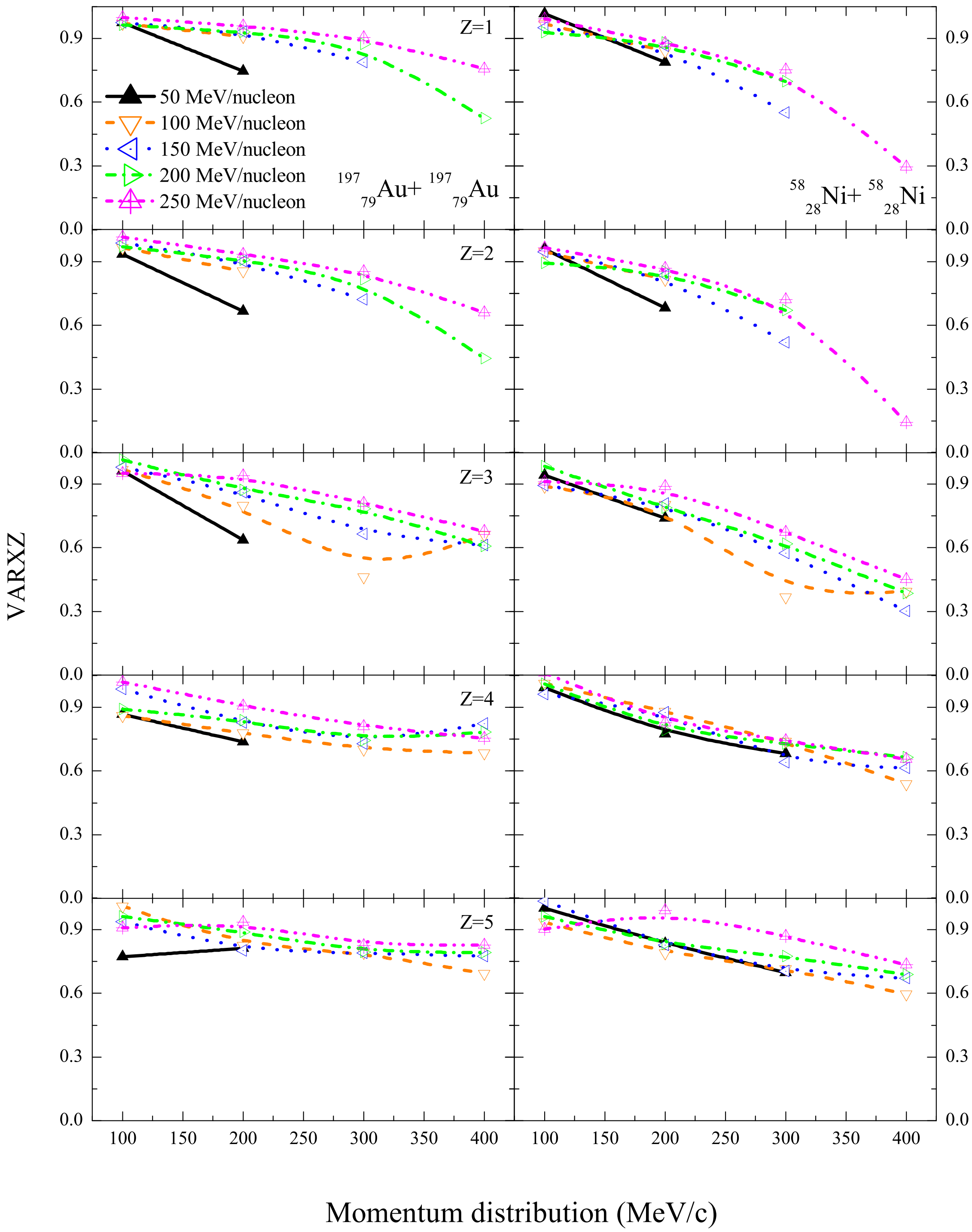

Figure 4.9: VARXZ as a function of momentum associated with the fragments.

(right panels). One can clearly see that nuclear stopping decreases with increase in the momentum associated with the particles. This is due to the reason that, at saturation time of a reaction, the charge fragments with large momentum associated with them moves away from the participant zone and contribute the least in nuclear stopping.

4.2.8 Stopping parameter (VARXZ) as a function of incident energy: Comparison with the experimental data

Lastly, we have shown the sensitivity of the free protons with a specific momentum towards the nuclear stopping as a function of incident energy. One can clearly see that at low incident energies ($\leq$ 400 MeV/nucleon) nuclear stopping increases with incident energy and then decreases significantly for all the momentum distribution (M-ALL) taken into account. Whereas, for a specific range of momentum distribution, there is a sharp increase in the nuclear stopping upto 400 MeV/nucleon. After this energy, there is a slight variation (increase/flatness) in the nuclear stopping.

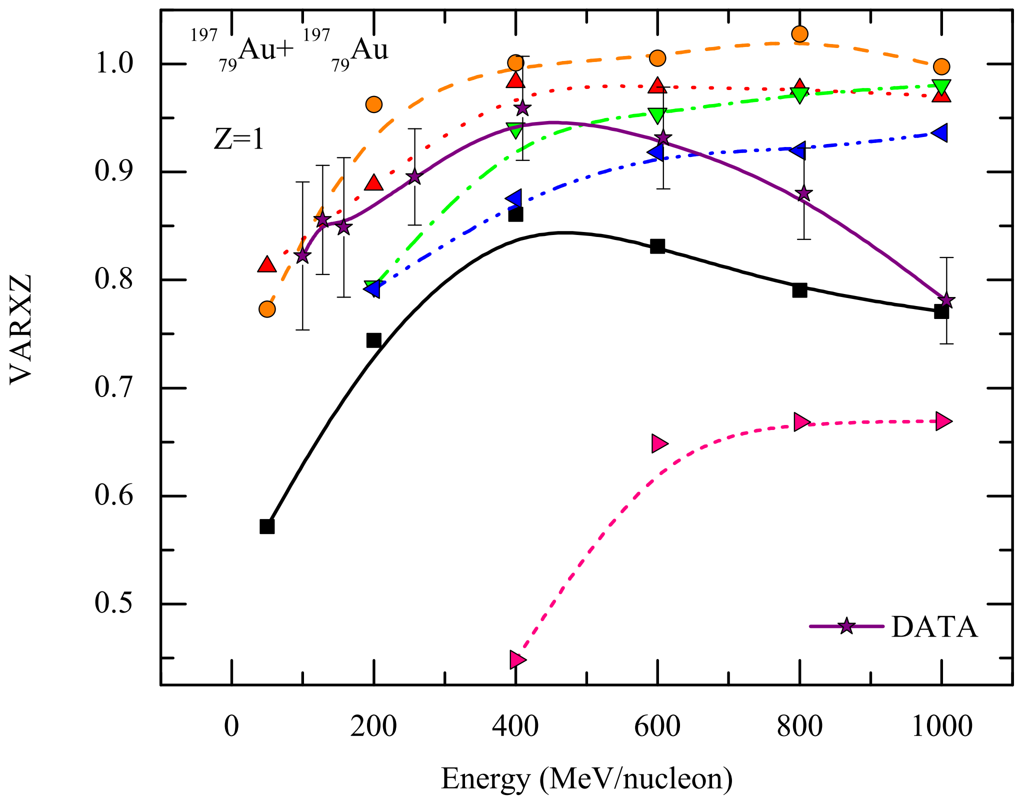

Figure 4.10: VARXZ as a function of incident energy for free protons of the system $^{197}_{79}$Au+$^{197}_{79}$Au.

These results are in agreement with findings of Reisdorf *et al.* [1] that a maximum stopping is observed at 400 MeV/nucleon. For the verification of our results, we have also compared our calculations with the available experimental data [16]. A closer look at Fig. 4.10 indicates that at low incident energies, fragments contributing to nuclear stopping lie in MBIN(I) and MBIN(II). With an increase in the incident energy, the momentum range of the fragments also shifts towards the higher end. Upto 600 MeV/nucleon, the fragments causing nuclear stopping lies in the bin MBIN(II), MBIN(III), MBIN(IV). Above 600 MeV/nucleon, higher momentum bin particles are playing a dominant role in the nuclear stopping. At 1000 MeV/nucleon, there are lesser number of fragments carrying high momentum which contribute in nuclear stopping.

Although the fragments lying in the higher momentum bins contribute more but still their contribution in nuclear stopping is the least. The comparison of theoretical calculations with the experimental data indicate that average effect of all the momentum distributions follows the similar trend as recorded by experimental data.

4.3 Summary

In summary, we presented the effect of isospin content as well as the contribution of various components of nuclear potential on the nuclear stopping of protons and neutrons for the reaction $^{120}_{50}$Sn+$^{120}_{50}$Sn using IQMD model. It is observed that momentum dependent interactions affect the nuclear stopping to a larger extent compared to other components of the nuclear potential. The isospin dependent cross section, however, affects the nuclear stopping in central collisions only. Further, influence of various momentum constraints on nuclear stopping has also been investigated. The comparison of our results with experimental data reveals that at a particular incident energy, a significant number of particles having a specific momentum are produced and maximum stopping is observed for the lowest range of momentum distribution. Moreover, for all the momentum distribution taken into account the nuclear stopping first increases sharply upto 400 MeV/nucleon and then decreases significantly with increase in incident energy.

Bibliography

[1] W. Reisdorf *et al.*, Phys. Rev. Lett. **92**, 232301 (2004).

[2] A. Schüttauf *et al.*, Nucl. Phys. A **607**, 457 (1996).

[3] R. E. Renfordt *et al.*, Phys. Rev. Lett. **53**, 763 (1984).

[4] B. Hong *et al.*, Phys. Rev. C **66**, 034901 (2002).

[5] D.T. Khoa *et al.*, Nucl. Phys. A **542**, 671 (1992).

[6] D.T. Khoa *et al.*, Nucl. Phys. A **548**, 102 (1992).

[7] R.K. Puri *et al.*, Nucl. Phys. A **575**, 733 (1994).

[8] G. Lehaut *et al.*, Phys. Rev. Lett. **104**, 232701 (2010).

[9] O. Lopez *et al.* (INDRA collaboration), Phys. Rev. C **90**, 064602 (2014).

[10] J. Aichelin, Phys. Rep. **202**, 233 (1991).

[11] Q. Li, J.Q. Wu and C.M. Ko, Phys. Rev. C **39**, 849 (1989).

[12] C. Hartnack, R.K. Puri, J. Aichelin, J. Konopka, S.A. Bass, H. Stöcker and W. Greiner, Eur. Phys. J. A **1**, 151 (1998).

[13] C. Hartnack, H. Oeschler, Y. Leifels, E.L. Bratkovskaya and J. Aichelin Phys. Rep. **510**, 119 (2012).

[14] W. Bauer, Phys. Rev. Lett. **61**, 2534 (1988).

[15] B. Hong *et al.*, Phys. Rev. C **57**, 244 (1998).

[16] W. Reisdorf *et al.*, Nucl. Phys. A **848**, 366 (2010).

[17] Y.F. Yang, J.Y. Liu, W. Zuo, W.J. Guo and Q. Zhao, Chin. Phys. Lett. **18**, 1040 (2001).

[18] J.Y. Liu, W.J. Guo, S.J. Wang, W. Zuo, Q. Zhao, and Y.F. Yang, Phys. Rev. Lett. **86**, 975 (2001).

[19] Q.F. Li and Z.X. Li, Chin. Phys. Lett. **19**, 321 (2002).

[20] J.Y. Liu, W.J. Guo, Y.Z. Xing, W. Zou and X.G. Lee, Phys. Rev. C **67**, 024608 (2003).

[21] J.Y. Liu, W.J. Guo, Y.Z. Xing, X. G. Li, and Y. Gao, Phys. Rev. C **70**, 034610 (2004).

[22] S. Kumar and S. Kumar, Chin. Phys. Lett. **27**, 062504 (2010).

[23] S. Kumar, S. Kumar, and R.K. Puri, Phys. Rev. C **81**, 014601 (2010).

[24] X.F. Luo, X. Dong, M. Shao, K.J. Wu, C. Li, H.F. Chen, and H.S. Xu, Phys. Rev. C **76**, 044902 (2007).

[25] X.F. Luo, X. Dong, M. Shao, C. Li, H.F. Chen, K.J. Wu and H.S. Xu, Indian J. Phys. **85**, 947 (2011).

[26] G.Q. Zhang, Y.G. Ma, X.G. Cao, C.L. Zhou, X.Z. Cai, D.Q. Fang, W.D. Tian, and H. W. Wang, Phys. Rev. C **84**, 034612 (2011).

[27] J. Su and F.S. Zhang, Phys. Rev. C **87**, 017602 (2013).

[28] J. Su, K. Cherevko, W.J. Xie, and F.S. Zhang, Phys. Rev. C **89**, 014619 (2014).

[29] G. Peilert, H. Stöcker, and W. Greiner, Rep. Prog. Phys. **57**, 533 (1994).

[30] A. Ono *et al.*, Phys. Rev. C **47**, 2652 (1993).

[31] P. Chung *et al.*, Phys. Rev. C **66**, 021901(R) (2002).

[32] K.S. Vinayak and S. Kumar, J. Phys. G: Nucl. Part. Phys. **39**, 095105 (2012).

[33] M. Begemann-Blaich *el al.*, Phys. Rev. C **48**, 610 (1993).

[34] V. Kaur and S. Kumar, Phys. Rev. C **81**, 064610 (2010).

[35] A. Jain, S. Kumar, and R.K. Puri Phys. Rev. C **84**, 057602 (2011).

Chapter 5

Influence of rapidity constraints on fragment production

5.1 Introduction

The knowledge of nucleon-nucleon interaction potential is a fundamental theoretical tool in the analysis of heavy-ion collisions. It is a key ingredient for constructing the nuclear EOS. Thus it would be of great interest to explore the EOS of nuclear matter by studying the contribution of different components of interaction potential separately, which is the essential input for simulation of heavy-ion collisions within a transport model. Many attempts have been made in the literature to study the mechanism behind the HIC by using the NN interaction potential [1–3]. The general trend of using the NN potential in the simulation of heavy-ion collisions is to parameterize the same as a function of density (as it is done for Skyrme interaction) [3]. While parameterizing the potential, one starts with the fundamental interaction i.e. the Skyrme interaction and then adds other components of potential such as Yukawa, Coulomb, momentum dependent interactions and symmetry potential. In past decade, extensive attempts have been made using various parameterizations of the Skyrme force to understand the heavy-ion collision dynamics at low energies [4, 5]. In contrast, very few attempts have been made in the literature to study such effects at the intermediate energies [6]. The momentum dependence of mean field potential also plays a crucial role in the dynamics of heavy-ion collisions. A significant change in fragment production is observed by taking into account the momentum dependent interactions [7]. The Coulomb potential is also found to affect the fragment production at low incident energies [8]. Studies show that the Coulomb potential affects the balance energy for mass asymmetric reactions [9]. The symmetry potential, a hot topic in physics community, plays an important role in understanding the astrophysical happenings e.g. supernova explosion, neutron star etc. The density dependence of symmetry potential has been found to affect the fragmentation, elliptical flow and transverse flow [10,11]. The role of different components of interaction potential on energy of vanishing flow and nuclear stopping has been studied in Chapter 3 and Chapter 4, respectively. Unfortunately, it is still unknown that how these different components of NN potential affect multifragmentation of heavy-ions at intermediate energies by taking into account the effect of mass asymmetry of the reaction.

In a heavy-ion reaction, the phase space configuration of the fragments produced is characterized by the degree of chaoticity produced in the reaction after the freeze-out density. Due to the interplay between compression-expansion, excited nucleus disintegrate into number of light, intermediate and heavy mass fragments. The yields of these highly excited fragments depend on the contribution of various components of NN interaction potential in addition to input parameters/ingredients of a reaction i.e. incident energy, masses of colliding nuclei and impact parameter. Moreover, the mass asymmetry (η) of reaction also plays a remarkable role in reaction dynamics. In symmetric reaction ($\eta = 0$) the excitation energy is available in the form of compressional energy in contrast to asymmetric reaction ($\eta \neq 0$) in which excitation energy is stored in the system in the form of thermal energy. The aim of multifragmentation studies is to relate the experimental observations to the properties of the nuclear matter phase diagram. The onset of fragmentation affects significantly the kinematical properties of the fragments, which can provide useful information about the equation of state of hot and dense nuclear matter and other phenomena at intermediate energy heavy-ion collisions.

Multifragmentation in heavy-ion collisions is studied via average multiplicity of fragments, d/p ratio, dlike/plike ratio, composite particle production of fragments, yield ratios, isoscaling and isospin fractionation ratio etc. [12–18]. Light elements such as protons(p), neutron (n), deuteron (d), tritons , ^{3}He and alpha particles have also been observed experimentally(see e.g Ref. [19] and references therein). In 1983, Gutbrod *et al.* [15] reported the sensitivity of d/p ratio on the size of the participant volume. Aichelin and coworkers [16] found d/p ratio to be insensitive towards the momentum dependent interactions, but is rather sensitive to the nuclear equation of state at least for the heavier colliding systems. Chen *et al.* [20] shed light on the multiplicity and energy spectra of light fragments and found it to be sensitive towards the density dependence of nuclear symmetry energy. Doss *et al.* [17] studied the yield ratios of light fragments to protons for $^{93}_{41}$Nb + $^{93}_{41}$Nb and $^{197}_{79}$Au + $^{197}_{79}$Au within the framework of QMD model [21–24] and further advanced by Peilert *et al.* [18], it was found that the light fragments to proton ratio increases with increase in multiplicity of charged particles and decrease in incident energy. In addition, it was also stated that the true multifragmentation events are found in the central collisions for bombarding energy between 30 and 110 MeV/nucleon. Despite lots of findings are present in the literature on the fragmentation of light as well as intermediate mass fragments (IMF) [25–29], while the contribution of various components of NN potential towards the aforesaid observables within different rapidity regions with varying mass asymmetry has been rarely studied.

Among the various interesting observables used for the study of heavy-ion reactions, the production of different fragments in different rapidity domains is quite useful. The rapidity distribution is an important parameter to explore the participant-spectator contribution in heavy-ion collisions at intermediate energies. There are two procedures reported in the literature to differentiate participant and spectator matter. In one of the procedures, a nucleon is considered to be originating from participant if it has suffered at least single collision. A nucleon which has not suffered even a single collision is treated as spectator nucleon. Alternatively, one can define participant spectator matter in terms of rapidity distribution (see Eq. 1.3). Here, the different cuts in rapidity distribution can be imposed to differentiate participant spectator matter [30]. The participant and spectator matter by adopting the later procedure is defined. In this chapter, we aim to investigate the dependence of fragment production (LCP, IMF) and reaction dynamics on various components of NN interaction potential in participant rapidity (PR) as well as quasi participant rapidity (QPR) region. In the present work, the PR region is defined as $|\frac{Y_{c.m.}}{Y_{beam}}| \leq 0.5$ and QPR region is defined as $|\frac{Y_{c.m.}}{Y_{beam}}| > 0.5$. The role of mass asymmetry of the reaction is also explored by keeping the total mass of system fixed A_{total} =240.

5.2 Results and discussion

Several thousand events were simulated for the central collisions of the reactions $^{120}_{50}$Sn + $^{120}_{50}$Sn (η = 0), $^{82}_{36}$Kr + $^{158}_{64}$Gd (η = 0.3), $^{56}_{26}$Fe + $^{184}_{74}$W (η = 0.5) and $^{35}_{17}$Cl + $^{205}_{81}$Tl (η = 0.7) at incident energies between 50 to 200 MeV/nucleon. In order to study the role of mass asymmetry of the reaction, the reactions are chosen in such a way that the mass asymmetry of the reactions varies between 0 to 0.7 while the total mass remains constant i.e. A_{total} = 240 units. A soft equation of state has been employed in present work. It has been stated in Ref. [31, 32] that the results obtained with σ_{nn}^{free} deviate from the experimental data by 25%, so, a reduced cross section $\sigma_{red} = 0.8\sigma_{nn}^{free}$ is used in the present study. It has been observed that in case of collision of lighter nuclei, the system thermalize earlier compared to the collision of heavier nuclei [21]. Since the fragmentation is a subsaturation phenomena, we take the observations at saturation time (i.e. 200 fm/c). After this time, there is no further change in the phase space configuration of nuclear matter.

To study the contribution of each component of nuclear interaction potential in different observables, one starts with the basic potential and then resimulate the reaction each time by adding gradually the other components of nuclear potential. Different acronym used in this chapter have the same meaning as in Chapter 3.

5.2.1 Trajectory of nucleon under the influence of various components of NN potential

Fig. 5.1 shows the 3D trajectory of a single nucleon for the central collision of the reaction $^{120}_{50}$Sn + $^{120}_{50}$Sn at E = 50 MeV/nucleon. The phase space of the reaction is stored at various time steps between t = 0.1 to 200 fm/c. Initially, at t=0.1 fm/c the phase space of the nucleon for different sets of components of NN potential coincide with each other. A slight change in time ordering of collisions may yield completely different trajectories. As the particle propagates, the role of different potentials comes into picture. The trajectory of nucleon under the influence of SY set of potential shows a linear path. The addition of Coulomb potential deviates the nucleon from its original path due to its repulsive nature. The addition of momentum dependent potential and symmetry potential further, adds repulsion to the system and deviate the path of nucleon further.

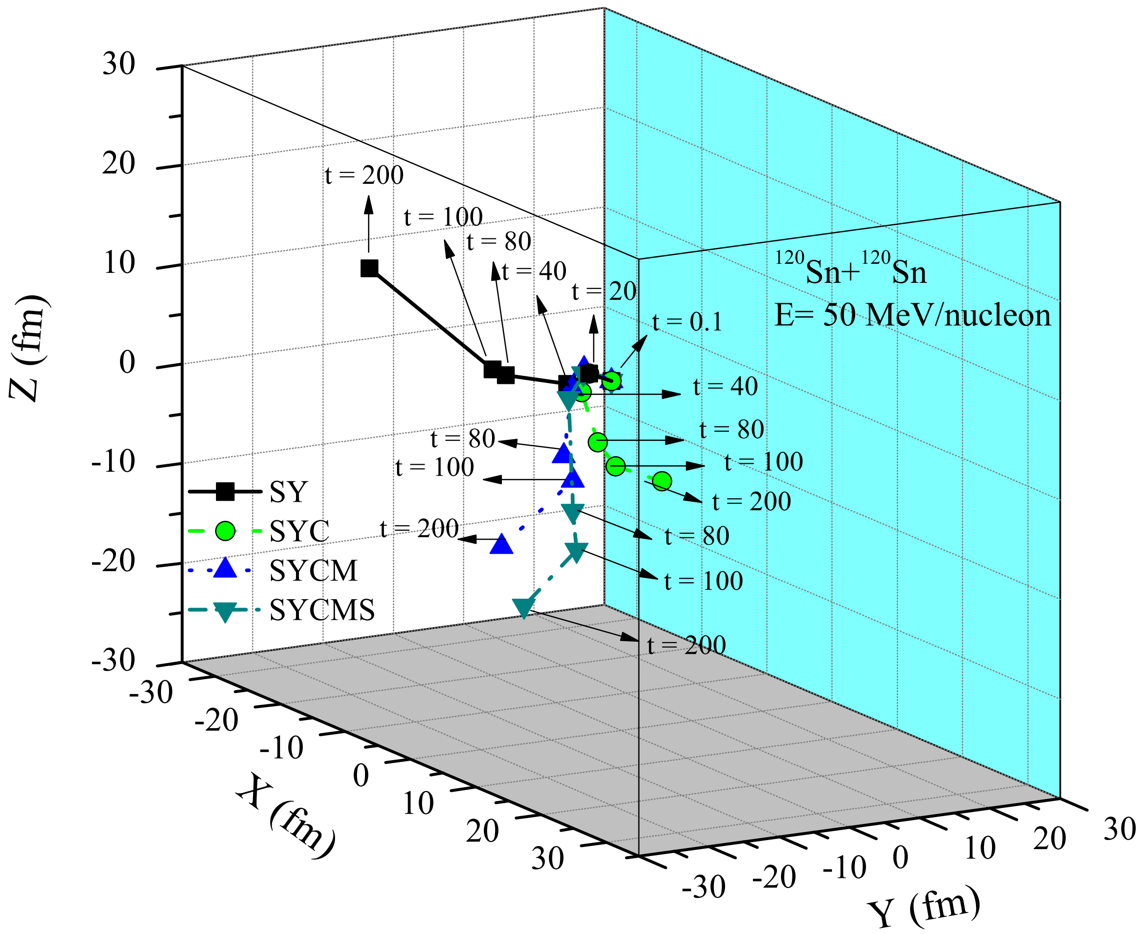

Figure 5.1: 3D Trajectory of single nucleon under the influence of different components of nuclear potential for symmetric $^{120}_{50}$Sn + $^{120}_{50}$Sn reaction.

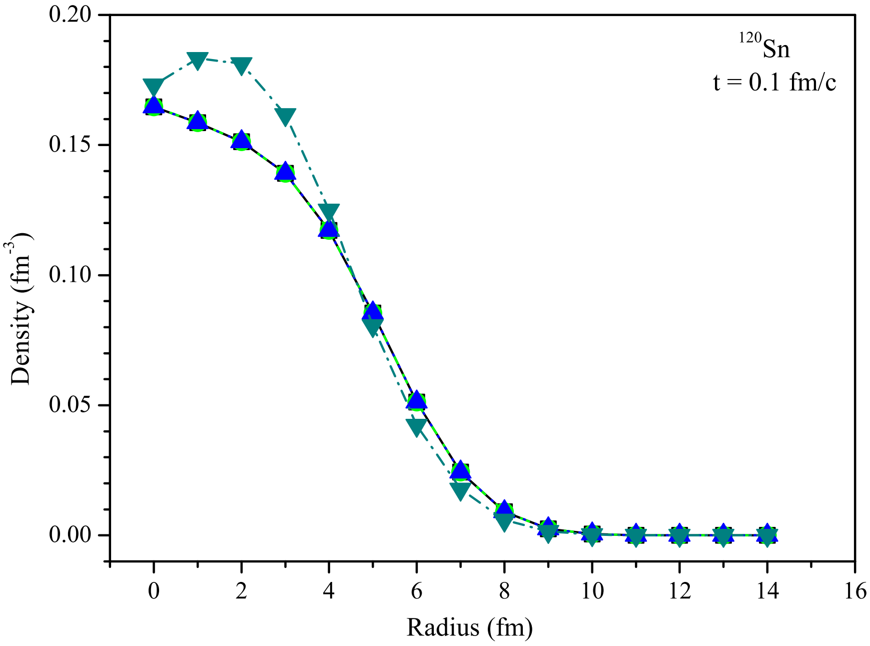

Figure 5.2: Variation of ground state density as a function of radius at T= 0.1 fm/c for $^{120}_{50}$Sn nucleus.

Fig.5.2 shows ground state density of $^{120}_{50}$Sn nucleus as a function of radius at t= 0.1 fm/c. We note that density remains same for SY, SYC, SYCM potentials. One can see that addition of various components of NN potential does not show a significant change in the ground state density of the nucleus except the symmetry potential. This is due to density dependent nature of symmetry potential which increases its contribution in the core of the nucleus as compared to its surface. With increase in radius, the ground state density starts decreasing. This decrease is more rapid in case of SYCMS as compared to SY, SYC, SYCM potentials as the Yukawa potential (surface potential) plays a dominant role at the surface of nucleus.

5.2.2 Charge distribution of fragments

Fig. 5.3 shows the charge distribution of the fragments for the central collision of the reaction $^{120}_{50}$Sn + $^{120}_{50}$Sn (50 MeV/nucleon), $^{197}_{79}$Au + $^{197}_{79}$Au (150 MeV/nucleon) and $^{40}_{20}$Ca + $^{40}_{20}$Ca (50 MeV/nucleon). All the symbols have the same meaning as in Fig. 5.1. Stars represent the experimental data of INDRA and FOPI collaboration. The reason for selecting the aforesaid energies for the corresponding reactions is the availability of experimen-

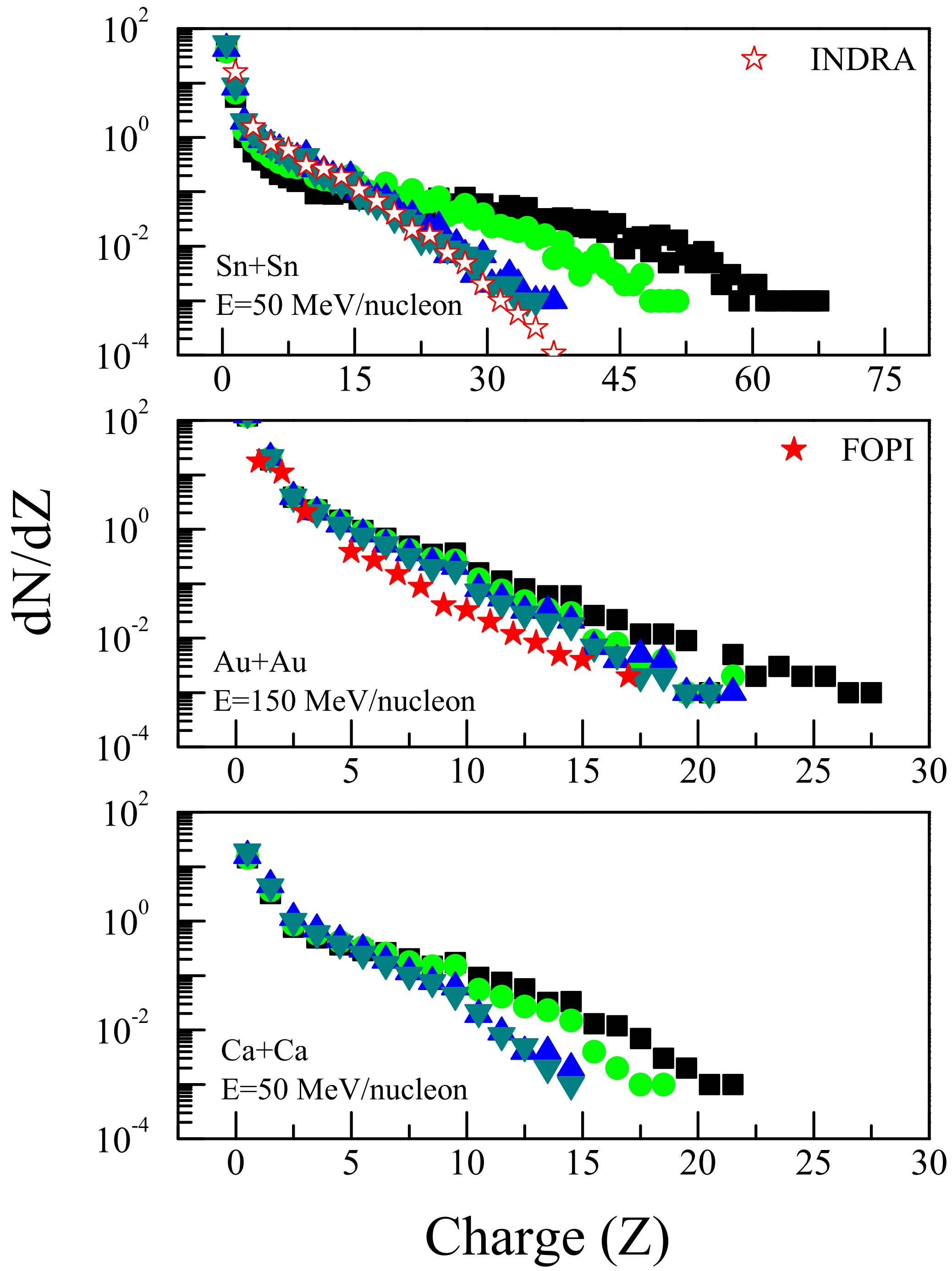

Figure 5.3: Charge distribution of fragments for the central collision of the reactions $^{120}_{50}$Sn + $^{120}_{50}$Sn (η = 0), $^{82}_{36}$Kr + $^{158}_{64}$Gd (η = 0.3) and $^{56}_{26}$Fe + $^{184}_{74}$W ($\eta = 0.5$), $^{35}_{17}$Cl + $^{205}_{81}$Tl ($\eta = 0.7$) at E = 50 MeV/nucleon.

tal data [33, 34]. One can see that the complete set of components of nuclear potential (SYCMS) lead to enhanced emission of light fragments at all colliding geometries. The Skyrme and Yukawa interaction, due to their attractive behavior, are not able to break the correlation among the nucleons and give rise to large number of heavy mass fragments. The addition of Coulomb interaction results in repulsive interaction between the colliding nucleons, due to which very heavy fragments can not be produced. At higher incident energies (e.g. in Fig. 5.3 (b)), the difference in the mass distribution due to different components of nuclear potential diminishes. With the increase in incident energy, more destruction of nuclear matter takes place due to violent phase of the reaction, which leads to large number of free nucleons and light fragments. Comparison between our calculations and the experimental data reveals that a combination of all the components of nuclear potentials is necessary to explain the fragment production.

5.2.3 Incident energy dependence of fragment multiplicity

In order to explore the contribution of various components of nuclear potential towards the fragment production in different rapidity domains, the complete range of rapidity distribution is divided into two different regions, namely, the participant rapidity (PR) region and quasi participant rapidity (QPR) region. Fig. 5.4 shows the variation of multiplicity of LCPs in PR and QPR region with energy for different mass asymmetric reactions. In both PR and QPR region, the multiplicity of LCPs decreases with increase in mass asymmetry (η) because of decrease in participant zone. The multiplicity of LCPs increases with energy due to increase in violence of collision with energy. For a particular η, the multiplicity is less for SY set of potential. It is because of their attractive nature, most of the matter is in the form of heavy mass fragments. With addition of Coulomb, momentum dependent and symmetry components of potential, the multiplicity of LCPs increases due to breaking of heavy mass fragments into smaller ones because of repulsive nature of these potentials added.

Fig. 5.5 is similar to Fig. 5.4 except that it is plotted for IMFs. In both PR and QPR region, the multiplicity of IMFs decreases with increase in mass asymmetry which is due to breaking of heavy mass fragments into more number of free nucleons and LCPs. In QPR region, the IMFs shows the well known trend of rise and fall with energy. The

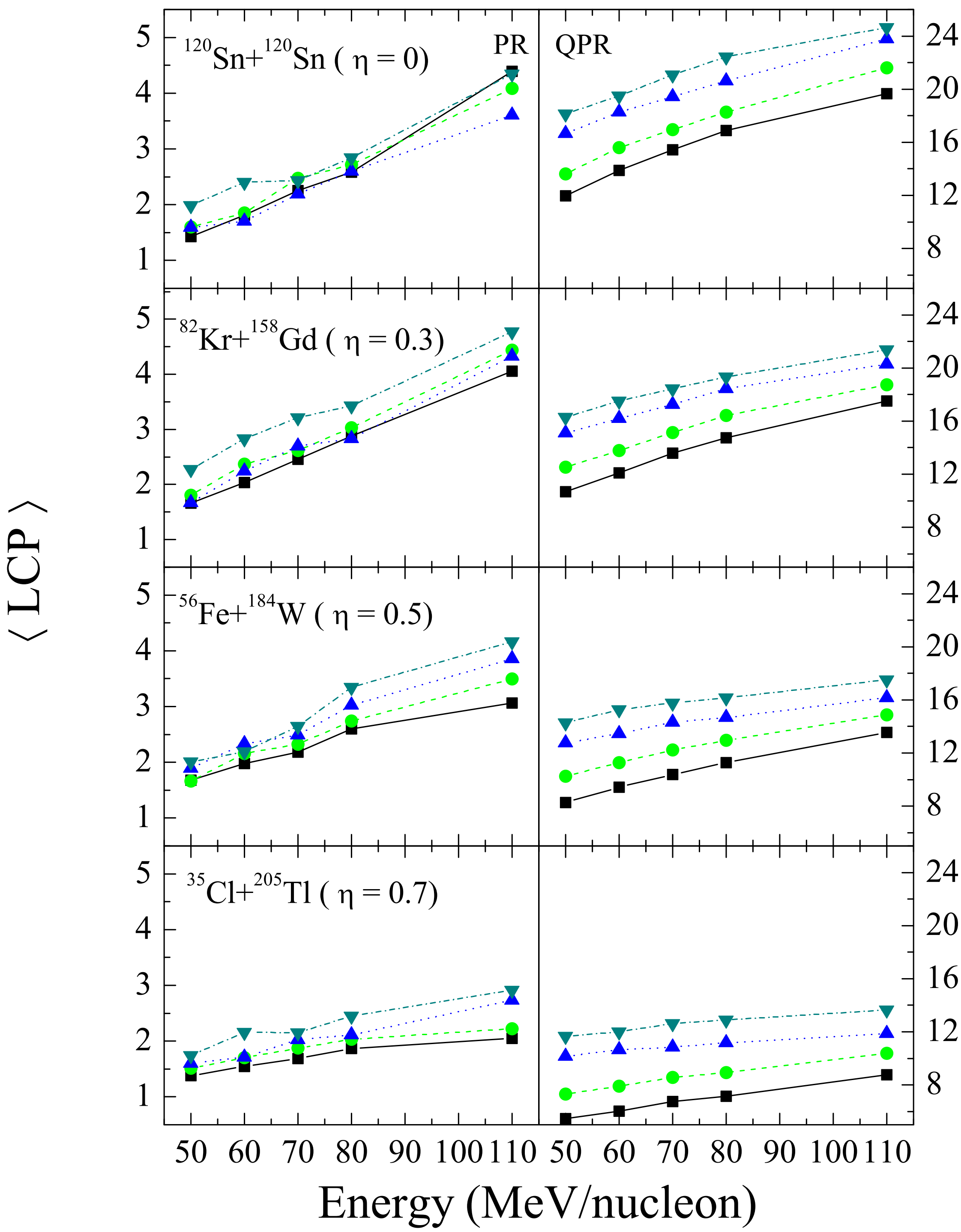

Figure 5.4: Variation of light charged particle multiplicity in participant region (PR) and quasi participant region (QPR) with energy for different η. Various symbols have same meaning as in Fig. 5.1.

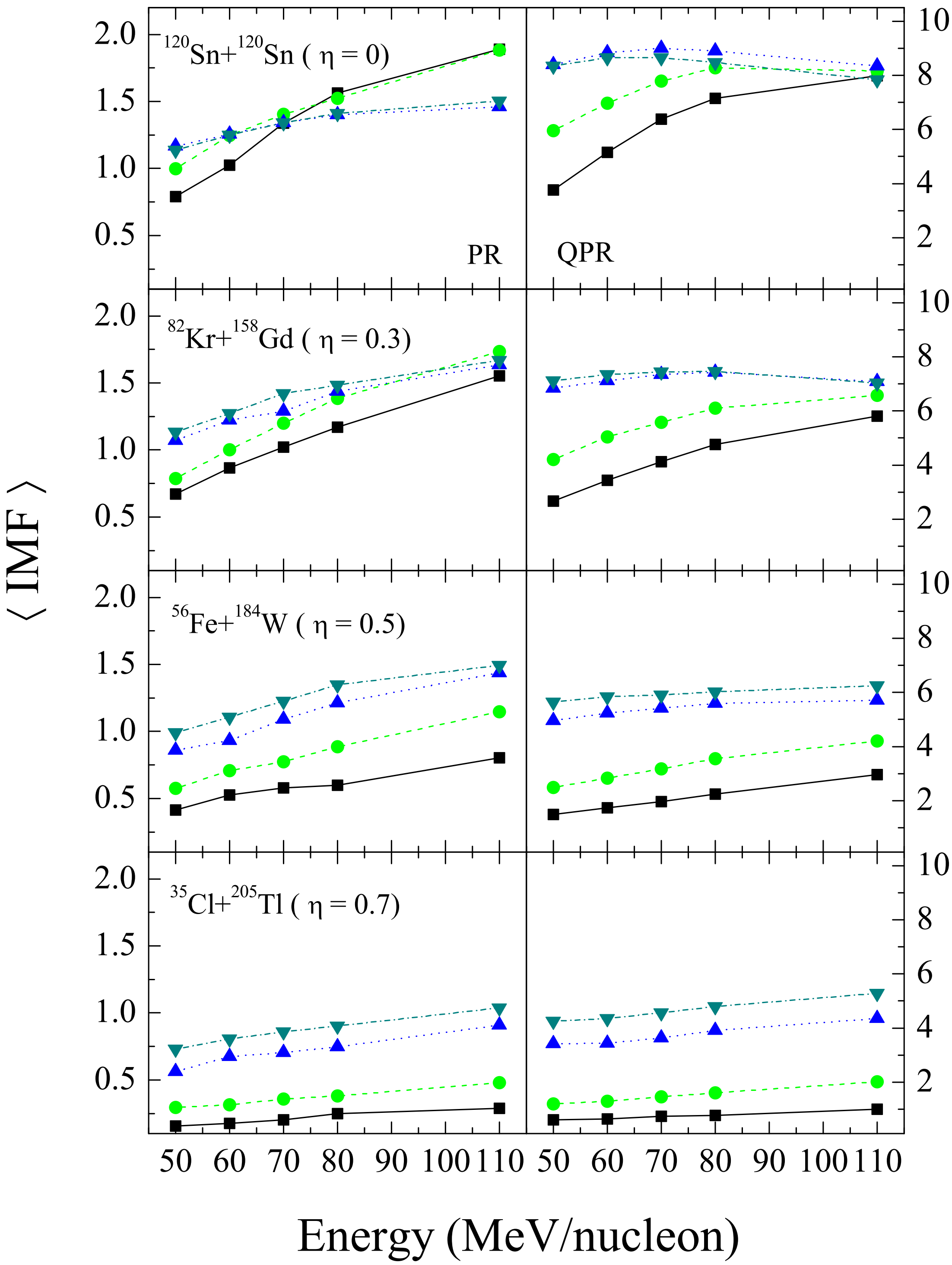

Figure 5.5: Same as Fig. 5.4 but for IMFs multiplicity in participant region (PR) and quasi participant region (QPR) with energy for different η.

peak shifts towards right with increase in mass asymmetry (η) of the reaction because more energy is needed to break the heavier fragments due to less compression in mass asymmetric reactions. For η=0.7 the multiplicity of IMFs shows only the rise as also observed in [8].

5.2.4 Mass asymmetry dependence of fragment multiplicity

Fig. 5.6 depicts the variation of multiplicity of LCPs and IMFs with mass asymmetry (η) in both PR and QPR regions at E =110 MeV/nucleon under the influence of different components of potential. It is clear that with increase in η, the multiplicity of LCPs decreases because of decrease in participant zone. In PR region, multiplicity of LCPs

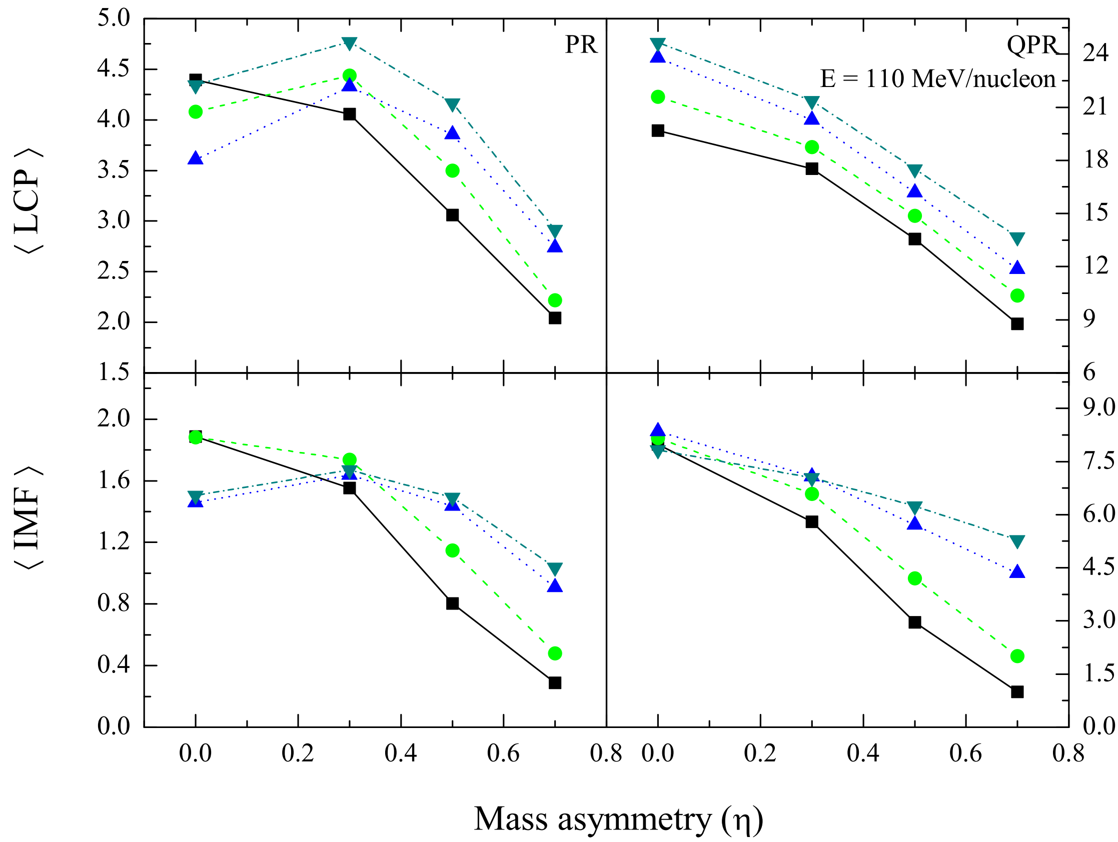

Figure 5.6: Variation of light charged particle multiplicity in participant region (PR) and quasi participant region (QPR) with η at E =110 MeV/nucleon. Various symbols have same meaning as in Fig. 5.1.

decreases with increase in η for SY set of potential as the part of repulsive potential is missing from the SY potential. Once the repulsive potential like Coulomb, MDI and symmetry potential is added, the rise and fall in the multiplicity of LCPs has been observed around η=0.2. This indicates that at incident energy 110 MeV/nucleon, maximum participant matter contributes in the formation of LCPs. The value will go towards the higher side with increase in incident energy because of the break-up of initial correlation among the nucleons, even in the spectator matter. This is due to the violent NN collisions in the participant matter with increase in incident energy. However, in QPR region, with increase in η, the spectator matter is increasing uniformly and hence LCPs production is decreasing uniformly. Since at saturation time (t=200fm/c), most of matter is driven into QPR region, therefore the multiplicity of fragments is less in PR region as compared to QPR region. Moreover, the role of different components of nuclear interaction potential is visible in this region. The SY potential being attractive does not break the heavy fragments into LCPs. But with addition of Coulomb, momentum dependent and symmetry potential, the LCPs and IMFs multiplicity increases due to their repulsive nature of these potentials.

5.3 Summary

In conclusion, the role of different components of nuclear potential on fragment production has been explored by varying the mass asymmetry and keeping A_{total} =240 units fixed, within the framework of IQMD model. The different components of NN potential have remarkable role in fragment production. The multiplicity of LCPs and IMFs increases with the addition of different components of interaction potential. With the increase in mass asymmetry, the multiplicity of LCPs and IMFs decreases in both the rapidity regions. However, the multiplicity of LCPs and IMFs is less in PR region as compared to QPR region. The comparison of charge distribution for $^{120}_{50}$Sn + $^{120}_{50}$Sn reaction with experimental data reveals that all the components of nuclear potential are necessary to explain the experimental charge distribution.

Bibliography

[1] R.K. Puri, Rashmi Arora, and R.K. Gupta, Phys. Rev. C **60**, 054619 (1999).

[2] V. Zanganeh, N. Wang, and O.N. Ghodsi, Phys. Rev. C **85**, 034601 (2012).

[3] D.T. Khoa, N. Ohtsuka, and M.A. Matin *et al.*, Nucl. Phys. A **548**, 102 (1992).

[4] R.K. Puri, P. Chattopadhay, and R.K. Gupta, Phys. Rev. C **43**, 315 (1991).

[5] R.K. Puri and R.K. Gupta, Phys. Rev. C **45**, 1837 (1992).

[6] S.A. Bass, C. Hartnack, H. Stocker, and W. Greiner, Phys. Rev. Letter **71**, 1144 (1993).

[7] S. Kumar and R.K. Puri, Phys. Rev. C **60**, 054607 (1999); J. Singh, S. Kumar, and R.K. Puri, Phys. Rev. C **63**, 054603 (2001); Y.K. Vermani, S. Goyal, and R.K. Puri, Phys. Rev. C **79**, 064613 (2009).

[8] V. Kumar and S. Kumar, Phys. Rev. C **81**, 064610 (2010).

[9] S. Goyal and R. K. Puri, Nucl. Phys. A **853**, 164 (2011).

[10] S. Gautam, R. Kumari, and R.K. Puri, Phys. Rev. C **86**, 034607 (2012).

[11] K.S. Vinayak and S. Kumar, Eur. Phys. Jour. A **47**, 144 (2011); K.S. Vinayak and S. Kumar, Phys. Part. and Nucl. Lett. **9**, 583 (2012).

[12] M.B. Tsang *et al.*, Phys. Rev. Lett. **86**, 5023 (2001).

[13] W.P. Tan *et al.*, Phys. Rev. C **64**, 51901(R) (2001).

[14] J. Iglio *et al.*, Phys. Rev. C **74**, 024605 (2006).

[15] H.H. Gutbrod *et al.*, Phys. Lett. **127B**, 317 (1983).

[16] J. Aichelin *et al.*, Phys. Rev. Lett. **58**, 1926 (1987).

[17] K.G.R. Doss *et al.*, Phys. Rev. C. **32**, 116 (1985); *ibid* Phys. Rev. C **37**, 163 (1988).

[18] G. Peilert*et al.*, Phys. Rev. C **39**, 1402 (1989).

[19] S. Kowalski *et al.* Phys. Rev. C **75**, 014601 (2007).

[20] L.W. Chen, C.M. Ko, and B.A. Li, Phys. Rev. C **68**, 017601 (2003); *ibid* Nucl. Phys. A **729**, 809 (2003).

[21] J. Aichelin, Phys. Rep. **202**, 233 (1991).

[22] E. Lehmann *et al.*, Phys. Rev. C **51**, 2113 (1995).

[23] E. Lehmann, *et al.*, Prog. Part. Nucl. Phys. **30**, 219 (1993).

[24] S. Goyal, R. K. Puri, Phys. Rev. C **83**, 047601 (2011).

[25] M. Begemann-Blaich, *et al.*, Phys. Rev. C **48**, 610 (1993).

[26] M.B. Tsang, *et al.*, Phys. Rev. C **55**, R557 (1997).

[27] S. Kumar and S. Kumar, Pramana J. Phys. **74**, 731 (2010).

[28] A. Jain and S. Kumar, Pramana J. Phys. **78**, 749 (2012).

[29] A. Schuttauf *et al.*, Nucl. Phys. A **607**, 457 (1996).

[30] W. Reisdorf, Nucl. Phys. A **630**, 15c (1998).

[31] S. Gautam, J. Phys. G. **37**, 085102 (2010)

[32] S. Gautam, A.D. Sood, R.K. Puri, and J. Aichelin, Phys. Rev. C **83**, 014603 (2011).

[33] S. Hudan *et al.*, Phys. Rev. C **67**, 064613 (2003).

[34] C. Kuhn *et al.*, Phys. Rev. C **48**, 1232 (1993).

Chapter 6

Summary and outlook

" Education is what remains after one has forgotten what one has learned in school"........................Albert Einstein

This thesis contains a theoretical study of heavy-ion collisions dynamics. The basic goal was to study in detail the contribution of various components of interaction potential towards the transverse directed flow, energy of vanishing flow and other related phenomena like nuclear stopping and nuclear multifragmentation. The role of various isospin-dependent components was also explored for various observables. The isospin-dependent Quantum Molecular Dynamics Model is used to carry out the present study.
Starting with the origin of nuclear physics, we first presented an introduction to heavy-ion collisions and various phenomena occurring at intermediate energies i.e. collective flow, nuclear stopping and multifragmentation. The mass symmetric and mass asymmetric heavy-ion reactions were also described followed by the theoretical and experimental review of these observables. Brief survey of various primary and secondary models used in the literature to study the reaction dynamics is also presented. However, Isospin-dependent Quantum Molecular Dynamics (IQMD) model is explained in detail.
Collective flow was first predicted experimentally by Berkeley group at BEVALAC. Since then, intensive theoretical and experimental investigations were carried out to study collective flow and its disappearance but, few studies are available when we talk about the effect of various components of interaction potential on directed transverse flow. We have studied the contribution of different components of interaction potential on the directed flow and its disappearance for the reactions ${}^{58}_{26}$Fe+ ${}^{58}_{26}$Fe, ${}^{58}_{28}$Ni+ ${}^{58}_{28}$Ni, ${}^{86}_{36}$Kr+ ${}^{93}_{41}$Nb and ${}^{197}_{79}$Au+${}^{197}_{79}$Au. Interestingly, we found that the transverse directed flow becomes more

positive or less negative with the increase in the incident energy as well as with the addition of various components of potentials. The gradual contribution of various potentials impart additional repulsion to the colliding partners. As a result, the net transverse flow becomes more positive. We also found that with increase in impact parameter, the dominance of the Coulomb potential and MDI decreases considerably due to the decrease in the participant zone. As a result, there is a net reduction in the number of binary nucleon-nucleon collisions and hence the transverse directed flow. In addition, the E_{bal} decreases with the addition of the Coulomb potential, momentum dependence of the interactions, and the symmetry potential. Our study revealed the dominance of Coulomb potential and momentum dependent interactions over the other components of the potential for lighter colliding systems. However, the contribution of symmetry potential also become significant in the collision of heavier nuclei.

Apart from the transverse directed flow of all nucleons, the transverse directed flow of fragments with Z= 1, 2, 3 and 4 is also investigated to optimize the cluster recognition method (MST) which is mostly used. The regular MST method is modified by making it isospin-dependent. The comparison of our results with the experimental data shows that the light fragments produced by using isoMSTP(IV), are able to explain the experimental data. In addition, the energy of vanishing flow of charge fragments has also been explored and is found to be sensitive towards the charge of the fragment. The energy of vanishing flow of Z=1 fragments is found to be higher than the Z=2 fragments, in agreement with the existing studies. However, no specific conclusion can be drawn for the energy of vanishing flow of heavier fragments (Z $\geq$ 3).

Next, we studied the effect of isospin content as well as the contribution of various components of nuclear potential on the stopping ratio of protons and neutrons for the reaction $^{120}_{50}$Sn+$^{120}_{50}$Sn over a wide range of incident energy covering entire colliding geometry. We found that momentum dependent interactions affect the nuclear stopping to a larger extent compared to other components of the nuclear potential. The isospin dependent cross section, however, affects the nuclear stopping in central collisions only. We also investigated the nuclear stopping to get better insight of momentum distribution of particles for the central collisions of the reactions of $^{58}_{28}$Ni+ $^{58}_{28}$Ni and $^{197}_{79}$Au+$^{197}_{79}$Au. We found that at a particular incident energy, a significant number of particles having a specific momentum are produced and maximum stopping is observed for the lowest range of considered momentum distribution. Moreover, for all the momentum distribution taken into account the nuclear stopping first increases sharply upto 400 MeV/nucleon and then decreases slightly with increase in incident energy.

As a last step, we presented the role of different components of nuclear potential on fragment production for various mass symmetric and asymmetric reaction keeping A_{total} =240 units as fixed one. The different components of NN potential have remarkable role in fragment production. For a particular η, lesser number of light charged particles are produced for SY set of potential. It is because of the attractive nature of Skyrme and Yukawa interaction, that most of matter is in the form of heavy mass fragments. With addition of Coulomb, momentum dependent and symmetry components of potential, the multiplicity of LCPs increases due to breaking of heavy mass fragments into smaller ones because of repulsive nature of these potentials. Comparing the charge distribution for $^{120}_{50}$Sn + $^{120}_{50}$Sn reaction with experimental data, we found that all components of nuclear potential are necessary to explain the experimental charge distribution.

Though, we successfully studied the role of various components of interaction potential as well as other model ingredients such as isospin effects and nucleon-nucleon cross section on critical observables of heavy-ion collisions at intermediate energies but, there are still many challenges that desperately need to be solved. One can elaborate this work by studying the effect of different Skyrme parameterizations within the IQMD model. It will become interesting to study the role of different nucleon-nucleon potential including the isospin-dependent clusterization algorithm for elliptical flow. The isospin dependence of momentum dependent interactions is still a question of open debate.